

**Role of myelin-associated NAD<sup>+</sup>- dependent deacetylase  
Sirtuin 2 in modifying axonal degeneration**

Dissertation

for the award of the degree

“Doctor of Philosophy (PhD)”

Division of Mathematics and Natural Sciences  
of the Georg-August-Universität Göttingen

**submitted by**

Burcu Kasapoğlu

**from**

Istanbul, Turkey

Göttingen, 30.11.2011

***Prof. Klaus-Armin Nave, PhD (Reviewer)***

Department of Neurogenetics, Max-Planck-Institute of Experimental Medicine,  
Göttingen

***Prof. Dr. Nils Brose (Reviewer)***

Department of Molecular Neurobiology, Max-Planck-Institute of Experimental Medicine,  
Göttingen

***Dr. André Fischer***

Laboratory for Aging and Cognitive Diseases, European Neuroscience Institute, Göttingen

**Date of the oral examination: 01.02.2012**

## Declaration

Herewith I declare that I prepared the PhD thesis entitled "Role of myelin-associated NAD<sup>+</sup>-dependent deacetylase Sirtuin 2 in modifying axonal degeneration" on my own and with no other sources and aids than quoted. I would like to acknowledge specific contributions: Dr. Maria Carla Motta and Prof. Dr. Lenny Guarente for providing the Sirt2<sup>null</sup> mice, Prof. Dr. Thomas Bayer and Dr. Oliver Wirths for providing the 5xFAD transgenic mice, Torben Ruhwedel and Dr. Wiebke Möbius for high pressure freezing-freeze substitution and electron microscopy, Annette Fahrenholz for the assistance in histology, and Dr. Benoit Barrette for the induction of experimental autoimmune encephalomyelitis (EAE).

Burcu Kasapoğlu

Göttingen, 30.11.2011

*Onların varlığı ve desteği olmadan basaramazdım.*

*Hayattaki en kıymetlilerime,*

*Anneme ve babama....*

### Acknowledgements

I wish to express my gratitude to Prof. Klaus-Armin Nave for gathering so many lovely and friendly people in this terrific scientific environment of his lab, for giving me the opportunity to work on this interesting, complex and challenging project, for his support and discussions and for giving feedback on this manuscript.

I owe special thanks to Dr. Hauke Werner for his supervision and involvement in my project. I am grateful to him for the fruitful discussions on every detail of my project, for proofreading this manuscript and for any kind of support throughout the project.

I would like to thank Prof. Dr. Nils Brose and Dr. André Fischer for being a part of my PhD thesis committee and for contributing greatly to my project with their invaluable comments during our discussions.

I owe many thanks to Dr. Maria Carla Motta and Prof. Dr. Lenny Guarente for providing the *Sirt2<sup>null</sup>* mice, thereby not only contributing to, but also initiating my project.

I want to thank Prof. Dr. Michael Hörner from CMPB office, Kirsten Pöhlker, Christin Fischer and Christina Bach from GGNB office for being a part of a great organization team, for being so kind, understanding and helpful and for their great administrative support.

I am thankful to the "Sequencing team", Fritz Benseler, Ivonne and Dayana for every oligo synthesis and sequencing analysis.

It was great to have the "Proteomics Group", Dr. Olaf Jahn and Marina Reinelt for useful comments and discussions on biochemical experiments.

I am grateful to Kerstin Claus, Astrid Kanbach, Rainer Libal and all other animal caretakers of the Animal Facility of the MPI-EM for their excellent skills on taking care of our precious experimental animals.

I specially thank to Dr. Konstantin Radyushkin and Anja Ronnenberg for not only allowing me to use their Rotarod equipment, but also for the discussions on protocols and to Dr. Sergi Papiol for the discussion on sequencing and human genetic experiments.

I owe special thanks to Torben Ruhwedel and Dr. Wiebke Möbius for their excellence in electron microscopy and for creating beautiful images for my thesis. I should also mention here my many thanks to Annette Fahrenholz for her great assistance in the "Histology lab".

I would like to thank every member of the Neurogenetics lab for not being reluctant to help me with any problem, for providing useful experimental advices whenever needed. I acknowledge Dr. Benoit Barrette for the EAE induction experiment and his guidance in clinical scoring of the animals and; of course, Dr. Iva Tzvetanova for joining the "SIRT2 team", for the discussions and for the experiments we did and we will do in the future together.

Life in the lab would not be easy without having Ulli Bode, Martin Theuerkorn, and Harry Scherer around. And especially, I am grateful to Gabriele Endo and Michaela Schmalstieg for being there whenever I need help at administrative and bureaucratic issues. And special thanks go to our computer experts: Beate Beschke, Lothar Demel, Rolf Merker and Hajo Horn for having always time for my computer-related questions. I also want to thank Svea Dettmer and Birgit Gläser for their help at organizational matters.

Many thanks go to fellow graduate students and my colleagues: Patricia, Julia, Georg, Ulrike, Theresa and Viky, not only for their friendship, but also for their moral support and making the life in the lab fun and endurable.

I am especially lucky for having Patricia in my life as a close and real friend, with whom I could share not only the working space, but also the “real life” outside the lab.

And last but not least, I should mention my deepest gratitude to my closest friend Derya. We can be miles apart, but this could and will never stop us from being there whenever one needs the other. And I should also mention my special thanks to Cansu, Ramazan, Anil, Esra, Pinar and Tolga for being my small Turkish family here in Germany and making these 6 years of my life unforgettable and precious.

Above all, I am indebted from the depth of my heart to my family: my parents, my brother and my “sister” for their immense support, love, tolerance, and respect in my life. I owe every success in my life to my parents: I could not have done any of it without them.

## Table of Contents

<b><i>I. List of Figures</i></b>	<b><i>XI</i></b>
<b>1. Abstract</b>	<b>1</b>
<b>2. Introduction</b>	<b>3</b>
2.1 Oligodendrocytes and myelin	4
2.2 Axonal degeneration in the absence of myelin proteins	7
2.3 Changes in the protein composition of Plp <sup>null</sup> myelin	10
2.4 Class III sirtuin histone deacetylases	11
2.5 SIRT2: cytosolic NAD <sup>+</sup> -dependent deacetylase	14
2.6 SIRT2: an oligodendroglial protein	16
2.7 SIRT2 and oligodendroglial cell differentiation	18
2.8 SIRT2 and neuronal motility	18
2.9 SIRT2 and neurodegeneration	19
2.10 Protein acetylation and novel targets of SIRT2	19
2.11 Aim of the project	20
<b>3. Material and Methods</b>	<b>22</b>
3.1 Material	23
3.1.1 Kits and assays	23
3.1.2 General laboratory equipments	23
3.1.3 Instruments	23
3.1.4 Chemicals	23
3.1.5 Buffers and solutions	24
3.1.5.1 Molecular biology buffers and solutions	24
3.1.5.2 Protein biochemistry buffers and solutions	24
3.1.5.3 SDS PAGE and Western blotting buffers and solutions	25
3.1.5.4 Polyacrylamide gel staining solutions	29
3.1.5.5 Thin layer chromatography solutions	30
3.1.5.6 Immunohistochemistry buffers and solutions	30
3.1.5.7 Histology staining solutions	32
3.1.5.8 Epon embedding and EM contrasting solutions	34
3.1.6 DNA/protein markers and loading dyes	34
3.1.7 Oligonucleotides	34
3.1.7.1 Genotyping primers	34
3.1.7.2 Quantitative real time PCR primers	35
3.1.7.3 Additional primers	37
3.1.8 Enzymes and reaction buffers	37
3.1.9 Antibodies and recombinant peptides/proteins	38

3.1.10 Additional materials and reagents	40
3.1.11 Animals and mouse lines	40
3.1.12 Softwares	40
3.2 Methods	42
3.2.1 DNA isolation and purification	42
3.2.1.1 Preparation of murine genomic DNA	42
3.2.1.2 DNA extraction from agarose gels	42
3.2.2 DNA modification and analysis	42
3.2.2.1 DNA amplification by polymerase chain reaction (PCR)	42
3.2.2.2 Agarose gel electrophoresis for the size separation of DNA fragments	43
3.2.2.3 Determination of DNA/RNA concentrations	44
3.2.2.4 DNA sequencing	44
3.2.2.5 Primer designing	44
3.2.3 RNA isolation and analysis	45
3.2.3.1 Small scale RNA isolation	45
3.2.3.2 First strand cDNA synthesis	45
3.2.3.3 Quantitative real time PCR (qRT-PCR)	46
3.2.4 Protein biochemistry methods	46
3.2.4.1 Preparation of protein lysates from animal tissue	46
3.2.4.2 Enrichment of CNS myelin	47
3.2.4.3 Protein concentration measurement by Lowry assay	47
3.2.4.4 Preparation of the protein samples for SDS-polyacrylamide gel electrophoresis (PAGE)	48
3.2.4.5 SDS-polyacrylamide gel electrophoresis (PAGE)	48
3.2.4.6 Silver staining	49
3.2.4.7 Western blotting	49
3.2.4.8 Coomassie staining	50
3.2.4.9 Immunodetection of blotted proteins	50
3.2.4.10 Stripping of PVDF membranes	51
3.2.4.11 Densitometric evaluation of band intensity	51
3.2.5 Thin layer chromatography of lipids	51
3.2.6 Histology, immunohistochemistry and electron microscopy	52
3.2.6.1 Perfusion and fixation of mouse tissue for histology	52
3.2.6.2 Procedures for tissue embedding	52
3.2.6.3 Tissue sectioning	54
3.2.6.4 Haematoxylin-Eosin (HE) staining	54
3.2.6.5 DAB-based immunodetection on the paraffin sections	55
3.2.6.6 Automated staining using the Ventana Discovery® XT System	56
3.2.6.7 Methylene blue-Azur II staining of semithin sections	56



3.2.6.8 Tissue contrasting for electron microscopy	56
3.2.6.9 Freeze substitution of high-pressure frozen samples	57
3.2.7 Imaging	57
3.2.8 Morphometry and quantifications	57
3.2.9 Animal maintenance, handling and experiments	57
3.2.9.1 Genotyping of the mouse mutants	57
3.2.9.2 Rotarod test	59
3.2.9.3 Grid-running	59
3.2.9.4 Acrylamide treatment	59
3.2.9.5 EAE induction	59
<b>4. Results</b>	<b>61</b>
4.1 Localization of SIRT2 protein in the central nervous system	62
4.2 Analysis of the <i>Sirt2</i> <sup>null</sup> mice	63
4.2.1 <i>Sirt2</i> <sup>null</sup> mice	63
4.2.2 Myelination in the absence of SIRT2	66
4.2.3 Acetylation status of the proteins in the absence of SIRT2	75
4.2.4 Expression levels of other sirtuins and cytoplasmic HDACs in the absence of SIRT2	77
4.2.5 Analysis of CNS axonopathy and inflammation in the absence of SIRT2	80
4.3 Double mutant mice lacking the expression of <i>Sirt2</i> and <i>Cnp</i>	83
4.3.1 SIRT2 protein level in the <i>Cnp</i> <sup>null</sup> myelin	83
4.3.2 Premature lethality in <i>Sirt2</i> <sup>null*</sup> <i>Cnp</i> <sup>null</sup> mice	84
4.3.3 Enhanced axonal degeneration in <i>Sirt2</i> <sup>null*</sup> <i>Cnp</i> <sup>null</sup> mice	84
4.3.4 Enhanced inflammation and astrogliosis in <i>Sirt2</i> <sup>null*</sup> <i>Cnp</i> <sup>null</sup> mice	86
4.4 EAE induction in <i>Sirt2</i> <sup>null</sup> mice	88
4.5 Acrylamide treatment in <i>Sirt2</i> <sup>null</sup> mice to induce axonal stress	89
4.6 5XFAD mice with a decreased dose of <i>Sirt2</i> gene	92
<b>5. Discussion</b>	<b>94</b>
5.1 SIRT2 is an oligodendroglial protein	95
5.2 <i>Sirt2</i> <sup>null</sup> mice: a tool to study the effects of the lack of a myelin-associated deacetylase	95
5.3 SIRT2 is dispensable for myelin formation and maintenance	96
5.4 Potential substrates of SIRT2 in the central nervous system	99
5.5 Compensation of the absence of SIRT2 by other sirtuins and cytoplasmic histone deacetylases	100
5.6 Absence of CNS axonopathy and inflammation in <i>Sirt2</i> <sup>null</sup> mice	101
5.7 Modifying axonal degeneration by SIRT2	102
<b>6. References</b>	<b>106</b>
<b>7. Appendices</b>	<b>124</b>
<b>Appendix 1: Abbreviations</b>	<b>125</b>
<b>Appendix 2: Instruments</b>	<b>130</b>

## Table of Contents

---

<i>Appendix 3: Chemicals</i>	<b>132</b>
<i>Appendix 4: Curriculum vitae</i>	<b>134</b>

## List of Figures

<b>Figure 1.</b> Myelin ultrastructure	4
<b>Figure 2.</b> Architecture of the compact myelin sheath	5
<b>Figure 3.</b> Myelinated axon in the CNS	6
<b>Figure 4.</b> CNS myelin compartments	6
<b>Figure 5.</b> Structure of PLP/DM20 in myelin membranes	8
<b>Figure 6.</b> Ultrastructure of PLP-deficient CNS	9
<b>Figure 7.</b> Ultrastructure of CNP-deficient CNS	10
<b>Figure 8.</b> The network of SIRT2 regulation	16
<b>Figure 9.</b> SIRT2 is enriched in white matter tracts of the brain	62
<b>Figure 10.</b> Genotyping the <i>Sirt2</i> <sup>null</sup> mice	64
<b>Figure 11.</b> Absence of SIRT2 protein	65
<b>Figure 12.</b> Normal myelination in CNS of <i>Sirt2</i> <sup>null</sup> mice	66
<b>Figure 13.</b> Normal myelination in PNS of <i>Sirt2</i> <sup>null</sup> mice	67
<b>Figure 14.</b> Quantification of myelin thickness and axon diameter in CNS of <i>Sirt2</i> <sup>null</sup> mice	68
<b>Figure 15.</b> Quantification of myelin thickness and axon diameter in PNS of <i>Sirt2</i> <sup>null</sup> mice	69
<b>Figure 16.</b> Levels of myelin proteins in <i>Sirt2</i> <sup>null</sup> mice	71
<b>Figure 17.</b> Quantification of myelin proteins in developing CNS of <i>Sirt2</i> <sup>null</sup> mice	72
<b>Figure 18.</b> A closer look into peripheral myelination in <i>Sirt2</i> <sup>null</sup> mice at postnatal day 5	72
<b>Figure 19.</b> Analysis of the myelin lipids and expression of the genes regulating sterol biosynthesis in the absence of SIRT2	74
<b>Figure 20.</b> Acetylation levels of myelin proteins and $\alpha$ -tubulin in the absence of SIRT2	76
<b>Figure 21.</b> Acetylation levels of $\alpha$ -tubulin in the developing CNS of <i>Sirt2</i> <sup>null</sup> mice absence of SIRT2	77
<b>Figure 22.</b> Relative mRNA abundance of other sirtuins in <i>Sirt2</i> <sup>null</sup> mice	78
<b>Figure 23.</b> Relative mRNA abundance of cytoplasmic histone deacetylases (HDACs) in <i>Sirt2</i> <sup>null</sup> mice	79
<b>Figure 24.</b> <i>Sirt2</i> <sup>null</sup> mice showed neither axonal degeneration nor microglial activation in the brain	81
<b>Figure 25.</b> Motor performance and motoric behavior in <i>Sirt2</i> <sup>null</sup> mice	82
<b>Figure 26.</b> SIRT2 abundance in <i>Cnp</i> <sup>null</sup> myelin	83
<b>Figure 27.</b> Premature lethality in <i>Sirt2</i> <sup>null</sup> * <i>Cnp</i> <sup>null</sup> mice	84
<b>Figure 28.</b> <i>Sirt2</i> <sup>null</sup> * <i>Cnp</i> <sup>null</sup> mice showed enhanced axonal degeneration in comparison to <i>Cnp</i> <sup>null</sup> mice	86
<b>Figure 29.</b> <i>Sirt2</i> <sup>null</sup> * <i>Cnp</i> <sup>null</sup> mice showed enhanced neuroinflammation and astrogliosis in comparison to <i>Cnp</i> <sup>null</sup> mice	87
<b>Figure 30.</b> No change in the clinical course of EAE in <i>Sirt2</i> <sup>null</sup> mice	88
<b>Figure 31.</b> The effects of different doses of acrylamide on wild type mice	90
<b>Figure 32.</b> Monitoring the motoric behavior of acrylamide-intoxicated <i>Sirt2</i> <sup>null</sup> mice	91
<b>Figure 33.</b> Lifespan of <i>Sirt2</i> heterozygous mutant mice carrying the 5XFAD transgene	93

**1. Abstract**

In the central nervous system (CNS), oligodendrocytes (OLs) ensheath axons with lipid-rich myelin membranes that provide an electrical insulation and are essential for fast nerve impulse transmission. However, myelination is not the only function of OLs, which is important for neurons. The axo-glia interaction is vital for the long-term survival of the axons, independently from myelination. The novel role of OLs in supporting axonal integrity was best exemplified by the findings on mutant mice with the genetic deletion of two structural proteins of the CNS myelin, namely proteolipid protein (PLP) and 2'-3'-cyclic nucleotide phosphodiesterase (CNP1). Lack of these proteins led to an axonopathy in the CNS, despite the absence of major myelin abnormalities. Gel-based proteome analysis performed to explore possible secondary molecular alterations in Plp<sup>null</sup> myelin revealed that Sirtuin 2 (SIRT2) was the only protein, other than PLP and its splice isoform DM20, to be virtually absent. These findings suggested that the axonal pathology observed in Plp<sup>null</sup> mice may be at least partially due to the lack of SIRT2.

SIRT2 is one of the mammalian orthologs of the silent information regulator 2 (Sir2) protein, which is an nicotinamide adenine dinucleotide (NAD<sup>+</sup>)-dependent histone deacetylase and is involved in many cellular mechanisms in yeast and worms. SIRT2 has a cytoplasmic distribution, to colocalize with microtubule network and to deacetylate  $\alpha$ -tubulin at the lysine-40 residue. SIRT2 is highly expressed in the brain, specifically in oligodendrocytes at early stages of myelination and is incorporated into myelin in presence of PLP/DM20, being localized at the inner and outer loops and the paranodes of the CNS myelin.

To identify the role of SIRT2 in the axon protection, we analyzed mice lacking Sirt2 expression. Surprisingly, we found that SIRT2 is dispensable for myelin formation and maintenance, as axons of all calibers in both the central and peripheral nervous system were normally myelinated in the Sirt2<sup>null</sup> mice. In addition, these mice showed no apparent CNS axonopathy suggesting that SIRT2 may not be the only key player of the yet unexplained axonoprotective function of PLP.

To test the hypothesis that SIRT2 serves as an NAD<sup>+</sup>-dependent regulator of glial neuroprotection, we did not only use pharmacological approaches to induce axonal stress, but we also generated double mutant mice expressing neuronal and glial disease genes. For example, we found that the axonal degeneration caused by the lack of Cnp1 was dramatically enhanced by the additional absence of Sirt2. As a result, the Sirt2\*Cnp1 double null mutant mice displayed increased inflammation, and a significantly reduced lifespan. These findings support the hypothesis that SIRT2 is a myelin-associated sensor for axonal stress that is essential for long-term axonal survival.

**2. Introduction**

## 2.1 Oligodendrocytes and myelin

The neurons and their glial support cells are building up the mammalian nervous systems. The evolution of the mammalian nervous system has led to an increase in the numbers of the glial cells far beyond that of the neuronal. There are three major glial cell types in the central nervous system (CNS): oligodendrocytes (OLs), astrocytes and microglia.

The unique function of OLs is to wrap axons with a special structure called “myelin”. Myelin is assembled by the membrane processes extending from the OLs in the CNS. In the peripheral nervous system (PNS), Schwann cells (SCs) are the myelin-forming glial cells. OLs can myelinate up to 60 axonal segments at a time (Sherman and Brophy, 2005), whereas SCs are restricted to a single axon. These cells wrap the extensions of their plasma membranes spirally around the axon. The withdrawal of the majority of the cytoplasm is followed by the compaction of these membrane bilayers to finalize the formation of the myelin sheath. This sheath is clearly visible as a tightly packed membrane stack on electron micrographs (Figure 1). Upon the compaction of the cytoplasm, a major dense line (MDL) is formed. This electron dense layer is rich in proteins, and its main component is the myelin basic protein (MBP). The MDL alternates with two intraperiod lines (IPL). The IPL is thought to result from the compaction of the extracellular proteins (peripheral membrane proteins and extracellular parts of transmembrane proteins) (Figure 1 and 2).

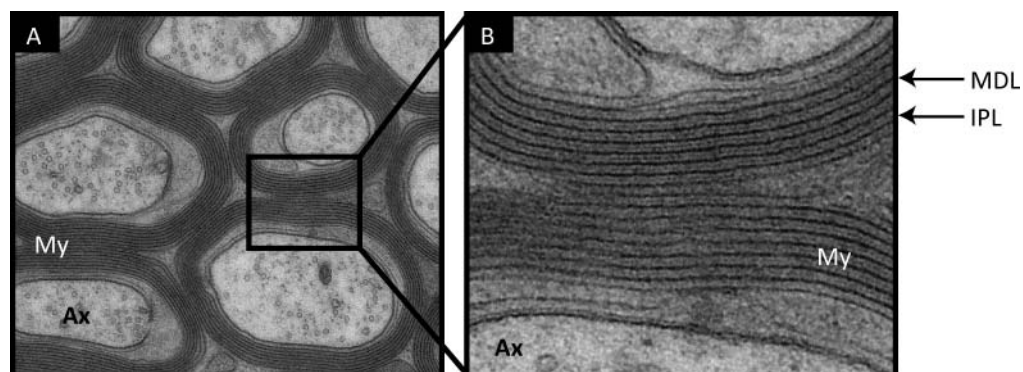


**Figure 1. Myelin ultrastructure**

(A) An electron micrograph of myelinated nerve fibers (Ax) within the optic nerve. (B) Higher magnification of the boxed area showing 2 opposing myelin sheaths, visible as tightly packed membrane stacks (My). The electron dense layer of myelin is called the major dense line (MDL), which results from the compaction of the cytoplasm of OLs. The compaction of the opposing outer leaflets form the intraperiod lines (IPL), which are interseparating the MDL (courtesy to Dr. Wiebke Möbius, EM Facility, Max-Planck-Institute of Experimental Medicine, Göttingen, Germany).

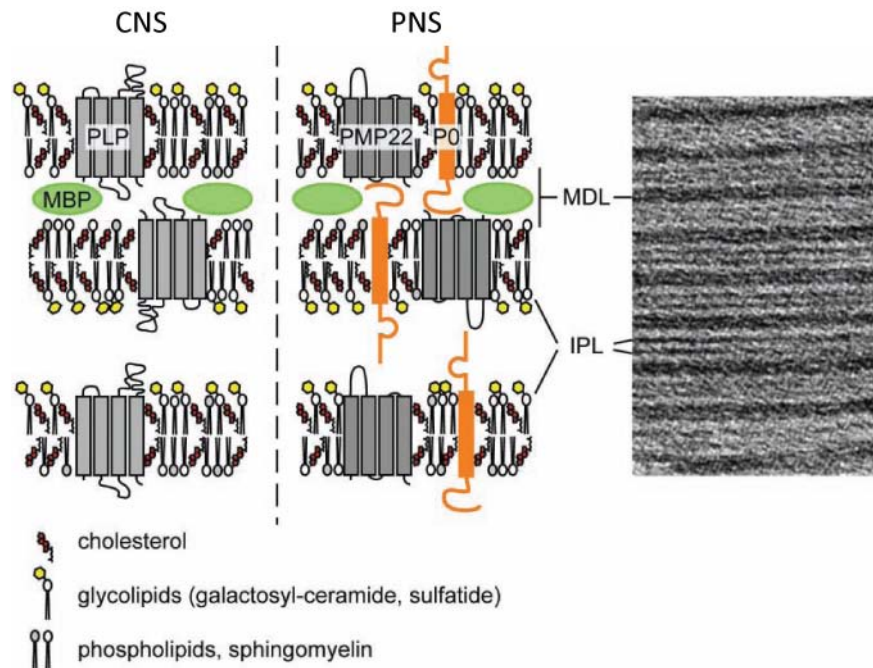


**Figure 2. Architecture of the compact myelin sheath**

Schematic representation of the protein and lipid composition of the compact myelin in the CNS and PNS. Major CNS myelin proteins: proteolipid protein (PLP), myelin basic protein (MBP) and major PNS myelin proteins: peripheral myelin protein 22 (PMP22) and myelin protein zero (P0) are depicted. Myelin membranes are rich in cholesterol and glycolipids. Electron micrograph at high magnification shows the protein-rich major dense line (MDL) and the intraperiod lines (IPL) interseperating MDLs (from Saher *et al.*, 2011).

Myelin serves as an electrical insulation around the axons, which enables rapid transmission of the nerve impulses by decreasing the capacitance and increasing the transverse resistance of the axonal membranes. Regions of axons myelinated at intervals are called the internodes (Figure 3). The nodes of Ranvier are the unmyelinated gaps regularly interrupting myelin, where the molecular machinery required for the propagation of action potentials is concentrated. Voltage-gated sodium ( $\text{Na}^+$ ) channels are confined to these unmyelinated regions (Pedraza *et al.*, 2001). These short unmyelinated segments of the axon allow the saltatory nerve impulse propagation (Hartline and Colman, 2007), as action potentials and ion currents are concentrated at defined and restricted regions on the axon surface. Because of that, the energy which neurons need to consume to restore the ion gradients is considered dramatically reduced (Poliak and Peles, 2003).



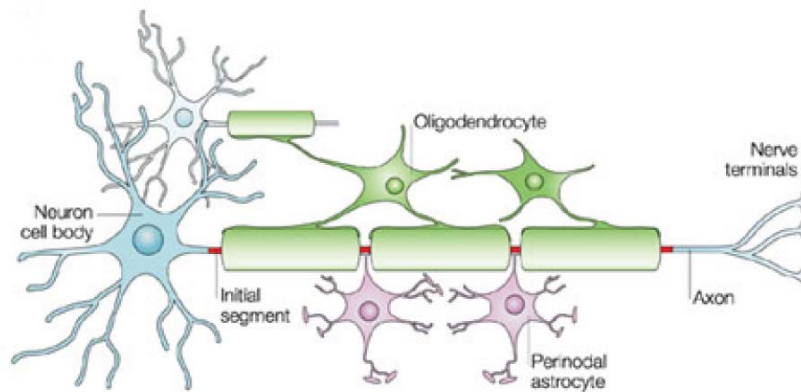


**Figure 3. Myelinated axon in the CNS**

In the CNS, OLs myelinate more than one axonal segment. Axons are myelinated at intervals. Myelinated regions are called the internodes. The nodes of Ranvier are the unmyelinated gaps interrupting myelin. The nodes are contacted by processes from perinodal astrocytes (from Poliak and Peles, 2003).

The region flanking both sides of the nodes is called the paranode, where the myelin loops contact the axonal membrane via septate-like junctions (Figure 4). The adjacent domains like the juxtaparanodal regions and the internodes extend directly underneath the compact myelin (Poliak and Peles, 2003).

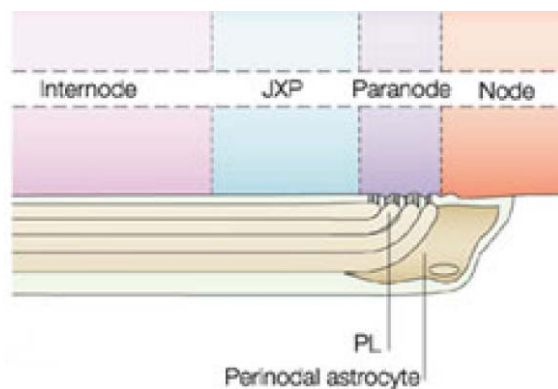


**Figure 4. CNS myelin compartments**

Schematic representation of a longitudinal section of a myelinated nerve fibre around the node of Ranvier. Perinodal astrocyte processes contact the node. At the paranodes, myelin loops (paranodal loops-PL) contact the axon via septate-like junctions. Adjacent to the paranode, the juxtaparanodal region (JXP) commences beneath the compact myelin sheath and is followed by the internode extension (from Poliak and Peles, 2003).

Myelin has a particularly unique structure and molecular composition. Myelin is a lipid-rich membrane, with 70% of the dry myelin weight composed of lipids (Norton, 1984). Glycosphingolipids and cholesterol constitute the majority of the lipid composition (Figure 2). Cholesterol plays a critical role in myelin biogenesis (Saher *et al.*, 2005). On the other hand, the protein composition of myelin is also as complex as that of the other membranes. The prominent diversity of myelin proteins has been revealed by several recent studies based on proteomic analysis (Taylor *et al.*, 2004; Vanrobaeys *et al.*, 2005; Roth *et al.*, 2006; Werner *et al.*, 2007; Dhaunchak *et al.*, 2010). Some of the proteins show a particular high abundance (Jahn *et al.*, 2009). Only few specific myelin proteins have been shown to be related to ultrastructural features of compacted myelin. For example, structural proteins of myelin as the cytoplasmic myelin basic protein (MBP) and the transmembrane proteolipid proteins (PLP/DM20) are required to be highly expressed for the compaction of myelin. According to the most recent mass spectrometry-based quantifications, 65% of the myelin proteome is constituted by previously unknown or novel myelin proteins. MBP and PLP, which were thought to compose 30-40% of the whole myelin proteome, make up to 8 and 17% of the total repertoire, respectively (Jahn *et al.*, 2009). The different myelin domains (compact and internodal myelin, juxtaparanodal and paranodal regions) possess distinct protein compositions (Nave, 2010).

Myelin is essential for proper neuronal functioning, and demyelination of nerve fibres leads to conduction block, possibly convulsions and paralysis. However, providing axons with myelin and thereby enabling the rapid signal transmission is not the sole function of OLs. Also, the interaction between glia and neurons is essential for proper functioning of the neurons, but the molecular mechanisms underlying this communication are not yet fully understood. However, there is increasing evidence indicating that the long-term survival of the axons depends on their interaction with glia, independently from their myelination. The oligodendroglial support of the axonal integrity is best demonstrated by the mouse mutants lacking the expression of major myelin proteins, which will be explained in the following chapters.

### **2.2 Axonal degeneration in the absence of myelin proteins**

The X-linked *Plp1* gene encodes PLP (and its splice isoform DM20), which is the major membrane proteolipid of the CNS myelin (Nave *et al.*, 1987) (Figure 5). Spiral membrane wrapping or myelin compaction are thought to require neither of these two proteolipid proteins; however, they are needed for stabilization of the ultrastructure of the CNS myelin by forming the IPL (Klugmann *et al.*, 1997). Additionally, many point mutations in the human and mouse gene cause

oligodendrocyte death, dysmyelination and eventually significant mortality in Pelizaeus-Merzbacher disease (PMD) and related animal models, due to cytotoxic effects of the misfolded PLP/DM20 (Werner *et al.*, 1998).

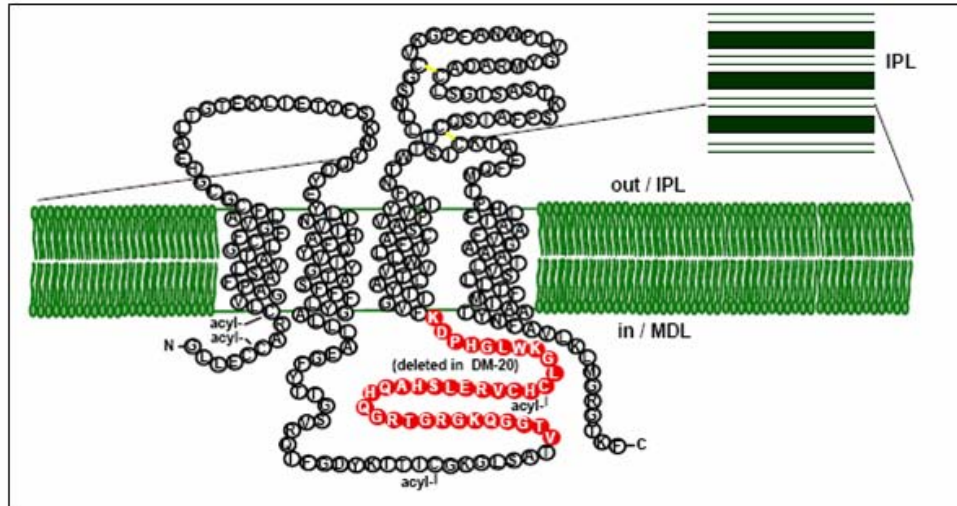


**Figure 5. Structure of PLP/DM20 in myelin membranes**

PLP is a four-helix-span membrane protein with a molecular mass of 30 kDa. A short 35 amino acid stretch in the intracellular loop is lacking in its splice isoform DM20 (shown as red-filled circles).

Mutant mice that lack PLP/DM20 exhibit a normal development without any dysmyelinating phenotype. Their OLs are morphologically normal and capable of assembling compacted myelin with appropriate thickness and of myelinating CNS axons of all diameters (Klugmann *et al.*, 1997) (Figure 6A). At the ultra-structural level, there are some minor differences such as a condensed electron-dense IPL of myelin, correlating with its reduced physical stability. Despite these differences, PLP-deficient myelin enables normal nerve transmission. However, from the age of 1.5-2 months on, axonal swellings and degeneration start to be developed in all areas of the CNS of these animals (Griffiths *et al.*, 1998b) (Figure 6B and C), and small-diameter nerve fibers, which are myelinated, are predominantly affected. Adult *Plp<sup>null</sup>* mice become ataxic and develop hind limb paralysis. This is caused by the impaired fast axonal transport, followed by length-dependent axonal loss (Edgar *et al.*, 2004). Similarly, human spastic paraplegia type 2 (SPG-2) patients with a null mutation in the *Plp* gene develop an axonopathy in the CNS without known myelin abnormalities (Inoue, 2005).

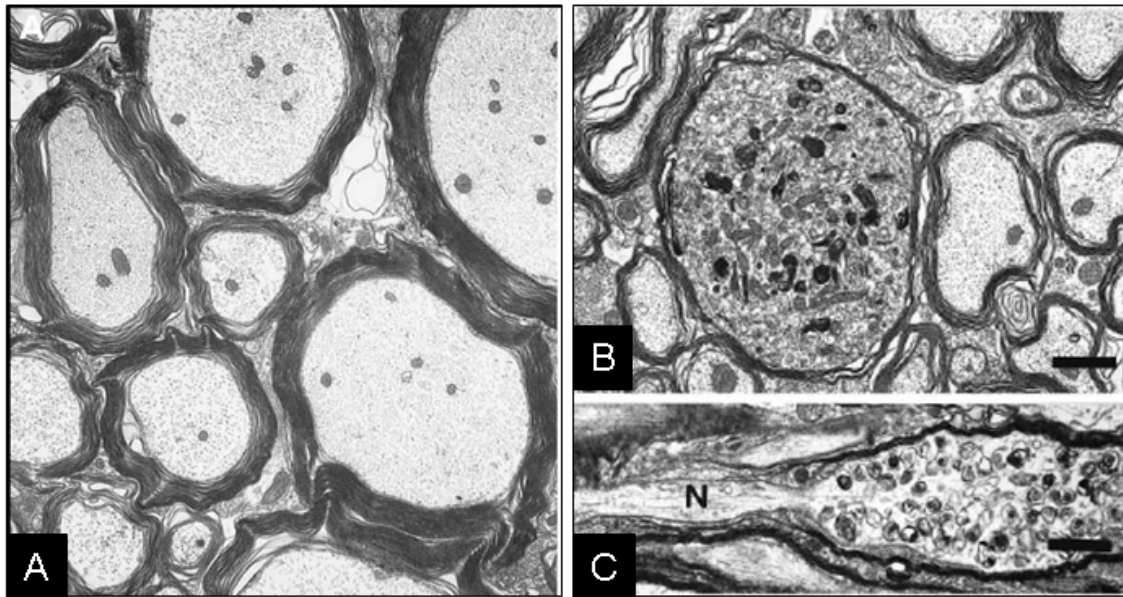


**Figure 6. Ultrastructure of the PLP-deficient CNS**

(A) Electron micrograph of the spinal cord from an adult  $Plp^{null}$  mouse. A properly compacted myelin sheath of an appropriate thickness surrounds both large- and small-diameter axons (adapted from Klugmann *et al.*, 1997). (B) Axonal spheroids in a cross-section of the spinal cord and (C) a longitudinal section of the optic nerve from  $Plp^{null}$  mouse at the age of 4 months (from Griffiths *et al.*, 1998b). Scale bar: 1  $\mu$ m. N: node of Ranvier.

Another example for uncoupling of two crucial functions of oligodendrocytes, myelination and axonal preservation, is the mouse mutant that lacks the 2', 3'-cyclic nucleotide phosphodiesterase (CNP). CNP constitutes 4% of the protein repertoire of the CNS myelin. This enzyme is widely used as a marker for myelin-forming glial cells (Vogel *et al.*, 1988; Sprinkle, 1989; Tsukada and Kurihara, 1992). CNP can be detected in OL lineage cells in the developing brain (Yu *et al.*, 1994) and mature OLs maintain its expression throughout their life. Overexpression of CNP in transgenic mice results in premature differentiation of OLs and deficits in myelin compaction (Gravel *et al.*, 1996; Yin *et al.*, 1997). On the other hand, mice which lack the expression of CNP develop axonal swellings and neurodegeneration throughout the brain, but are able to form compacted myelin with a normal ultrastructure, periodicity, and physical stability (Figure 7) (Lappe-Siefke *et al.*, 2003). This axonal degeneration starts very early in the postnatal life (Edgar *et al.*, 2009). When CNP-deficient OLs are transplanted into *shiverer* mice, which are normally dysmyelinated, these OLs are able to form compact myelin, but still induce the same degenerative phenotype (Edgar *et al.*, 2009).

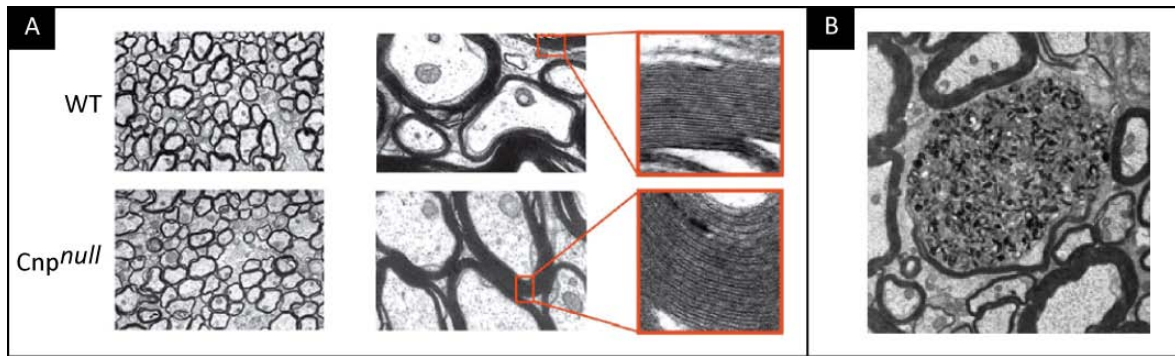


**Figure 7. Ultrastructure of the CNP-deficient CNS**

(A) Electron micrographs showing cross-sections of spinal cord from 2.5 month-old wild type (WT) and  $Cnp^{null}$  mice. Mutant mice can form normal compact myelin with regular spacing and periodicity. (B) Electron micrographs of spinal cord sections from 14 month-old  $Cnp^{null}$  mice showing axonal swellings containing membranous organelles and multivesicular bodies (from Lappe-Siefke *et al.*, 2003).

Altogether, these two mouse mutants,  $Plp^{null}$  and  $Cnp^{null}$  mice, serve as best examples for demonstrating the important role of OLs in axonal preservation, independently from myelination itself.

### 2.3 Changes in the protein composition of $Plp^{null}$ myelin

The genetic loss of a single myelin protein appears not sufficient to completely explain the progression of the phenotype in the well-myelinated  $Plp^{null}$  animals towards a degenerative state. Thereby, the question arises whether there are secondary molecular changes in  $Plp^{null}$  myelin contributing to the disease phenotype. To identify any alterations in the protein composition of the  $Plp^{null}$  myelin, which occur prior to the onset of axonal degeneration, a differential myelin proteome analysis had been performed using two-dimensional differential fluorescence intensity gel electrophoresis (2D-DIGE) (Unlu *et al.*, 1997) and protein identification by mass spectrometry (MS) (Werner *et al.*, 2007). A reduction (by about 40%) in abundance of three proteins of the septin family in the mutant myelin was revealed by this study. Sirtuin 2 (SIRT2), a protein deacetylase was the only undetectable protein in the mutant myelin. It has been found to be virtually absent already in 15 days old mutant mice, indicating that this molecular impairment precedes the axonal degeneration. The mRNA level of SIRT2 remains unchanged, but the protein fails to be incorporated into myelin in the absence of PLP/DM20. By immunolabeling, it was also shown that in the white matter of  $Plp^{null}$  mice, SIRT2 is retained in the cell bodies of oligodendrocytes.

## 2.4 Class III sirtuin histone deacetylases

Histone deacetylases (HDACs) and histone acetyltransferases (HAT), by two opposing enzymatic activities, control the level of acetylation of histones and other nonhistone proteins, which are acetylated at their lysine residues (Polevoda and Sherman, 2002). The deacetylation of histones leads to a tighter chromatin structure and thereby the transcription is repressed (Cheung *et al.*, 2000; Wu and Grunstein, 2000). Mammalian histone deacetylases are grouped into four classes based on their homology to yeast transcriptional repressors: Class I, II and IV non-sirtuin histone deacetylases, which are homologs of RPD3, HDA1 and HDAC11-related enzymes, respectively. Class III sirtuin histone deacetylases are homologs of yeast silent information regulator 2 (Sir2) (Denu, 2005). This class of deacetylases were specified as atypical HDACs due to their dependence on NAD<sup>+</sup> as an enzymatic cofactor (Blander and Guarente, 2004; Michan and Sinclair, 2007; Taylor *et al.*, 2008).

The gene family encoding the silent information regulator (SIR) proteins are conserved from archaeobacteria to eukaryotes (Frye, 2000). They play critical roles in transcriptional silencing at a number of loci, including the mating-type loci, telomeres, and ribosomal gene clusters (Gasser and Cockel, 2001).

The silent information regulator 2 (Sir2) protein is an NAD<sup>+</sup>-dependent histone deacetylase, which hydrolyzes one molecule of NAD<sup>+</sup> for every lysine residue that is deacetylated (Imai *et al.*, 2000). This sirtuin-mediated deacetylation results in the formation of O-acetyl-ADP-ribose (OAADPr) as a by-product (Figure 8) (Landry *et al.*, 2000; Sauve *et al.*, 2001). Additionally, many sirtuins carry a mono-ADP-ribosyl transferase activity with not well investigated biological significance (Michan and Sinclair, 2007).

In addition to transcriptional silencing, the yeast Sir2 protein and its mammalian homologs are involved in DNA repair and recombination, genome maintenance, cell-cycle regulation, microtubule organization, metabolism, longevity and in the regulation of aging. An increase in Sir2 activity extends the lifespan in yeast, worms and flies (Kaeberlein *et al.*, 1999; Rogina and Helfand, 2004). The control of life span is highly dependent on the metabolic state of the organism, because of the NAD<sup>+</sup> dependency of the Sir2 activity.

There are seven human orthologs of Sir2 proteins which are named sirtuins (SIRTs), from SIRT1 to SIRT7 (Frye, 1999 and 2000). They share a conserved catalytic core domain comprised of

approximately 275 aminoacids (Milne and Denu, 2008). Each member has distinct amino- and carboxy-terminal protein sequences flanking the conserved central catalytic domain, which most likely encode interaction motifs for partner proteins and cellular localization signals.

The founding member of this family is SIRT1, which is the most studied one among the seven sirtuins. It bears the highest homology to the yeast Sir2. SIRT1 has a nuclear localization, but it can shuttle between the nucleus and the cytoplasm (Blander and Guarente, 2004; Michan and Sinclair, 2007; Taylor *et al.*, 2008). It deacetylates a number of histones: histone H1, H3 and H4 (Imai *et al.*, 2000; Vaquero *et al.*, 2004) and thereby induces the formation of heterochromatin and thus gene repression (Blander and Guarente, 2004; Michan and Sinclair, 2007; Taylor *et al.*, 2008). Additionally, SIRT1 deacetylates components of the core RNA polymerase I transcriptional machinery and the HAT p300/CBP (Bouras *et al.*, 2005), also resulting in the reduction of gene expression (Muth *et al.*, 2001). Human SIRT1 protein binds, deacetylates and reduces the transcriptional activity of p53 (Luo *et al.*, 2001; Vaziri *et al.*, 2001) and the mammalian Forkhead transcription factor, FOXO3A, thereby reducing both forkhead- and p53-dependent apoptosis in response to DNA damage and oxidative stress (Motta *et al.*, 2004). SIRT1 can also increase FOXO3's ability to induce cell cycle arrest and resistance to oxidative stress (Brunet *et al.*, 2004). On the other hand, the application of specific SIRT1 inhibitors induces apoptosis in human cancer cells (Liu *et al.*, 2011). SIRT1 also physically interacts with and deacetylates the RelA/p65 subunit of the nuclear factor 'kappa-light-chain-enhancer' of activated B-cells (NF- $\kappa$ B) at lysine 310, thereby silences its transcription. As a result, cells become more sensitive to TNF $\alpha$ -induced apoptosis, when they are treated with small-molecule agonists increasing SIRT1 activity (Yeung *et al.*, 2004). Recently, it has been shown that the deacetylation of FOXO3 by SIRT1 facilitates its ubiquitination and thereby its subsequent degradation by the proteasome (Wang *et al.*, 2011). SIRT1 is shown to also act as a cell migration stimulator (Zhang *et al.*, 2009).

SIRT1 has been extensively studied in various neurodegeneration models, e.g. amyotrophic lateral sclerosis (ALS), Parkinson's, Huntington's and Alzheimer's disease and Wallerian degeneration models (Araki *et al.*, 2004; Dillin and Kelly, 2007; Outeiro *et al.*, 2008; Tang and Chua, 2008; Taylor *et al.*, 2008). Studies mainly reported SIRT1's neuroprotective effects (Anekonda, 2006; Qin *et al.*, 2006; Kim *et al.*, 2007; Donmez and Guarente, 2010). Wang *et al.* observed that SIRT1 protects neurons from glucose/oxygen deprivation (Wang *et al.*, 2009). It modulates the DNA damage response via deacetylating p53 in cortical neurons (Hasegawa and Yoshikawa, 2008). Additionally, it inhibits NF- $\kappa$ B signaling and thereby protects neurons against microglia-dependent amyloid-beta toxicity (Chen *et al.*, 2005). SIRT1 can also suppress beta-amyloid production by activating

the alpha-secretase gene ADAM10 (Donmez *et al.*, 2010). Moreover, SIRT1 activation protects dopaminergic neurons in midbrain slice cultures from various insults (Okawara *et al.*, 2007), mammalian and nematode neurons from mutant polyglutamine cytotoxicity (Parker *et al.*, 2005) and reduces plaque pathology in a transgenic model of Alzheimer's disease (Karuppagounder *et al.*, 2009). Interestingly, the neuroprotective effects of SIRT1 are independent from its deacetylase activity (Pfister *et al.*, 2008). SIRT1 can also be activated by excess NAD<sup>+</sup> synthesis and this leads to the delay of Wallerian degeneration (Araki *et al.*, 2004).

Much attention was drawn towards SIRT1, because of its beneficial effect for energy metabolism by mediating calorie restriction (Bishop and Guarente, 2007; Michan and Sinclair, 2007; Donmez and Guarente, 2010). SIRT1 protein is induced in liver during fasting, and interacts with and deacetylates the peroxisome proliferator-activated receptor gamma coactivator 1-alpha (PGC-1 $\alpha$ ), thereby controls the gluconeogenic/glycolytic pathways as a response to fasting (Rodgers *et al.*, 2005). Mice which overexpress SIRT1 were reported to be more metabolically active, and have reduced cholesterol levels (Bordone *et al.*, 2007). Milne *et al.* showed that these mice are protected against diabetes-induced obesity (Milne *et al.*, 2007). When SIRT1 is overexpressed, fat mobilization is increased (Picard *et al.*, 2004). Additionally, glucose tolerance is also increased, leading to decreased age-related insulin sensitivity. Resveratrol, which is a red wine component, can increase SIRT1 activity, and that is why the effect of its intake has been studied with the focus on preventing many age-related afflictions (e.g. obesity and diabetes) (Baur *et al.*, 2006; Lagouge *et al.*, 2006; Milne *et al.*, 2007; Bishop and Guarente, 2007; Michan and Sinclair, 2007).

SIRT3 is localized in the nucleus, but is translocated to the mitochondria upon cellular stress (Scher *et al.*, 2007). Its activity is regulated by the proteolytic processing of its N-terminus (Onyango *et al.*, 2002; Schwer *et al.*, 2002). SIRT3 can regulate the expression of various mitochondria-related genes by its two distinct enzymatic capabilities and plays a key role in adaptive thermogenesis in brown adipose tissue (Shi *et al.*, 2005). SIRT4 and SIRT5 are also localized in mitochondria, linked to aging and energy metabolism (Michishita *et al.*, 2005). SIRT4 has been shown to decrease reactive oxygen production and increase ATP production (Haigis *et al.*, 2006). SIRT6 and SIRT7 exhibit a constitutive nuclear localization in association with heterochromatic regions and nucleoli; however, they lack the *in vitro* deacetylation activity of histones or p53 peptides, unlike SIRT1 (Liszt *et al.*, 2005; Michishita *et al.*, 2005). Mice lacking the expression of SIRT6 showed impaired DNA repair associated with signs of premature aging (Mostoslavsky *et al.*, 2006). SIRT7 acts as an activator of RNA polymerase I transcription (Ford *et al.*, 2006).



## 2.5 SIRT2: cytosolic NAD<sup>+</sup>-dependent deacetylase

The mouse Sirt2 gene consists of 16 exons (Mahlknecht *et al.*, 2005) and encodes two splice isoforms: isoform 1 is a protein of 389 amino acids with a molecular weight of 43.2 kDa, whereas isoform 2 is a protein of 352 amino acids with a molecular weight of 39.5 kDa. Isoform 2 lacks the first three exons. A recent study reported a less abundant third, previously uncharacterized SIRT2 isoform (which is a protein with a molecular weight of 35.6 kDa translated from the mRNA lacking the exons 2, 3 and 4), which shows an age-dependent accumulation in murine the CNS (Maxwell *et al.*, 2011).

Human SIRT2 expression predominates in heart, brain, testis, and skeletal muscle tissues (Afshar *et al.*, 1999; Yang *et al.*, 2000). SIRT2 shows a cytoplasmic distribution and colocalizes with the microtubule network (North *et al.*, 2003). Both *in vitro* and *in vivo*, SIRT2 has been reported to deacetylate  $\alpha$ -tubulin at the lysine-40 residue. It co-immunoprecipitates *in vitro* in transiently-transfected human embryonic kidney (HEK 293T) cells with HDAC6, a class II histone deacetylase, which is also known to have tubulin deacetylation activity (Hubbert *et al.*, 2002; Matsuyama *et al.*, 2002; Zhang *et al.*, 2003). They are thought to function together in a complex. Hyperacetylated tubulin is observed after the inhibition of SIRT2 expression via small interference ribonucleic acid (siRNA). Considering the importance of the reversible acetylation of tubulin in the regulation of microtubule stability and function (Piperno *et al.*, 1987), SIRT2 appears important for cell structural integrity.

In addition to microtubule organization, SIRT2 has been identified to be involved in mammalian development by interacting with the homeobox transcription factor HOXA10, both in the cytoplasm and in the nucleus (Bae *et al.*, 2004). Indeed, SIRT2 can shuttle between the nucleus and the cytoplasm during mitosis (North and Verdin, 2007a) and plays an important role in the regulation of the cell cycle (Inoue *et al.*, 2007a). This mitotic regulation by SIRT2 is fine-tuned by cyclin-dependent kinase 1-dependent phosphorylation (North and Verdin, 2007b). During mitosis, SIRT2 preferentially deacetylates histone H4 at its Lys16 residue (Vaquero *et al.*, 2006) and also the SIRT2 protein level increases. Its overexpression results in a marked extension of the mitotic phase (Dryden *et al.*, 2003). Upon the down-regulation of SIRT2, a resistance to microtubule inhibitors is developed and chronic mitotic arrest is prolonged (Inoue *et al.*, 2009). SIRT2 has been reported to be functioning as a mitotic checkpoint protein of the early metaphase, blocking the entry to chromosome condensation in glioma cell lines in response to mitotic stress, thereby preventing chromosomal instability (Inoue *et al.*, 2007b). The function of SIRT2 in cell cycle

regulation is likely triggered upon stress-inducing stimuli on cells, because under normal cell culture conditions, SIRT2 does not affect the cell cycle progression (Pandithage *et al.*, 2008).

The abundance of SIRT2 protein is found to be reduced in gliomas and gastric carcinomas and it inhibits colony formation in glioma cell lines (Hiratsuka *et al.*, 2003). Recently, it has been shown that the inhibition of SIRT2 by specific inhibitors induces apoptosis in human cancer cells (Liu *et al.*, 2011). The downregulation of SIRT2 by siRNA leads to apoptosis in cancer cell lines such as HeLa cells because of a p53 accumulation, but not in normal cells (Li *et al.*, 2011). These findings led to the suggestion of SIRT2 to be a new molecular target for cancer therapy. When SIRT2 is silenced in the neuroendocrine cell line, this led to a decrease in the intracellular ATP levels, suggesting that the decrease in SIRT2 levels can compromise the antioxidation capacity of the cells (Nie *et al.*, 2011).

SIRT2 is the most abundant sirtuin in adipocytes and its expression is downregulated during preadipocyte differentiation and, as a consequence, FOXO1 becomes hyperacetylated (Jing *et al.*, 2007; Wang and Tong, 2008). The interaction between SIRT2 and FOXO1 triggers an insulin-stimulated phosphorylation of FOXO1, thereby regulating its subcellular localization. In their studies, Wang and Tong (2008) concluded that SIRT2 can respond to nutrient deprivation and to energy consumption to maintain homeostasis by favoring lipolysis and preventing adipocyte differentiation. In another study, it was shown that upon stress, FOXO1 dissociates from SIRT2 and becomes acetylated. This led to an altered autophagic process and to cell death (Zhao *et al.*, 2010).

Several studies showed that SIRT2 can be phosphorylated by a number of cyclin-cyclin dependent kinase (CDK) complexes (North and Verdin, 2007b; Pandithage *et al.*, 2008) and its de-phosphorylation is performed by CDC14B (Dryden *et al.*, 2003). Cyclin dependent phosphorylation of SIRT2 inactivates the protein, whereas its de-phosphorylation by CDC14B results in decreased protein levels of SIRT2.

An interesting mutual regulatory relationship exists between SIRT2 and p300/CREB-binding protein (CBP). SIRT2 can be inactivated when acetylated by p300/CBP (Han *et al.*, 2008) and contrarily, p300/CBP can be deacetylated by SIRT2 (Black *et al.*, 2008).

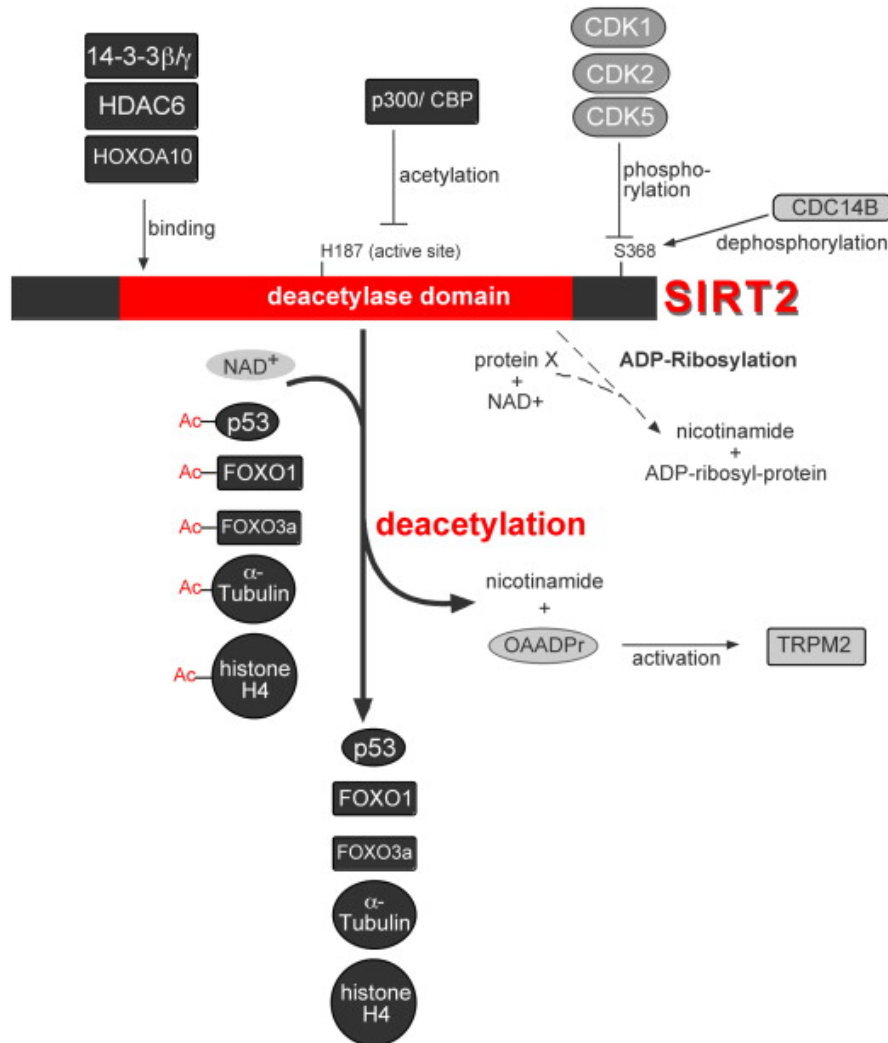


**Figure 8. The network of SIRT2 regulation**

SIRT2 protein has a central domain required for its deacetylase function. This catalytic core domain comprised of approximately 275 aminoacids is conserved among seven mammalian Sirtuins (Milne and Denu, 2008). p53, FOXO, tubulin and histone H4 are known to be deacetylated by SIRT2, whereas 14-3-3, HDAC6 and HOXA10 can bind to and interact with it. SIRT2 itself can be acetylated by the acetyltransferase p300/CBP, and dephosphorylated by CDK and CDC14B (from Harting and Knöll, 2010).

## 2.6 SIRT2: an oligodendroglial protein

Among all sirtuins, the expression of SIRT2 is strongest in the brain. SIRT2 is predominantly localized in the cytoplasm and not in the nucleus of OLs *in vivo* (Li *et al.*, 2007; Michan and Sinclair, 2007; Southwood *et al.*, 2007; Werner *et al.*, 2007) and *in vitro* (Li *et al.*, 2007; Werner *et al.*, 2007). Although it has been shown *in vitro* that HDAC6 and SIRT2 are binding partners (North *et al.*, 2003), this interaction occurs unlikely *in vivo*, as it has been shown that these two proteins are localized into different cell types in the brain (Southwood *et al.*, 2007). Whereas HDAC6 is

expressed in neurons, especially in cerebellar Purkinje cells, SIRT2 is localized specifically in OLs (mainly in pre-myelinating or early myelinating OLs) and SCs. According to Li *et al.* (2007) and Southwood *et al.* (2007), the main substrate for SIRT2 in OLs is the acetylated alpha-tubulin, but not histones, of which the acetylation levels remained mainly unchanged in cells transfected with SIRT2.

Both isoform 1 and 2 of SIRT2 are detected in total brain lysate by immunoblotting; however, only isoform 2 is enriched in myelin equivalent to that of PLP/DM20 and CNP (Werner *et al.*, 2007). The expression of SIRT2 in a heterogeneous OL progenitor population is similar to CNP (Sprinkle, 1989), suggesting that SIRT2 indeed can be a marker for OL differentiation (Williams and Price, 1992). By immunofluorescence labeling, SIRT2 is localized to the inner and outer loops and the paranodes of the CNS myelin sheaths (Southwood *et al.*, 2007).

SIRT2 expression was shown to be developmentally regulated in the CNS (Southwood *et al.*, 2007). It is expressed at very low levels in the developing (embryonic) CNS and its isoform 2 is accumulated in the cortex rather postnatally (Maxwell *et al.*, 2011). The expression profile of the protein indicates that SIRT2 is strongly expressed in OLs from the early stages on of myelinogenesis. Its expression reaches a peak at around postnatal age of 16 days (P16) and then its mRNA level starts to be downregulated. The SIRT2 expression coincides with that of *Nf155*, which is the 155 kDa isoform of neurofascin essential for the paranodal junction formation. Moreover, the peak of SIRT2 mRNA abundance in brain precedes that of PLP, which is a marker of compact myelin formation. These findings have suggested that SIRT2 might have a role in the early myelin sheath formation, which is currently unknown.

Though these studies collectively suggest that SIRT2 is largely expressed by OLs in the brain, several groups have observed SIRT2 expression in olfactory neurons *in vivo* and cultured hippocampal neurons *in vitro* (Yu *et al.*, 2005; Suzuki and Koike, 2007; Taylor *et al.*, 2008; Pandithage *et al.*, 2008). According to the Allen Brain Atlas ([www.brain-map.org](http://www.brain-map.org)), Sirt2 mRNA also localizes to neurons in the adult mouse brain. A recent study reported that the isoform 1 of SIRT2 is expressed in late-stage primary cultures of embryonic cortical neurons, that SIRT2 isoforms can be detected in both fiber tracts and neuronal NeuN-positive cell bodies throughout the cortex and in Purkinje cells, molecular layer neurons and fiber tracts in the cerebellum, and that there is an age-dependent accumulation only of the isoform 3, previously uncharacterized SIRT2 isoform, in the murine CNS (Maxwell *et al.*, 2011).

## 2.7 SIRT2 and oligodendroglial cell differentiation

Histone deacetylases, but not yet histone acetyltransferases, have been shown to govern OL differentiation by epigenetic patterning to facilitate myelin gene expression (Copravay *et al.*, 2009). Transcriptional regulators, like hairy and enhancer of split 5 protein (Hes5) or inhibitor of DNA binding 2 protein (Id2), do drive precursor cells into the neuronal lineage, and the HDAC-mediated deacetylation prevents their activation (Marin-Husstege *et al.*, 2002; He *et al.*, 2007; Shen *et al.*, 2008).

SIRT2 might govern OL differentiation by modifying the cytoskeleton and thereby moderates the alterations in OL morphology during differentiation. During their differentiation, OLs mature as they become multipolar with an extended process arborization. This is enabled by the polarized orientation of microtubules in their processes (Richter-Landsberg, 2000). During the formation of the multiple layers of the myelin sheath with its complex composition of specialized proteins and glycosphingolipids (Larocca and Rodriguez-Gabin, 2002; Sherman and Brophy, 2005; Simons and Trajkovic, 2006), the microtubule network is important for the proper incorporation of myelin proteins and sulfatides into myelin.

According to the available *in vitro* data, SIRT2 appears to be an inhibitor of OL differentiation. When SIRT2 was overexpressed, the complexity of the OL arborisation was decreased (Li *et al.*, 2007). When SIRT2 was knocked down, the expression of myelin basic protein (MBP) was elevated as a sign of accelerated OL differentiation. Also the overexpression of functional SIRT2 inhibited the arborization-inducing effect of co-transfected juxtandin (an OL-specific, differentiation-related protein with an actin-binding domain) (Zhang *et al.*, 2005). However, the recent findings of Ji *et al.* (2011) demonstrated an opposite effect of SIRT2 on OL differentiation. According to their data, the transcription factor Nkx2.2 binds to the Sirt2 promoter via HDAC1, which negatively regulated the expression of SIRT2 in oligodendroglial precursor cell lines. Subsequently, the decrease in the SIRT2 expression levels led to a delay in the differentiation of these precursor cells (Ji *et al.*, 2011).

## 2.8 SIRT2 and neuronal motility

When wild-type SIRT2 or a constitutively active SIRT2 mutant was overexpressed in cultured primary hippocampal neurons, neurite outgrowth was strongly impaired and proper growth cone collapse did not occur (Pandithage *et al.*, 2008). As expected, when SIRT2 was knocked down, the

opposite effect was observed. Considering that neuronal motility strongly depends on cytoskeletal dynamics (Creppe *et al.*, 2009), the modulation of neuronal motility may be explained by SIRT2 acting on the candidate substrates localizing in the cytoplasm.

The acetylation levels of the suggested cytoplasmic target of SIRT2, alpha-tubulin, is altered upon overexpression of SIRT2 in neurons (Pandithage *et al.*, 2008). When microtubules are acetylated, they become more stable and resistant to depolymerizing chemicals (Dent and Gertler, 2003; Fukushima *et al.*, 2009). Acetylated microtubules are rather observed in the axon than in the dendrites of neurons (Witte *et al.*, 2008). Taking together, SIRT2 might contribute to neuronal motility by deacetylating microtubules, and thereby decreasing the levels of stable microtubules. In addition to alpha-tubulin, 14-3-3 proteins are also shown to be interacting with SIRT2 (Figure 8) (Jin *et al.*, 2008; Lynn *et al.*, 2008), thereby deacetylating p53 and decreasing its activity (Jin *et al.*, 2008).

### **2.9 SIRT2 and neurodegeneration**

Previous studies on the effect of microtubule acetylation on the cellular processes, which are pathological features common to diverse neurodegenerative diseases (De Vos *et al.*, 2008; Janke and Kneussel, 2010; Perdiz *et al.*, 2011), have focused mainly on the activity of HDAC6 (Dompierre *et al.*, 2007; Tapia *et al.*, 2010; Chen *et al.*, 2010). However, several recent studies pinpointed the effects of the SIRT2 activity in different neurodegenerative models and, unlike SIRT1, SIRT2 has been reported to promote neurodegeneration. When the SIRT2 function was blocked, a rescue of alpha synuclein toxicity was observed in several Parkinson's disease models (Outeiro *et al.*, 2007) and, contrarily, when it is overexpressed, the resistance of axonal degeneration in the Wallerian mouse model was hindered (Suzuki and Koike, 2007). The neuroprotective effects of the SIRT2 inhibition have been attributed to the decrease in the expression levels of several key genes which are important for sterol biosynthesis (Luthi-Carter *et al.*, 2010).

### **2.10 Protein acetylation and novel targets of SIRT2**

Posttranslational modification of proteins by reversible acetylation at their lysine residues emerges as a mechanism to fine-tune the biological activity of the target proteins and regulates many key cellular processes (Kouzarides, 2000; Plevoda and Sherman, 2002; Haberland *et al.*, 2009; Choudhary *et al.*, 2009). Recently, it has been shown that SIRT2, along with SIRT1, can also deacetylate FOXO3 and thereby facilitate its ubiquitination and subsequent degradation by the

proteasome (Wang *et al.*, 2011). It should be noted that FOXO transcription factors have important roles in many biological pathways, including cancer development. Rothgiesser *et al.* (2010) identified SIRT2 as a deacetylase of the transcription factor p65 and this regulates the expression of specific NF- $\kappa$ B-dependent genes. This suggests an involvement of SIRT2 also in the immune and inflammatory cellular response.

Supporting data are emerging to indicate that protein acetylation can be a key regulatory mechanism for cellular metabolism. The acetylated proteins identified by global screens of lysine acetylation consists mainly of metabolic enzymes (Zhang *et al.*, 2009) and covers a considerable proportion of mitochondrial proteins (Kim *et al.*, 2006; Schwer *et al.*, 2006). Sirtuins were reported to deacetylate and activate the mitochondrial enzyme acetyl-CoA synthetase (Hallows *et al.*, 2006). Recently, Jiang *et al.* (2011) showed in their recent study that the acetylation regulates the stability of the gluconeogenic rate-limiting enzyme phosphoenolpyruvate carboxykinase (PEPCK1), and SIRT2 deacetylated and thus stabilized PEPCK1, at least *in vitro*.

It is also important to note that myelin proteome analysis (Werner *et al.*, 2007) has revealed several acetylated proteins being present in CNS myelin, which are potential novel SIRT2 substrates, based on their changed acetylation patterns in the Plp<sup>null</sup> myelin. The acetylated protein found in the CNS myelin by immunoblotting is  $\alpha$ -tubulin, which is a known *in vitro* substrate of SIRT2. However, it is not observed as hyperacetylated in the PLP<sup>null</sup> myelin. There are several myelin proteins interacting with or regulating microtubules (e.g. CNP, MBP or MOG) (Pirollet *et al.*, 1992; Johns and Bernard, 1999; Hill *et al.*, 2005; Galiano *et al.*, 2006) which have the potential to be targets of SIRT2, and this interaction can modulate microtubule stability in OLS and axon-glia interaction. At least, some myelin proteins, including MBP, MOG are acetylated proteins, but the functional relevance is unclear. Therefore, it is important to pursue future studies to verify myelin proteins as SIRT2 substrates.

### 2.11 Aim of the project

The analysis of Plp<sup>null</sup> and CNP<sup>null</sup> mice has led to the hypothesis that OLS in the CNS serve two independent functions: myelination and axonal preservation. In the absence of either of these myelin proteins, a normal amount of myelin is formed. However, a length-dependent progressive axonal degeneration was observed, likely due to impaired glia-axonal support. The most striking secondary difference in the protein composition of the Plp<sup>null</sup> myelin is the virtual absence of the NAD<sup>+</sup>-dependent tubulin deacetylase, SIRT2.

The aim of this project was to identify the putative role of SIRT2 in the PLP-dependent axon protection and to understand the molecular basis of the oligodendroglial support in axonal integrity by analyzing mice lacking the expression of Sirt2 with respect to myelination and CNS axonopathy. Additionally, pharmacological approaches were used to induce axonal stress, as well as generation of double mutant mice expressing neuronal and glial disease genes, to test the hypothesis that SIRT2 might serve as an NAD<sup>+</sup>-dependent regulator of glial neuroprotection.



**3. Material and Methods**

### 3.1 Material

#### 3.1.1 Kits and assays

- ❖ Bio-Rad DC Protein Assay kit
- ❖ DAB Substrate Kit High Contrast (Zytomed)
- ❖ Dako LSAB2 System-HRP Kit
- ❖ DAB MAP Kit (Ventana Medical Systems Inc.)
- ❖ Enhanced Chemiluminescence (ECL) Western blot detection kit: Western Lightning™ Plus-ECL, Enhanced luminol reagent plus, Perkin Elmer Life Sciences, Inc.
- ❖ QIAquick Gel Extraction Kit, QIAGEN
- ❖ RNeasy Mini Prep Kit, QIAGEN

#### 3.1.2 General laboratory equipments

The following laboratory equipments were used during this study: microcentrifuge tubes from Eppendorf, 15- and 50 ml conical bottom Falcon tubes from BD Biosciences, 15- and 50 ml brown conical bottom tubes (CELLSTAR) from Greiner, pipetmans from Gilson, tips from MolecularBioProducts, Eppendorf or Gilson, multichannel pipettes from BRAND, multipipettes from Eppendorf, glassware from Schott Duran, pasteur pipettes from WU Mainz, glass pipettes from Hirschmann (EM Techcolor, Germany), ultracentrifuge tubes from Beckman, dissection equipments from KLS MARTIN Group, MicroAmp Fast Optical 96-well plates for qRT-PCR from AB Applied Biosystems, 96-well PCR plates from Thermo Scientific, cell scrapers from Nunc (179707), 96-well plates and cell culture dishes from Greiner or Falcon, infusion sets from Braun, syringes and needles from BD, scintillation vials from Perkin Elmer, coverslips from MenzelGläser, microscope slides from Marienfeld or ThermoScientific (SuperFrost Plus, MenzelGläser), and disposable cuvettes from Eppendorf.

#### 3.1.3 Instruments

See Appendix 2.

#### 3.1.4 Chemicals

See Appendix 3.

### 3.1.5 Buffers and solutions

#### 3.1.5.1 Molecular biology buffers and solutions

##### 10x modified Gitschier buffer (MGB)

- ❖ 6.7 ml 1.0 M Tris/HCl, pH 8.8
- ❖ 1.66 ml 1.0 M  $(\text{NH}_4)_2\text{SO}_4$
- ❖ 650  $\mu\text{l}$  1.0 M  $\text{MgCl}_2$

Complete the volume up to 10 ml with ddH<sub>2</sub>O.

##### 1x MGB buffer (Working solution)

- ❖ 1.0 ml 10x MGB
- ❖ 500  $\mu\text{l}$  10% Triton X-100
- ❖ 8.5 ml ddH<sub>2</sub>O

##### 50x Trisacetate EDTA (TAE) buffer

- ❖ 2.0 M Tris-acetate, pH 8.0
- ❖ 50 mM EDTA
- ❖ 57.1 ml glacial Acetic acid

Complete the volume up to 1L with ddH<sub>2</sub>O.

##### Ethidiumbromide (stock solution)

1.0% solution in ddH<sub>2</sub>O (10 mg/ml)

(final concentration in a gel: 1.0  $\mu\text{g}/\text{ml}$ )

##### 10 mM dNTP (50x stock) (Boehringer)

200  $\mu\text{M}$  final concentration in a PCR reaction (50  $\mu\text{M}$  each nucleotide)

#### 3.1.5.2 Protein biochemistry buffers and solutions

##### 10x Phosphate buffered saline (PBS)

- ❖ 1.7 M NaCl
- ❖ 34 mM KCl
- ❖ 40 mM  $\text{Na}_2\text{HPO}_4 \times 2\text{H}_2\text{O}$
- ❖ 18 mM  $\text{KH}_2\text{PO}_4$

Adjust pH 7.2 with 1.0 N NaOH.

### **Modified RIPA buffer (protein lysis buffer)**

- ❖ 50 mM Tris/HCl, pH 7.4
- ❖ 150 mM NaCl
- ❖ 1.0 mM EDTA
- ❖ 0.1% SDS
- ❖ 1.0% Sodium deoxycholate
- ❖ 1.0% Triton X-100

### **1x Tris buffered saline (TBS)**

- ❖ 137 mM NaCl
- ❖ 20 mM Tris/HCl, pH 7.4

(filtered before use)

### **Solutions for CNS myelin enrichment**

0.85 M Sucrose solution (sterile filtered) in ddH<sub>2</sub>O

0.32 M Sucrose solution (sterile filtered) in ddH<sub>2</sub>O

### **Deacetylase inhibitors**

TSA, 5 mM in DMSO, Sigma-Aldrich (500 nM final concentration)

Nicotinamide, SIGMA (10 mM final concentration)

### **Protease inhibitors**

PMSF (1.0 mM final concentration)

Complete Mini protease inhibitor tablets (1.0 tablet per 10 or 50 ml solution)

\*When needed, buffers were supplied with the desired deacetylase and protease inhibitors freshly before use.

### **3.1.5.3 SDS PAGE and Western blotting buffers and solutions**

#### **Polyacrylamide stacking gel (4 gels, each 0.75 mm thick)**

- ❖ 6.1 ml ddH<sub>2</sub>O
- ❖ 1.3 ml 30% Acrylamide/Bis-acrylamide (29:1)

- ❖ 2.5 ml 0.5 M Tris/HCl, pH 6.8
- ❖ 100 µl 10% SDS
- ❖ 50 µl 10% APS
- ❖ 10 µl TEMED

### **12% Polyacrylamide separating gel (20 ml)**

- ❖ 6.6 ml ddH<sub>2</sub>O
- ❖ 8.0 ml 30% Acrylamide/Bis-acrylamide (29:1)
- ❖ 5.0 ml 1.5 M Tris/HCl, pH 8.8
- ❖ 200 µl 10% SDS
- ❖ 200 µl 10% APS
- ❖ 8.0 µl TEMED

### **10% Polyacrylamide separating gel (20 ml)**

- ❖ 7.9 ml ddH<sub>2</sub>O
- ❖ 6.7 ml 30% Acrylamide/Bis-acrylamide (29:1)
- ❖ 5.0 ml 1.5 M Tris/HCl, pH 8.8
- ❖ 200 µl 10% SDS
- ❖ 200 µl 10% APS
- ❖ 8.0 µl TEMED

### **1x SDS running buffer**

- ❖ 25 mM Tris base
- ❖ 192 mM Glycine
- ❖ 0.1% SDS

### **20x MOPS/SDS running buffer**

- ❖ 1.0 M Tris base
- ❖ 1.0 M MOPS
- ❖ 20.5 mM EDTA
- ❖ 69.3 mM SDS

pH 7.7 (do not adjust the pH with acid or base)

### **1x SDS sample buffer**

- ❖ 62.5 mM Tris/HCl, pH 6.8

- ❖ 2.0% SDS
- ❖ 10% Glycerol
- ❖ 0.01% Bromophenol Blue

### **2x SDS sample buffer**

- ❖ 125 mM Tris/HCl, pH 6.8
- ❖ 4.0% SDS
- ❖ 20% Glycerol
- ❖ 0.02% Bromophenol Blue

### **6x SDS sample buffer**

- ❖ 375 mM Tris/HCl, pH 6.8
- ❖ 12% SDS
- ❖ 60% Glycerol
- ❖ 0.06% Bromophenol Blue

### **4x LDS sample buffer (10 ml)**

- ❖ 4.0 g Glycerol
- ❖ 0.682 g Tris Base
- ❖ 0.666 g Tris-HCl
- ❖ 0.800 g LDS
- ❖ 0.006 g EDTA
- ❖ 0.75 ml of 1.0% solution of Serva Blue G250
- ❖ 0.25 ml of 1.0% solution of Phenol Red

Complete the volume up to 10 ml with ddH<sub>2</sub>O.

pH 8.5 for 1X (do not adjust the pH with acid or base)

### **10x Tris-Glycine transfer buffer**

- ❖ 390 mM Glycine
- ❖ 480 mM Tris base

### **2x Tris-Glycine transfer buffer**

- ❖ 78 mM Glycine
- ❖ 96 mM Tris base
- ❖ 20% Methanol

**1x Tris-Glycine transfer buffer**

- ❖ 39 mM Glycine
- ❖ 48 mM Tris base
- ❖ 20% Methanol

**1x Transfer buffer (for Invitrogen gels)**

- ❖ 25 mM Bicine
- ❖ 25 mM Bis-Tris
- ❖ 0.6 g EDTA
- ❖ 20% Methanol

Complete the volume up to 2L with ddH<sub>2</sub>O.

pH 7.2 (do not adjust the pH with acid or base)

**20x Tris buffered saline (TBS)**

- ❖ 1.0 M Tris base
- ❖ 3.0 M NaCl

Adjust the pH to 7.4 with fuming HCl.

**1x TBS with Tween-20 (TBST)**

- ❖ 50 mM Tris/HCl, pH 7.4
- ❖ 150 mM NaCl
- ❖ 0.05% Tween-20

**1x TBST (for Western blotting with antibodies against acetylated lysine)**

- ❖ 10 mM Tris/HCl, pH 7.4
- ❖ 150 mM NaCl
- ❖ 0.1% Tween-20

**1x PBS**

- ❖ 170 mM NaCl
- ❖ 3.4 mM KCl
- ❖ 4.0 mM Na<sub>2</sub>HPO<sub>4</sub> x 2H<sub>2</sub>O
- ❖ 1.8 mM KH<sub>2</sub>PO<sub>4</sub>

**1x PBST**

1x PBS + 0.1% Tween-20

**Blocking and primary/secondary antibody dilution buffer**

5.0% non fat dry milk powder in 1x TBST

**Blocking and secondary antibody dilution buffer for Western blotting with antibodies against acetylated lysine**

5.0% non fat dry milk powder in 1x TBST (0.1% Tween-20)

**Primary antibody dilution buffer for Western blotting with antibodies against acetylated lysine**

5.0% BSA in 1x TBST (0.1% Tween-20)

**Blocking buffer for Western blotting with IRDye secondary antibodies**

5.0% non fat dry milk powder and 5.0% goat serum in 1x TBS

**Primary and secondary antibody dilution buffer for Western blotting with IRDye secondary antibodies**

5.0% non fat dry milk powder and 5.0% goat serum in 1x TBST (0.1% Tween-20)

**Stripping buffer**

- ❖ 0.2 M Glycine/HCl, pH 2.5
- ❖ 0.1% Tween-20

**3.1.5.4 Polyacrylamide gel staining solutions**

❖ **Coomassie blue**

Staining solution:

0.25% Coomassie brilliant blue (R-250), 50% Methanol, 10% Acetic acid

Destaining solution:

25% Methanol, 7.5% Acetic acid

❖ **Silver staining**

Fixation solution:

40% Ethanol, 10% Acetic acid



Washing solution:

30% Ethanol

Sensitization solution:

0.8 mM Na<sub>2</sub>S<sub>2</sub>O<sub>3</sub> (0.02%)

Silver staining solution:

0.2% AgNO<sub>3</sub>, 0.05% HCOH (37%)

Developing solution:

3.0% Na<sub>2</sub>CO<sub>3</sub>, 0.05% HCOH (37%)

Reaction stop solution:

5.0% Acetic acid

### 3.1.5.5 Thin layer chromatography solutions

- ❖ Chloroform/Methanol (2:1)
- ❖ Chloroform/Methanol (1:1)
- ❖ 75 mM K<sub>2</sub>SO<sub>4</sub>
- ❖ Fluid phase: Chloroform/Methanol/Water (65:25:4)
- ❖ 10% Sulfuric acid, 5.0% Methanol

### 3.1.5.6 Immunohistochemistry buffers and solutions

#### Avertin

- ❖ 2.0 g Tribromethanol
- ❖ 2.0 ml Amyl alcohol
- ❖ 96 ml ddH<sub>2</sub>O (pre-warmed to 40°C)

Stir the solution for 30 min and sterile filter it. Store it away from light and at 4°C.

#### Phosphate buffer (stock solutions)

0.2 M Sodium dihydrogenphosphate (NaH<sub>2</sub>PO<sub>4</sub>)

0.2 M Disodium hydrogenphosphate (Na<sub>2</sub>HPO<sub>4</sub>)

#### 0.1 M Phosphate buffer (working solution - pH 7.4)

- ❖ 20 ml 0.2 M Sodium dihydrogenphosphate (NaH<sub>2</sub>PO<sub>4</sub>)
- ❖ 80 ml 0.2 M Disodium hydrogenphosphate (Na<sub>2</sub>HPO<sub>4</sub>)
- ❖ 100 ml ddH<sub>2</sub>O

### **PBS/BSA**

- ❖ 20 ml 0.2 M Sodium dihydrogenphosphate ( $\text{NaH}_2\text{PO}_4$ )
- ❖ 80 ml 0.2 M Disodium hydrogenphosphate ( $\text{Na}_2\text{HPO}_4$ )
- ❖ 1.8 g Sodium chloride
- ❖ 1.0 g Bovine Serum Albumin (BSA)
- ❖ 100 ml ddH<sub>2</sub>O

### **16% Paraformaldehyde (PFA)**

Add 16 g PFA into 90 ml ddH<sub>2</sub>O, heat it up to 65°C while stirring, and let it be stirred at 60°C for 15-20 min. Add droplets of 5 N NaOH until the solution becomes clear.

(cooled, filtered, stored at -20°C)

### **4.0% Paraformaldehyde (PFA)**

- ❖ 100 ml 0.2 M Phosphate buffer (20 ml 0.2 M Sodium dihydrogenphosphate ( $\text{NaH}_2\text{PO}_4$ ) + 80 ml 0.2 M Disodium hydrogenphosphate ( $\text{Na}_2\text{HPO}_4$ ))
- ❖ 50 ml 16% PFA (pre-heated at 60°C for 30-45 min)
- ❖ 1.6 g NaCl

Complete the volume up to 200 ml with ddH<sub>2</sub>O.

### **4.0% Paraformaldehyde (PFA) in 0.1 M PB**

- ❖ 100 ml 0.2 M Sodium dihydrogenphosphate ( $\text{NaH}_2\text{PO}_4$ )
- ❖ 400 ml 0.2 M Disodium hydrogenphosphate ( $\text{Na}_2\text{HPO}_4$ )
- ❖ 100 ml 37% Formaldehyde
- ❖ 400 ml ddH<sub>2</sub>O

(filtered)

### **Karlsson and Schultz fixative (K&S)**

- ❖ 0.36 g Sodium dihydrogenphosphate ( $\text{NaH}_2\text{PO}_4$ )
- ❖ 3.1 g Disodium hydrogenphosphate ( $\text{Na}_2\text{HPO}_4$ )
- ❖ 1.0 g Sodium chloride (final concentration: 0.5%)
- ❖ 50 ml 16% PFA (pre-heated at 60°C for 30-45 min, final concentration: 4.0%)
- ❖ 20 ml 25% Glutaraldehyde (final concentration: 2.5%)

Complete the volume up to 200 ml with ddH<sub>2</sub>O and filter.

### **Citrate buffer (stock solutions)**

0.1 M Citric acid ( $C_6H_8O_7 \cdot xH_2O$ )

0.1 M Sodium citrate ( $C_6H_5O_7Na_3 \cdot 2H_2O$ )

(stored at 4°C)

### **Citrate buffer (working solution, 0.01 M, pH 6.0)**

- ❖ 9.0 ml 0.1 M Citric acid ( $C_6H_8O_7 \cdot xH_2O$ )
- ❖ 41 ml 0.1 M Sodium citrate ( $C_6H_5O_7Na_3 \cdot 2H_2O$ )
- ❖ 450 ml ddH<sub>2</sub>O

### **Tris buffer (stock solution)**

0.5 M Tris base

Adjust pH 7.6 with HCl.

(store at 4°C)

### **Tris buffer (working solution)**

- ❖ 100 ml 0.5 M Tris base (pH 7.6)
- ❖ 9.0 g Sodium chloride

Complete the final volume up to 1L with ddH<sub>2</sub>O.

### **Washing buffer (2.0% milk in Tris buffer)**

20 g of non-fat milk powder in a final volume of 1000 ml with working solution of Tris buffer

### **Blocking buffer**

20% Goat serum in PBS/BSA

### **3.1.5.7 Histology staining solutions**

#### **Mayer's Haematoxylin solution**

Dissolve 1.0 g Haematoxylin in 1L ddH<sub>2</sub>O.

Add 0.2 g Sodium iodate and 50 g of Potassium aluminium sulphate under constant shaking.

Add 50 g Chloralhydrate and 1.0 g Citric acid.

Filter the solution before use.

### **Eosin stock solution (10x)**

10 g of Eosin in 100 ml of ddH<sub>2</sub>O

(left to mature)

### **Eosin working solution**

Add 2.5 ml of stock solution to 250 ml ddH<sub>2</sub>O and finish by adding 12 drops of glacial Acetic acid.

### **Scott's solution**

❖ 2.0 g Potassium bicarbonate (KHCO<sub>3</sub>)

❖ 20 g Magnesium sulfate (MgSO<sub>4</sub>)

Complete the final volume up to 1L with ddH<sub>2</sub>O.

### **HCl-Alcohol**

❖ 1.25 ml concentrated HCl

❖ 350 ml Ethanol

❖ 150 ml ddH<sub>2</sub>O

### **Solutions for Methylene blue-Azur II staining of semithin sections**

#### ❖ **Methylene blue stock solution**

1.0 g Na-tetraborat (Borax)

1.0 g Methylene blue

Complete the volume up to 100 ml with ddH<sub>2</sub>O.

(stable for one month)

#### ❖ **Azur II stock solution**

1.0 g Azur II in 100 ml ddH<sub>2</sub>O

(stable for one month)

#### ❖ **Methylene blue-Azur II working solution**

Mix both staining solutions in a 1:1 ratio and filter through a syringe filter tip when applying to the sections.

### 3.1.5.8 Epon embedding and EM contrasting solutions

#### Epon mix

- ❖ 171.3 g Glycidether 100
- ❖ 115 g DDSA (Dodeceny succinic anhydride)
- ❖ 89 g MNA (Methyl nadic anhydride)

Mix using magnet stirrer for 10 min and then add 6.5 ml DMP-30.

Mix using magnet stirrer for 20 min.

#### Chemicals for EM contrasting

4.0% Uranyl acetate (light sensitive)

Reynolds lead citrate

### 3.1.6 DNA/protein markers and loading dyes

GeneRuler 1 kb DNA ladder (Fermentas)

GeneRuler 100 bp DNA ladder (Fermentas)

PageRuler Plus Prestained Protein Ladder (Fermentas)

6x DNA loading dye (Fermentas)

### 3.1.7 Oligonucleotides

All oligonucleotides were synthesized at “DNA Core Facility” of the Max-Planck-Institute of Experimental Medicine. They are provided at 50 pM concentration.

#### 3.1.7.1 Genotyping primers

##### **Cnp<sup>null</sup> mice**

CNP-forward: 5'-GCCTTCAAACGTCCATCTC-3' (#2016)

CNP-reverse: 5'-CCCAGCCCTTTTATTACCAC-3' (#7315)

EllaCre forward: 5'-CCTGGAAAATGCTTCTGTCCG-3' (#4193)

EllaCre reverse: 5'-CAGGGTGTATAAGCAATCCC-3' (#4192)

Amplification products: 643 bp (wt) and 400 bp (mutant)

### **5xFAD transgenic mice**

Forward: 5'-CCGCGCAGAACAGAAGGACAGAC-3' (#19746)

Reverse: 5'-GGGCGGGCATCAACAGGCTCAACT-3' (#19747)

Amplification product: 438 bp (transgene)

### **Plp<sup>null</sup> mice**

Forward: 5'-GGAGAGGAGGAGGGAAACGAG-3' (#2729)

Reverse: 5'-TCTGTTTTGCGGCTGACTTTG-3' (#2731)

Hwneo: 5'-TTGGCGGCGAATGGGCTGAC-3' (#1864)

Amplification products: 150 bp (wt) and 300 bp (mutant)

### **Sirt2<sup>null</sup> mice**

Forward: 5'-GGCCCCTGACTCCTGACTGTTCTA-3' (#12201)

Reverse: 5'-ACCTGGCCTGTCTTTTCCTTGTTA-3' (#12202)

Puro: 5'-CATAGCCTGAAGAACGAGA-3' (#1955)

Amplification products: 448 bp (wt) and 200 bp (mutant)

### **3.1.7.2 Quantitative real time PCR primers**

#### **Atp5b**

Forward: 5'-GGCACAATGCAGGAAAGG-3' (#10568)

Reverse: 5'-TCAGCAGGCACATAGATAGCC-3' (#10569)

#### **Cnp**

Forward: 5'-CGCTGGGGCAGAAGAATA-3' (#8890)

Reverse: 5'-AAGCCTTGCCATACGATCT-3' (#8893)

#### **Fdft1**

Forward: 5'-TCAATCAGACCAGTCGCAGC-3' (#4350)

Reverse: 5'-GTGCCGTATGTCCCATCC-3' (#4351)

#### **Hdac4**

Forward: 5'-CACACCTCTTGAGGGTACAA-3' (#17639)

Reverse: 5'-AGCCCATCAGCTGTTTTGTC-3' (#17640)

**Hdac5**

Forward: 5'-GAGTCCAGTGCTGGTTACAAAA-3' (#17641)

Reverse: 5'-TACACCTGGAGGGGCTGTAA-3' (#17642)

**Hdac6**

Forward: 5'-GAAGGAGGAGCTGATGTTGG-3' (#17643)

Reverse: 5'-TCATGTACTGGGTTGTCTCCAT-3' (#17644)

**Hdac7**

Forward: 5'-CCATGGGGGATCCTGAGT-3' (#18049)

Reverse: 5'-GCAAACCTCTCGGGCAATG-3' (#18050)

**Hmgcr**

Forward: 5'-TGAAGAGGACGTGCTGAGCA-3' (#4342)

Reverse: 5'-ATGTACAGGATGGCGATGCA-3' (#4343)

**Nfkbib**

Forward: 5'-ACAGTGACAGTGACAACAGAGATG-3' (#18051)

Reverse: 5'-AAGGCGGTTGTTCGGTTTT-3' (#18052)

**Plp**

Forward: 5'-TCAGTCTATTGCCTTCCCTAGC-3' (#8740)

Reverse: 5'-AGCATTCCATGGGAGAACAC-3' (#8741)

**Rinl**

Forward: 5'-CTTGCCACGCCTACTGT-3' (#18053)

Reverse: 5'-TGAGGTGTCCACCTGGATG-3' (#18054)

**Sirt1**

Forward: 5'-TCGTGGAGACATTTTTAATCAGG-3' (#18060)

Reverse: 5'-GCTTCATGATGGCAAGTGG-3' (#18061)

**Sirt2**

Forward: 5'-CACTACTTCATCCGCCTGCT-3' (#9167)

Reverse: 5'-CCAGCGTGTCTATGTTCTGC-3' (#9168)

**Sirt3**

Forward: 5'-CTGCTACTCATTCTTGGGACCT-3' (#17633)

Reverse: 5'-TCTGTAAGCTTCAGACAAGCTG-3' (#17634)

**Sirt4**

Forward: 5'-TGATGTCCAAAGGCTGGAA-3' (#17635)

Reverse: 5'-AGAGTTGGAGCGGCATTG-3' (#17636)

**Sirt5**

Forward: 5'-CCAGCTTTAGCAGGAAAAGG-3' (#17637)

Reverse: 5'-GACTGGGATTCTGGCGTCT-3' (#17638)

**Sirt6**

Forward: 5'-GACCTGATGCTCGCTGATG-3' (#18062)

Reverse: 5'-GGTACCCAGGGTGACAGACA-3' (#18063)

**Sirt7**

Forward: 5'-TGCAACTCCTCATGAATGAACT-3' (#18064)

Reverse: 5'-CGCCAAGGAGAAGATTGG-3' (#18065)

**Top1**

Forward: 5'-AATGAGAGGGGACAGCAAAC-3' (#10576)

Reverse: 5'-CCTTGTCTGTGGCCTTCG-3' (#10577)

**3.1.7.3 Additional primers**

**For mouse Sirt2 cDNA**

5'-ACACGATGGGCTGGATGAAAGAGA-3' (#13183)

5'-TCCACCGCGCTTCTTCTCCTG-3' (#13184)

5'-GTCTGGCCTGTCTTTTCCTTGTTA-3' (#13185)

**3.1.8 Enzymes and reaction buffers**

First-Strand buffer, 5x (Invitrogen)

GoTaq polymerase, 5.0 U/ $\mu$ l (Promega)



GoTaq reaction buffer, green, 5x (Promega)  
 Power SYBR Green PCR master mix (Applied Biosystems)  
 Proteinase K (Roth)  
 REDTaq DNA polymerase, 1.0 U/μl (Sigma-Aldrich)  
 REDTaq reaction buffer, 10x (Sigma-Aldrich)  
 Superscript III Reverse Transcriptase (Invitrogen)

**3.1.9 Antibodies and recombinant peptides/proteins**

**Primary antibodies**

<b>Antibody</b>	<b>Species</b>	<b>Dilution</b>	<b>Application</b>	<b>Vendor</b>
Acetylated lysine	rabbit	1:500-1000	IB	Cell Signaling (#9441)
Acetylated lysine (Ac-K-103)	mouse	1:1000	IB	Cell Signaling (#9681)
Acetylated lysine	rabbit	1:1000	IB	Immunechem (ICP0380)
Acetylated tubulin (Clone 6-11B-1)	mouse	1:5000	IB	Sigma-Aldrich (T6793)
APP, A4 (Clone 22C11)	mouse	1:750	IHC	Millipore (MAB 348)
CNP (Clone 11-5B)	mouse	1:1000- 10000/1:150	IB/IHC	Sigma-Aldrich (C5922)
GAPDH	mouse	1:5000	IB	Stressgen
GAPDH (GC5)	mouse	1:1000	IB	Santa Cruz (sc-32233)
GFAP	mouse	1:1000/1:200	IB/IHC	Novocastra (NCL-GFAP-GA5)
HDAC4	rabbit	1:1000	IB	Upstate (#07-040)
HDAC5	rabbit	1:1000	IB	Santa Cruz
HDAC6 (H-300)	rabbit	1:500	IB	Santa Cruz (sc-11420)
HDAC7 (H-273)	rabbit	1:1000	IB	Santa Cruz (sc-11421)
Mac3 (M3/84)	rat	1:400	IHC	BD Pharmingen (553222)

<b>Antibody</b>	<b>Species</b>	<b>Dilution</b>	<b>Application</b>	<b>Vendor</b>
MAG (Clone 513)	mouse	1:500	IB	Poltorak et al., 1987
MBP	rabbit	1:5000	IB/IHC	DAKO (A0623)
MOG (8-18c5)	mouse	1:2500	IB	Linnington et al., 1984
PLP/DM20 (A431)	rabbit	1:5000	IB	Jung et al., 1996
Septin 8	rabbit	1:200	IB	received from Makoto Kinoshita
SIRT2 (H95)	rabbit	1:2000/1:100	IB/IHC	Santa Cruz (sc-20966)
SIRT2	rabbit	1:5000/1:1000	IB/ICC	Southwood et al., 2006
$\alpha$ -tubulin (Clone B-5-1-2)	mouse	1:5000	IB	Sigma-Aldrich (T5168)

**Secondary antibodies**

<b>Antibody</b>	<b>Species</b>	<b>Dilution</b>	<b>Application</b>	<b>Vendor</b>
Biotinylated anti rat	rabbit	1:100	IHC	Vector (BA-4001)
HRP anti rabbit	goat	1:5000- 10000	IB	Dianova 111-035-144
HRP anti mouse	goat	1:5000- 10000	IB	Dianova 115-035-003
IRDye 800 anti rabbit	goat	1:5000	IB	LI-COR Odyssey Infrared Imaging System
IRDye 800 anti mouse	goat	1:5000	IB	LI-COR Odyssey Infrared Imaging System

**Recombinant peptides and proteins**

Acetylated BSA (Immunechem)

MOG peptide, 35-55, 2.5 mg/ml (synthesized by the Proteomics Group of the Max-Planck-Institute of Experimental Medicine, Göttingen)

Purified BSA, 100x, 10  $\mu$ g/ $\mu$ l (New England BioLabs)

### 3.1.10 Additional materials and reagents

Betaine (Sigma-Aldrich)

Bis-Tris 1.0 mm precasted polyacrylamide gels, 4.0-12% or 12% (NuPAGE, Invitrogen)

DTT (0.1 M, Invitrogen)

ECL-Hyperfilms (Amersham Biosciences)

Goat serum (Gibco)

HBSS (Lonza)

Horse serum (Pan Biotech)

PVDF membrane, Hybond P pore size 0.45  $\mu\text{m}$  (GE Healthcare)

Shandon coverplates (ThermoScientific)

Silica gel 60 (Merck, Darmstadt, Germany)

Trizol reagent (Invitrogen)

### 3.1.11 Animals and mouse lines

The mice lacking Sirt2 expression (unpublished) were generated by Dr. Maria Carla Motta in the group of Prof. Van Lohuizen, The Netherlands Cancer Institute, Amsterdam, The Netherlands, and kindly provided by Dr. Maria Carla Motta in the group of Prof. Dr. Lenny Guarente, The Massachusetts Institute of Technology, Cambridge, USA. The mouse line was generated by using Fvb inbred mouse strain. Throughout this project, we backcrossed these mice up to 10 generations into c57/n background. Experiments were performed after at least one generation of backcrossing; however, most of the data shown in this manuscript were obtained with the material from the animals backcrossed 3 or more generations into c57/n background.

#### **Additional mouse lines used:**

Plp<sup>null</sup> mice (Klugmann et al., 1997)

Cnp<sup>null</sup> mice (Lappe-Siefke et al., 2003)

5XFAD transgenic mice (Oakley et al., 2006)

### 3.1.12 Softwares

Adobe Illustrator CS3: for preparation of the figures of the thesis manuscript

Adobe Photoshop CS3: for preparation of the figures of the thesis manuscript

BioRAD Quantity One free trial software: for densitometric evaluation of the intensities of protein bands

DNASar software package (SeqMan, EditSeq and PrimerSelect):

for analysis of nucleotide and protein sequences, of the results of DNA sequencing, and for designing primer pairs

EndNote X4: for organizing the references used in this thesis

7500 Fast System SDS Software Ver 1.3 (Applied Biosystems): for the analysis of qRT-PCR data

GraphPad Prism 5 free trial software: for calculations, statistical analysis, and preparation of the graphs

ImageJ: for processing the electron and light microscopic images

Kappa Image Base Software Ver 2.7.2.: for taking the light microscopic images

Microsoft Office Excel, 2003: for preparing data tables and calculations

Microsoft Office Word, 2003: for writing the thesis manuscript

Odyssey 2.1 Software: for densitometric evaluation of the intensities of protein bands

### 3.2 Methods

#### 3.2.1 DNA isolation and purification

##### 3.2.1.1 Preparation of murine genomic DNA

To prepare murine genomic DNA for genotyping, 5.0 mm large pieces of tail biopsies were digested in 200  $\mu$ l of lysis buffer (180  $\mu$ l of 1x MGB and 20  $\mu$ l of proteinase K (10 mg/ml)) in tightly closed microfuge tubes O/N at 56°C with vigorous shaking. Once the digestion was complete, proteinase K was heat-inactivated at 95°C for 15 min. Lysates were then centrifuged at 5000 rpm for 5 min to pellet the undigested material. The supernatants were collected in clean tubes and diluted (1:2) or (1:5) with ddH<sub>2</sub>O, depending on the PCR reaction to be performed and 1.0  $\mu$ l of the diluted DNA was used for each genotyping PCR reaction.

##### 3.2.1.2 DNA extraction from agarose gels

DNA extraction from agarose gels was performed using Qiagen's "QIAquick Gel Extraction Kit". The principle of the gel extraction kit is based on the ability of DNA fragments to bind to silica-membranes under high-salt conditions at pH 7.5. Briefly, the desired DNA fragment was excised under UV light from the agarose gel and placed into an microfuge tube. DNA fragments were isolated from agarose following the manufacturer's protocol. Finally, the DNA was eluted in 30-50  $\mu$ l of prewarmed (50°C) ddH<sub>2</sub>O.

#### 3.2.2 DNA modification and analysis

##### 3.2.2.1 DNA amplification by polymerase chain reaction (PCR)

PCR is a method that permits the *in vitro* enzymatic amplification of a selected DNA sequence (Mullis et al., 1986). The DNA synthesis is catalyzed by the DNA polymerase from the thermophilic bacterium *Thermus aquaticus* (Taq Polymerase), which is stable at the melting temperature of the double stranded DNA (95°C) and has an optimal activity at 72°C. Template sequence for amplification is defined with the primers flanking the sequence to be amplified. Primers are single stranded oligonucleotides, which can anneal to the sense and antisense strand of the amplicon due to their sequence, complementary to the target DNA. PCR amplification is carried out by a thermocycler through multiple repetitions (25-40 times) of the three stepped PCR cycle. In the first

step, the double stranded DNA template is denatured at 95°C. In the second step, primers anneal to the complementary sequences of the template DNA at varying temperatures defined by the sequence of the primers. Then, each strand is replicated by the elongation of the primer sequence by the Taq Polymerase which adds nucleotides complementary to the template sequence. In addition to the DNA template, the primers and the polymerase enzyme, each reaction mixture contains dNTPs and the appropriate buffer to provide the optimal salt and pH conditions.

Standard PCR reaction mix:

- 1.0-2.0 µl DNA (100 pg-100 ng)
- 1.0-2.0 µl forward primer (10 pM)
- 1.0-2.0 µl reverse primer (10 pM)
- 2.0 µl dNTP mix (2.0 mM)
- 2.0 µl 10x RedTaq buffer or 4.0 µl 5x GoTaq buffer (green)
- 0.8 µl Betaine (optional)
- 1.0 µl RedTaq polymerase (1.0 U/µl) or 0.15 µl GoTaq polymerase (5.0 U/µl)
- ddH<sub>2</sub>O up to 20 µl

### 3.2.2.2 Agarose gel electrophoresis for the size separation of DNA fragments

In order to separate DNA fragments, 1.0-2.0% agarose gels were used. Agarose was dissolved in 1x TAE buffer by cooking in a microwave. EtBr was added with a final concentration of 1.0 µg/ml into the gel, which had cooled down to around 60°C. The gel was slowly poured into custom-made gel trays and combs were placed to form wells into the gel. Solidified gels were placed into an electrophoresis chamber, which was filled then with 1x TAE buffer until the gel surface was covered by and the wells were filled with buffer. Then the combs were removed gently. Standard DNA markers (100 bp or 1 kb ladder) and DNA samples in sample buffer were loaded into the wells. After the loading was completed, the chamber was connected to a power supply and the gel was run at a constant voltage of 120 V (approximately 8.0-10 V/cm length of gel) until the desired fragment separation was achieved. For documentation, snapshots of the UV trans-illuminated gels were taken.

### 3.2.2.3 Determination of DNA/RNA concentrations

The concentration and purity of nucleic acids were determined spectrophotometrically according to the Lambert-Beer law. This law states that the concentration of a substance in an aqueous solution is proportional to its absorption.

The absorptions at 260 nm (A<sub>260</sub>) and 280 nm (A<sub>280</sub>) represent the absorption maxima for nucleic acids and proteins, respectively. And these values correspond to the amount of DNA/RNA in the solution, and the protein contamination in the sample, respectively. The absorbance at 320 nm (A<sub>320</sub>) provides a general measurement of the turbidity of the sample. The A<sub>320</sub> value as a background reading is subtracted from the A<sub>260</sub> one to calculate the nucleic acid concentration. Phenol and guanidium salt contaminations are detected by absorbance measurement at 230 nm (A<sub>230</sub>).

To read the absorbance of the sample in question at the wavelengths listed above, it was diluted 1:100 with ddH<sub>2</sub>O in a final volume of 100 µl, pipetted into a disposable cuvette and analysed by using a UV spectrophotometer. A nucleic acid sample with a good quality should have a ratio of A<sub>260</sub>/A<sub>280</sub> between 1.7–2.0 and of A<sub>260</sub>/A<sub>230</sub> greater than 1.5. For an accurate measurement, the A<sub>260</sub> value must be between 0.1 and 1.0.

### 3.2.2.4 DNA sequencing

DNA samples were sequenced at the “DNA Core Facility” of the Max-Planck-Institute of Experimental Medicine. 16 µl of DNA samples (100 ng/µl) diluted in ddH<sub>2</sub>O and sequencing primer information were submitted for sequencing. Resulting sequence was analyzed by using the DNASTar (SeqMan) software package and verified on public domain databases like 'National Centre for Biotechnology Information' (NCBI).

### 3.2.2.5 Primer designing

Forward and reverse primers (24-32 oligonucleotides) with a melting point between 50-65°C and an appropriate GC content were manually designed based on the template sequence information by using NCBI database, and the DNASTar (EditSeq and PrimerSelect) software package. All primers were synthesized at the “DNA Core Facility” of the Max-Planck-Institute of Experimental

Medicine. The oligonucleotide stocks with a concentration of 50 pM were diluted 1:5 with ddH<sub>2</sub>O before use.

Primers to be used for quantitative RT-PCRs were designed by the help of Universal Probe Library of Roche, on the following website: <http://www.roche-applied-science.com/sis/rtpcr/upl/index.jsp?id=UP030000>.

### **3.2.3 RNA isolation and analysis**

#### **3.2.3.1 Small scale RNA isolation**

Small scale RNA isolation from animal tissue was performed by using Qiagen's "RNeasy Mini Prep Kit" to purify up to 100 µg total RNA. The kit is based on a selective binding of RNAs bigger than 200 bases to a silica-gel based membrane under high-salt conditions, which excludes binding of 5S, 5.8S and tRNAs. RNA isolation and purification was carried out following the manufacturer's instructions.

Briefly, frozen (at -80°C) brain tissue was lysed and homogenized in Trizol with an Ultra-Turrax T8 for 20-30 sec. Chloroform was added to the homogenates and after the spin, the upper aqueous phase was collected. After addition of ethanol for optimal binding, the samples were applied onto RNeasy mini columns where total RNA binds to the membrane and contaminants are efficiently washed away. Finally, RNA was eluted from the column twice with 30 µl RNase-free ddH<sub>2</sub>O.

#### **3.2.3.2 First strand cDNA synthesis**

In order to analyze the gene expression profile of tissues in interest, the isolated RNA repertoire is converted into the more stable complementary single stranded DNA (cDNA) library. cDNA synthesis is possible, because eukaryotic messenger RNAs harbor defined polyadenylated tail on the 3' end. Total RNA is mixed with random nanomer and oligo-dT primers. The amplification reaction is carried out by Superscript III reverse transcriptase (Gerard et al., 1986; Kotewicz et al., 1985) at 55°C providing high specificity and yields of cDNA (from 100 bp to >12 kb).

To coprecipitate RNA and primers, 1.0 µl of dT-mix primer (0.6 pmol/µl, #9578, anchored oligo dT-mix), 1.0 µl of N9 primer (120 pmol/µl, #4542) and 1.0 µg total RNA were mixed in a nuclease-free microfuge tube. The mixtures were incubated at 70°C for 2 min and then put on ice. 4.0 µl of 5x



First-Strand Buffer, 2.0  $\mu$ l of 0.1 M DTT, 1.0  $\mu$ l of dNTPs (10 mM), and 1.0  $\mu$ l Superscript III (200 U/ $\mu$ l) were added into the tubes (final volume: 20  $\mu$ l). The reactions were incubated in the thermocycler with the following settings: (lid should be at 65°C) at 25°C for 10 min, then at 50°C for 45 min, and finally at 55°C for 45 min. Synthesized cDNAs were diluted 10 times with ddH<sub>2</sub>O before further analysis.

### 3.2.3.3 Quantitative real time PCR (qRT-PCR)

qRT-PCR was performed by using Light Cycler 480 (Roche) and SYBR Green Master Mix (Applied Biosystems). For each reaction, 5.0  $\mu$ l of SYBR Green Master Mix, 20-200 ng of cDNA, forward and reverse primers with a final concentration of 1.0 pM each were mixed and the volume was adjusted to 10.2  $\mu$ l with ddH<sub>2</sub>O. The samples were pipetted into a 96-well plate. All reactions were performed in triplicates. PCR reaction was carried out for 45 cycles under following temperature conditions: at 95°C for 15 sec and at 60°C for 60 sec. Analysis of the measurements was done with 7500 Fast System SDS Software Ver 1.3 (Applied Biosystems). The relative quantity (RQ) values were calculated with respect to the housekeeping genes of Atp5b or Top1. Results were displayed as histograms of normalized RQ values, after the mean of the normalized RQ values for the control group were adjusted to 1.0.

### 3.2.4 Protein biochemistry methods

#### 3.2.4.1 Preparation of protein lysates from animal tissue

Mice were sacrificed by cervical spinal cord dislocation and were instantly decapitated using sharp scissors. Brains were removed as quickly as possible, kept cold and micro dissected under binoculars. The various brain regions such as cortex, hippocampus, cerebellum and brain stem were collected in 2.0 ml microfuge tubes, snap frozen on dry ice and stored at -80°C until further processing. For every 100 mg of tissue, 1.0 ml of 'modified RIPA Buffer' supplemented with protease and deacetylase inhibitors was used for homogenization. Protein lysates were prepared using an Ultra-turrax T8 at highest settings (20-30 sec). After incubation of lysates for about 20-30 min at 4°C while rotating, the insoluble cellular debris were pelleted by centrifugation at 14000 rpm at 4°C for 30 min and the supernatant was used for further analysis or stored at -80°C.

To prepare proteins out of frozen sciatic nerves, the tissues were homogenized in 1x TBS supplemented with protease and deacetylase inhibitors. Homogenization was carried out by the

Precellys homogenizer (at 5000 rpm, 2-3 times for 10 sec). Lysed tissue was then centrifuged at 4°C for 30 min at 14000 rpm. The supernatant containing the soluble proteins was transferred into a new tube and kept at -20 or -80 °C until use.

### **3.2.4.2 Enrichment of CNS myelin**

The enrichment of CNS myelin was performed according to Norton and Poduslo, 1973. Mice were sacrificed by spinal cord dislocation and decapitated. The brains were removed and homogenized in cold 0.32 M sucrose, supplemented with protease and deacetylase inhibitors, by using a homogenizer. The homogenates were carefully layered over a 0.85 M sucrose solution in an ultracentrifuge tube of the appropriate volume. In the sucrose gradient step, the samples were centrifuged for 30 min at 23800 or 24400 rpm, depending on the rotor used (SW-28 or SW-40 Ti, respectively) in a Beckman Ultracentrifuge XL70. Myelin was recovered from the 0.32 M and 0.85 M sucrose interphase. Myelin was washed once in a large volume of cold water and centrifuged for 15 min at 23800 or 24400 rpm, depending on the rotor used (SW-28 or SW-40 Ti, respectively). Then, the myelin-enriched fractions were exposed to two rounds of osmotic shock for 10 min by resuspension of the pellet in a large volume of cold water and centrifuged for 15 min after each round at 9500 or 9700 rpm, depending on the rotor used (SW-28 or SW-40 Ti, respectively). The myelin pellets were resuspended in cold 0.32 M sucrose supplemented with protease and deacetylase inhibitors, and subjected to a second sucrose gradient centrifugation. The purified myelin was collected from the interphase, and washed once more in a large volume of cold water. Finally, myelin pellet was resuspended in a small volume of 1x TBS supplemented with protease and deacetylase inhibitors, by using Ultra-Turrax T8 and stored at -20 and -80°C.

### **3.2.4.3 Protein concentration measurement by Lowry assay**

The protein concentration was measured by using the Bio-Rad DC Protein Assay kit according to manufacturer's "microplate assay" protocol. The assay was performed in a 96-well plate (flat bottom) and absorbance reading was done at 650 nm with a microtitre plate reader.

The working principal of the kit is similar to the Lowry assay (Lowry et al., 1951). The two step assay is based on the reaction of proteins with an alkaline copper tartrate solution, followed by the reduction of the Folin reagent by the copper-treated protein. Primarily the amino acids tyrosine and tryptophan are oxidized and Folin reagent is reduced by losing its oxygen atoms, and

this leads to production of a number of reduced species, which harbour a characteristic blue color with maximum absorbance at 750 nm and minimum absorbance at 405 nm.

Briefly, 5  $\mu$ l of BSA standards (with various concentrations) and samples (diluted or non-diluted) were pipetted into a 96-well plate. 1 volume of Reagent A' and 50 volumes of Reagent A were mixed, and 25  $\mu$ l of the final mix was added into each well. Finally, 200  $\mu$ l of Reagent B was added into each well. After 15 min, the plate was read at 650 nm by using a microtitre plate reader.

### **3.2.4.4 Preparation of the protein samples for SDS-polyacrylamide gel electrophoresis (PAGE)**

The sample preparation was performed on ice. The samples were diluted either with 2x, 6x SDS or 4x LDS sample buffer, and the desired volume was adjusted by adding ddH<sub>2</sub>O or 1x SDS sample buffer. Each sample was adjusted to contain 10%  $\beta$ -ME (the samples planned to be probed with MAG antibody (clone 513, Poltorak et al., 1987) should not include  $\beta$ -ME). Before loading, myelin samples were incubated either at 40°C for 10-20 min or left at room temperature (RT), and the samples of brain, cells and other lysates were incubated at 70°C for 10 min. Then, they were spun briefly and kept at RT until loading.

### **3.2.4.5 SDS-polyacrylamide gel electrophoresis (PAGE)**

In 1970, Laemmli described today's most widely used denaturing and discontinuous polyacrylamide gel electrophoresis (PAGE) method to separate proteins. In this method, buffers of distinctive pH and polyacrylamide concentration generate a discontinuous pH and voltage gradient in the gel. The discontinuity in the pH and the voltage concentrates proteins of each sample into narrow bands thereby allowing the separation of very dilute samples. The protocol primarily relies on the denaturation of the proteins by heating in the presence of SDS and  $\beta$ -mercaptoethanol ( $\beta$ -ME). Under these conditions, the proteins are dissociated and their biological activities are lost. Most proteins bind to SDS in a constant weight ratio, leading to an identical charge densities for the denatured proteins. Thus, the SDS-protein complexes migrate into the polyacrylamide gel according to size, not charge. Most proteins are resolved on polyacrylamide gels containing from 5.0-15% Acrylamide and 0.2-0.5% Bisacrylamide. The detailed theory and protocol for one dimensional gel electrophoresis has been described in following references (Gallagher, 2006; Hames, 1990).

The SDS-PAGE was performed by using the Mini-Protean 3 system (BIO-RAD). A sandwich of a short glass plate and a 0.75 or 1.5 mm spacer plate was assembled according to the manufacturer's instructions. The separating gels with 10 or 12% Acrylamide concentration were prepared, poured between the glass plates, and the gel surface was covered with water-saturated isobutanol to isolate the gel from the air until the polymerization was completed. After the residual alcohol was removed, the stacking gel was poured on top of the separating gel. A 0.75 or 1.5 mm plastic comb with 10 or 15 teeth was inserted into the layer of stacking gel solution to form the wells for the sample application and the gel was left to polymerize. The chamber and gels were assembled according to the manufacturer's instructions. For the separation, the 1x SDS running buffer was used. For the separation of the acetylated proteins, precasted NuPage 4.0-12% or 12% Bis-Tris gels with a thickness of 1.0 mm from Invitrogen were used with the 1x MOPS buffer. 5.0 µl of prestained protein ladder was loaded on each gel as a molecular weight standard and to monitor electroblotting. Samples were loaded into prewashed wells and the gels were run with a constant current of 15-30 mA per gel in BIO-RAD system and 50-100 mA per gel in Invitrogen system, with a maximum voltage of 150-180 V. The run was stopped when the dye in the sample buffer reached the bottom end of the gel.

### **3.2.4.6 Silver staining**

The silver staining was performed according to the modified versions of the protocols of Blum, et al. (1987) and Soerensen et al. (2002). All steps were carried out at RT and by using autoclaved clean glass wares. After SDS-PAGE, the gel was fixed in 40% Ethanol/10% Acetic acid for at least an hour. It was washed twice in 30% Ethanol and once in ddH<sub>2</sub>O for 20 min each. It was incubated for 1 min in 0.02% Na<sub>2</sub>S<sub>2</sub>O<sub>3</sub> for sensitization. It was followed by 3 washes with ddH<sub>2</sub>O for 20 sec each. The gel was stained for 20 min in 0.2% Silver nitrate solution with 0.02% HCOH and then washed 3 times with ddH<sub>2</sub>O for 20 sec each. The gel was developed in 3.0% Na<sub>2</sub>CO<sub>3</sub> with 0.02% HCOH till staining is satisfactory. The reaction was stopped by incubating the gel in 5.0% Acetic acid. The gel was washed with and stored in ddH<sub>2</sub>O at RT. The gel was scanned for documentation purpose.

### **3.2.4.7 Western blotting**

Towbin and his colleagues in 1979 introduced for the first time western blotting as a method for immunological detection of the proteins in biological samples. When an electric current is applied to the blotting module, the negatively charged proteins migrate from the cathode to the anode

and are immobilized on the polyvinylidene difluoride (PVDF) membrane by electrostatic and hydrophobic interactions.

PVDF membranes were activated in methanol for 30 sec, washed briefly in ddH<sub>2</sub>O, and kept in transfer buffer until blotting. Whatman papers and blotting pads were presoaked in transfer buffer. When XCellSureLock wet blotting chambers from Invitrogen were used, 1x transfer buffer with 20% Methanol was used and the gel was not dipped into the transfer buffer before the blotting starts. On the other hand, when Novex Semi-Dry Blotter from Invitrogen was used, 2x Transfer buffer with 20% Methanol was used and the gel was incubated for 10 min on a shaker in 2x Transfer buffer with 20% Methanol prior to blotting. Presoaked papers, pads, gel and membrane were assembled into a blotting sandwich according to manufacturer's instructions. Proteins were transferred at constant 30 V (and 250 mA) for 1 hr at RT when using the wet blotting chambers and at constant 20 V for 1 hr at RT when using the SemiDry blotting apparatus.

### **3.2.4.8 Coomassie staining**

After SDS-PAGE, the gels were stained with Coomassie blue stain to verify the protein transfer. Briefly, the gel was covered with and incubated in Coomassie blue stain solution at RT for a couple of hours and then destained in destaining solution until the protein bands were clearly visible. Staining solution can be recycled.

### **3.2.4.9 Immunodetection of blotted proteins**

After electrophoretic transfer, the membranes were blocked for at least 1 hr at RT in the appropriate blocking buffer. For the detection of acetylated proteins, blots were washed once in TBST (TBS with 0.1% Tween-20) for 5 min before blocking, blocked for 1 hr at 4°C in the appropriate blocking buffer and washed once in TBST for 15 min. Membranes were placed into 50-ml Falcon tubes to be incubated in primary antibodies (diluted in 5 to 10 ml appropriate dilution buffer) (O/N) at 4°C with constant and gentle rotation. Next day, blots were washed three times (each 15 min) in appropriate TBST or five times (each 5 min) in PBST (PBS with 0.1% Tween-20). Membranes were incubated with appropriate HRP-conjugated or IRDye secondary antibodies (diluted in the appropriate dilution buffer) for at least 1 hr at RT. The incubation of the membranes with IRDye secondary antibodies was done in brown colored, conical bottom tubes. This was followed by 4 washes (each 15 min) of the membranes with appropriate TBST or 3 washes (each 5 min) with PBST and 2 times (each 5 min) with PBS. Membranes treated with HRP-

conjugated secondary antibodies were treated for 1 min with Enhanced Chemiluminescence Detection Kit according to manufacturer's instructions. The high performance chemiluminescence films (Amersham) were then exposed to the treated membranes for desired durations in closed cassettes designed for this purpose and developed by KODAK X-OMAT. The membranes treated with IRDye secondary antibodies were scanned by Odyssey Infrared Imaging System 9201, LI-COR at the wavelength of 800 nm.

### **3.2.4.10 Stripping of PVDF membranes**

In order to reprobe a previously analysed membrane with another antibody, the membrane was incubated with the stripping buffer twice for 20 min at 55°C. Then the membrane was reactivated in methanol for 5 min at RT. After washes several times in appropriate TBST, the membrane was blocked again in the appropriate blocking buffer for 30 min-1 hr at RT and probed with the next antibody desired.

### **3.2.4.11 Densitometric evaluation of band intensity**

The exposed films were scanned at grayscale as a 16-bit (600 dpi resolution) using an EPSON F-3200 scanner. Intensities of individual bands were quantified with the BIO-RAD Quantity-One software. The membranes treated with IRDye secondary antibodies were scanned by Odyssey Infrared Imaging System 9201, LI-COR at the wavelength of 800 nm and the intensities of individual bands were measured by Odyssey 2.1 software. The values were normalized to loading controls used. The normalized values ( $\pm$ SEM) were plotted as histograms and the statistical analysis (unpaired t-test) was performed by using the GraphPad Prism 5 software.

### **3.2.5 Thin layer chromatography of lipids**

10  $\mu$ g myelin proteins were diluted in 200  $\mu$ l ddH<sub>2</sub>O and vortexed thoroughly after adding 600  $\mu$ l Chloroform/Methanol (2:1) and 40  $\mu$ l of K<sub>2</sub>SO<sub>4</sub> (75mM). The samples were centrifuged at 7000 g for 10 min. The aqueous phase was discarded and the organic phase was transferred into a new microfuge tube and dried using a vacuum concentrator. The pellets were diluted in 20  $\mu$ l Chloroform/Methanol (1:1) and applied on a silica gel. A mixture of Chloroform/Methanol/Water (65:25:4) was used as the liquid phase in a chromatography chamber. Chamber was equilibrated with the liquid phase for at least 1 hr and its walls were covered with wet Whatman papers. After separation of the lipids on the silica plate in the opposite direction of gravity, the plates were air-

dried and the lipids were detected by carbonization. A solution of 10% Sulfuric acid and 5.0% Methanol was applied using a vaporizer and plates were heated up to 140°C for 10 min.

### **3.2.6 Histology, immunohistochemistry and electron microscopy**

#### **3.2.6.1 Perfusion and fixation of mouse tissue for histology**

Mice were anesthetized by the intraperitoneal injection of 2.5% Avertine with a dose of 0.017 ml per gram of body weight. After anesthesia, the mouse was fixed onto a styrofoam board with the ventral side up and a piece of the tail was cut and kept for the confirmation of the genotype. The abdomen of the mouse was wiped with 70% Ethanol and the skin was removed from the ventral side. A transversal cut was done just below the diaphragm and the rib cage was slowly opened until the heart was exposed. A 27 gauge needle butterfly connected to a peristaltic pump was inserted into the left ventricle and the flow was immediately started. The right atrium was open by a small cut to ensure the blood to flow out of the body instead of re-circulating in it. The position of the needle was tightly fixed in order to prevent it from piercing through the ventricle. With help of the peristaltic pump, warm HBSS was forced through the aorta to clean the blood vessels. After 2-3 min, the tubing of the pump was changed carefully from HBSS to the appropriate cold fixative (4.0% PFA in PB for IHC analysis and K&S solution for Epon embedding and EM analysis) without introducing any air bubbles into the system and then the mouse was let to be perfused with 20-40 ml of the cold fixative. Fixed brain, optic nerve, spinal cord, and sciatic nerves were dissected and placed in cold perfusion fixative (in a scintillation plastic vial) for post-fixation. Tissues for paraffin embedding were post-fixed (O/N) in 4.0% PFA in PB. Tissues intended for Epon embedding and EM analysis were postfixed (O/N) in K&S solution and can be kept longer than O/N in this fixative. For very long storages, tissues should be transferred into 1.0% PFA to avoid over-fixation.

#### **3.2.6.2 Procedures for tissue embedding**

##### **Paraplast impregnation and embedding of the tissue**

After the post-fixation, the tissue was washed 3 to 4 times with PBS. The brains were cut into half for sagittal sectioning and transferred into plastic perforated chambers for dehydration and paraplast impregnation. Spinal cords (cut into 3 to 4 pieces) and sciatic nerves were first embedded in 2.0% agar blocks and then also placed into plastic perforated chambers. An

automated system was used for dehydration and paraplast impregnation. The tissue was dehydrated by incubating them in an increasing alcohol concentration at RT:

- ❖ 50% Ethanol (1 hour)
- ❖ 70% Ethanol (2 times, 1 hour each)
- ❖ 96% Ethanol (2 times, 1 hour each)
- ❖ 100% Ethanol (2 times, 1 hour each)
- ❖ Isopropanol (1 hour)
- ❖ Xylene (2 times, 2 hours each)

After dehydration, the tissue was impregnated 2 times with paraplast for 2 hours each at 60°C. Embedding molds were filled with molten paraplast. The tissue was then immediately transferred into these paraplast-filled molds by using hot forceps. Labelled casts were placed on the filled molds. Tissue blocks with casts were left to harden on a cold plate. Blocks were removed from the molds and stored stably and for years at room temperature.

### **Epon embedding**

Tissues for subsequent EM imaging were embedded using an automated system in a multi step process involving osmification, dehydration and Epon impregnation. Epon mix was prepared 30 min prior to embedding. Before embedding, tissues were washed from the fixative with 0.1 M phosphate buffer and placed into plastic chambers. Chambers were then placed into the machine for embedding and tissues were processed using following settings:

- ❖ Phosphate buffer (3 times, 10 min each, at 4°C)
- ❖ 2.0% OsO<sub>4</sub> (4 hours, at 4°C)
- ❖ ddH<sub>2</sub>O (3 times, 10 min each, at 4°C)
- ❖ 30% Ethanol (20 min, at 4°C)
- ❖ 50% Ethanol (20 min, at 4°C)
- ❖ 70% Ethanol (20 min, at 4°C)
- ❖ 90% Ethanol (20 min, at 4°C)
- ❖ 100% Ethanol (4 times, 10 min each, at 4°C)
- ❖ Propylenoxide (3 times, 10 min each, at RT)
- ❖ Propylenoxide/Epon, 2:1 (2 hours, at RT)
- ❖ Propylenoxide/Epon, 1:1 (2 hours, at RT)



- ❖ Propylenoxide/Epon, 1:2 (4 hours, at RT)
- ❖ Epon (4 hours, at RT)

Tissues were then placed into labelled and Epon-filled molds and left (O/N) at 60°C for Epon polymerization.

### 3.2.6.3 Tissue sectioning

Cooled paraffin blocks of embedded tissue were cut into 5-7 µm thick sections by using a microtome. Sections were transferred into a water bath filled with 42°C -warm water to flatten the tissue. Floating sections were picked with positively charged glass slides and left to dry (O/N) at 37°C.

Epon embedded tissue was cut with diamond knives (Diatome Histo 45° and Ultra 45°) into semi- (500 nm) and ultra-thin (50 nm) sections, respectively, by using a microtome. Each section cut was released from the block into a water filled pool on the knife holder. For light microscopy, floating 500 nm sections were picked and collected on a glass slide, dried on a hot plate at 60°C and stained. For electron microscopy, 50 nm sections were placed on a slot grid coated with Formvar polyvinyl and contrasted.

### 3.2.6.4 Haematoxylin-Eosin (HE) staining

Haematoxylin-Eosin (HE) staining is used to obtain information of the overall tissue structure. Basophilic nuclei were stained by haematoxylin in dark purple and cytoplasm is stained by eosin in pink, which enables the cells to be easily differentiated.

Paraffin sections were first incubated at 60°C for 10 min before being de-paraffinised. For de-paraffinisation, the slides were incubated 2 times for 10 min each in Xylol and then once for 10 min in Xylol/Isopropanol (1:1). This was followed by re-hydration of the slides by incubating them for 5 min in the alcohol solutions with decreasing concentrations (100%, 90%, 70%, and 50%). After 5 min wash in ddH<sub>2</sub>O, sections were stained with 0.1% Haematoxylin for 5 min and washed again with ddH<sub>2</sub>O. To differentiate the dark purple coloration, sections were dipped once in HCl-Alcohol solution. To stop the differentiation process and properly develop the color, sections were incubated for 5 min in Scott's blueing solution. After a short rinse in ddH<sub>2</sub>O to remove excessive salts, they were counterstained with 0.1% Eosin for 3-5 min to reveal cellular details.

The excess dye was washed off with ddH<sub>2</sub>O. Sections were dehydrated by incubating them for 5 min in the alcohol solutions with increasing concentrations (50%, 70%, 90%, and 100%). Sections were then incubated for 10 min in Xylol/Isopropanol (1:1) and 2 times for 10 min each in Xylol. At the end, they were mounted with the Xylol based mounting medium Eukitt.

### 3.2.6.5 DAB-based immunodetection on the paraffin sections

This method is based on the enzymatic reaction of Horseradish Peroxidase (HRP) conjugated to a secondary antibody and DAB substrate, which forms a stable brown precipitate that can be visualized with light microscopy (Harlow and Lane, 1988).

Paraffin sections were de-paraffinised and re-hydrated as described in section 3.2.7.4. After 5 min wash in ddH<sub>2</sub>O, sections were incubated for 5 min in citrate buffer. For antigen retrieval, sections were cooked for 10 min in boiling citrate buffer at 650 W in a microwave. Sections were left in citrate buffer for 20 min or longer at RT to cool them down. Sections planned to be stained with SIRT2 (polyclonal rabbit, Santa Cruz) antibody were treated with proteinase K (diluted 1:500 in PBS) for 1 min at 37°C. This was followed by a 5 min wash in Tris buffer with 2.0% milk powder. Slides with sections were fixed with plastic cover plates and then washed with Tris buffer with 2.0% milk powder to adjust the proper flow. Endogenous peroxidases were inactivated by incubating the slides with 100 µl of 3.0% Hydrogen peroxide for 5 min. To minimize the unspecific binding of the antibody and to reduce the background staining, the blocking of free sites on the tissue sections was achieved by incubating the slides with 100 µl of Goat serum diluted in PBS/BSA (1:5) for 20 min at RT. Sections were incubated in 100 µl of the primary antibody diluted in PBS/BSA (O/N) at 4°C. Next day, sections were washed with Tris buffer with 2.0% milk powder in order to remove excess or unbound primary antibodies. They were incubated with 100 µl of the bridging antibody i.e. biotinylated secondary antibody (Dako LSAB2, yellow bottle: solution A) for 10 min at RT. After washing in Tris buffer with 2.0% milk powder, 100 µl of tertiary antibody i.e. HRP-Streptavidine complex (Dako LSAB2, red bottle: solution B) was applied onto the sections and they were incubated for 10 min at RT. Sections were washed with Tris buffer without milk powder to wash off unspecifically bound antibodies. Then slides and plastic cover plates were disassembled and 100 µl of DAB substrate solution (1.0 ml Dako Substrate buffer with 2 drops of DAB) was applied on the sections. After 10 min, sections were rinsed with ddH<sub>2</sub>O twice for 5 min. Sections were counterstained with Haematoxylin for 30 sec, and then dehydrated and mounted as described in section 3.2.7.4.

### 3.2.6.6 Automated staining using the Ventana Discovery® XT System

Automated stainings for some antibodies and for some experiments were performed by the Discovery XT Staining Module (Ventana Medical Systems Inc.) with DAB MAP Kit. The slides were de-paraffinised according to manufacturer's protocol. Tris-EDTA-buffer, pH 8.0 (Cat. # 950-124, Ventana Medical Systems Inc.) was used as cell conditioner. Sections planned to be stained with SIRT2 (polyclonal rabbit, Santa Cruz) antibody were treated with protease (supplied by the manufacturer) for 4 min. The following steps were carried out according to manufacturer's instructions. The primary antibodies were diluted in PBS/BSA and titrated manually. The slides were incubated in primary antibodies for 60 min. For the slides stained with primary antibodies derived from rat, the biotinylated secondary anti-rat IgG antibody was applied manually in a dilution of 1:100 and incubated for 20 min. For mouse and rabbit antibodies, Universal Secondary Antibody (supplied by the manufacturer) was used. The counterstaining was performed by treating the slides with Haematoxylin counterstain (Cat. # 760-2021, Ventana Medical Systems Inc.) for 4 min at 37°C. Bluing reagent (Cat. # 760-2037, Ventana Medical Systems Inc.) was applied for post-counterstaining for 4 min. After the staining procedure was complete, the slides were removed from the machine and rinsed in ddH<sub>2</sub>O with soap to remove oil residues. Sections were then dehydrated and mounted as described in section 3.2.7.4.

### 3.2.6.7 Methylene blue-Azur II staining of semithin sections

To stain myelin on semithin sections, freshly prepared Methylene blue-Azur II working solution was applied through a syringe filter tip onto the dry slides on a hot plate at 60°C. After 1 min of incubation, the Methylene blue-Azur II was washed with ddH<sub>2</sub>O and slides were left to dry. Slides were finally mounted with Eukit.

### 3.2.6.8 Tissue contrasting for electron microscopy

Grids were placed with the shiny side up on the drops and treated as follows:

- ❖ 30 min Uranyl acetate (light sensitive)
- ❖ 3 times 1 min ddH<sub>2</sub>O
- ❖ 6 min Reynolds lead citrate
- ❖ 4 times 1 min ddH<sub>2</sub>O

Grids were carefully dried with a stripe of filter paper.

### **3.2.6.9 Freeze substitution of high-pressure frozen samples**

Freeze substitution of high-pressure frozen samples were carried out by Dr. Wiebke Möbius and Torben Ruhwedel according to the protocol standardized in the lab.

### **3.2.7 Imaging**

The light microscopic observations were performed by using a Zeiss Axiophot and Leica DMRX4 microscope. The following objectives were used: 4X (achroplan, 4x/0.10), 10X (achroplan, 10x/0.30), 20X (planneofluar, 20x/0.50), 40X (planneofluar, 40x/0.75), 100X (planneofluar, 100x/1.30 Oil) and 100X/1.40 Oil PH3. The images were captured by a Kappa camera system (Kappa optoelectronics GmbH, Gleichen, Germany) and the Kappa Image Base Software (2.7.2. version).

### **3.2.8 Morphometry and quantifications**

Light microscopic images or digitalized electron micrographs were analysed by ImageJ software to quantify the DAB-based stainings on paraffin sections or to count the myelinated/unmyelinated axons and to make g-ratio calculations on EM images. The g-ratio was determined by dividing the circumference of an axon (without myelin) by the circumference of the same axon including myelin. The calculations were performed by Microsoft Office Excel, 2003. More than 100 randomly chosen axons per animal were analysed. Statistical analysis was performed by using GraphPad Prism 5 software.

### **3.2.9 Animal maintenance, handling and experiments**

All mouse mutants used in this study were maintained and bred in the animal facility of the Max-Planck-Institute of Experimental Medicine. Experiments were in compliance with the animal policies of the Max-Planck-Institute of Experimental Medicine, approved by the German federal state of Niedersachsen. Only male animals at the indicated age were used unless indicated.

### 3.2.9.1 Genotyping of the mouse mutants

At the 3 weeks of age, mice tail biopsies were taken. DNA for genotyping was prepared as described in section 3.2.1.1. Genotyping PCRs were performed by using the primers listed in section 3.1.8.1.

20 µl genotyping PCR reaction:

- 1 µl tail DNA (diluted 1:2 or 1:5)
- 1-2 µl genotyping forward primer (10 pM)
- 1-2 µl genotyping reverse primer (10 pM)
- 2 µl dNTP mix (2 mM)
- 2 µl 10x RedTaq buffer or 4 µl 5x GoTaq buffer (green)
- 0.8 µl Betaine (optional)
- 1 µl RedTaq polymerase (1.0 U/µl) or 0.15 µl GoTaq polymerase (5.0 U/µl)
- (ddH<sub>2</sub>O up to 20 µl)

PCR programs:

<b>CNP<sup>null</sup></b>	<b>5xFAD</b>	<b>PLP<sup>null</sup></b>	<b>Sirt2<sup>null</sup></b>
1. 95°C, 3 min	1. 95°C, 2 min	1. 95°C, 2.5 min	1. 95°C, 2 min
2. 56°C, 30 sec	2. 66°C, 25 sec	2. 56°C, 30 sec	2. 61°C, 30 sec
3. 72°C, 1 min	3. 72°C, 40 sec	3. 72°C, 1 min	3. 72°C, 45 sec
4. 95°C, 30 sec	4. 95°C, 25 sec	4. 95°C, 30 sec	4. 95°C, 30 sec
(step 2 to 4, 37 cycles)	(step 2 to 4, 30 cycles)	(step 2 to 4, 36 cycles)	(step 2 to 4, 30 cycles)
5. 56°C, 1 min	5. 66°C, 1 min	5. 56°C, 1 min	5. 61°C, 1 min
6. 72°C, 10 min	6. 72°C, 10 min	6. 72°C, 10 min	6. 72°C, 10 min
7. 4°C	7. 4°C	7. 4°C	7. 4°C

### 3.2.9.2 Rotarod test

The rotarod test was performed during the light phase using the Accelerator Rotarod 7650 for mice, Ugo Basile, Italy (Jones & Roberts). The mice were habituated for 2 min on the motionless rod, then allowed for another 30 sec at constant speed of 4 rpm. The rotarod accelerator was set to the highest speed configuration (from 4 to 40 rpm), accelerating every 30 sec in increments of 4 rpm over the duration of 5 min (maximal trial time). Latency of the mice to fall from the rod after switching the machine to the acceleration mode was measured. The mice were subjected to 3 or 6 trials per day, with 2-3 min rest between each trial. Results of all trials on a single day were pooled to generate a mean and SEM. Results were compared by the two-tailed Student's t-test. Values of  $p < 0.05$  were considered significant.

### 3.2.9.3 Grid running

For the grid running experiment, mice were allowed to walk a total distance of 2 m on an elevated grid (dimensions: 50 x 10 cm), with a distance of 1 cm between the grid bars. The experiments were performed during the light phase and recorded. The videos, which were 4 times slowed down, were analyzed to count the number of slips of each mouse per 2 m distance travelled.

### 3.2.9.4 Acrylamide treatment

Groups of 6-to-9-week-old male mice were treated with acrylamide by adding it to the drinking water at 200 ppm. Each mouse was housed in separate cages throughout the experimental period. Mice were trained before acrylamide treatment on 3 consecutive days by performing on the rotarod as described in section 3.2.10.2. After initiation of acrylamide treatment, the rotarod performance of mice were tested every third or fourth day. Results of all 6 trials on one day were pooled to generate a mean and SEM. Results were compared by the two-tailed Student's t-test. Values of  $p < 0.05$  were considered significant.

### 3.2.9.5 EAE induction

To induce experimental autoimmune encephalomyelitis (EAE), MOG (35-55) peptide (2.5 mg/ml) was emulsified in complete Freund adjuvant (CFA). Female mice at the age of 6-8 weeks were immunized by subcutaneous bilateral injection (in the inguinal and the scapular area) of 200  $\mu$ l of MOG peptide, 50  $\mu$ l in each injection site ( $\pm$ 200  $\mu$ g total MOG peptide per mouse). Once right

after the immunization and once more 48 hours later, 500 ng of Pertussis toxin is administered intraperitoneally. The mice were clinically scored on a daily basis.

### Clinical scoring

0.5	loss of tail tip tone
1.0	loss of tail tone
1.5	ataxia mild walking deficits (slipping of the grid)
2.0	mild hindlimb weakness less frequent walking can grip the flipped grid with hindlimbs shortly twisting of the tail results into rotation of the whole body
2.5	moderate hindlimb weakness can not walk by itself, but after nudging can not grip the flipped grid with hindlimbs but can stay on a upright tilted grid (water and food have to be located inside the cage at this point.)
3.0	complete hindlimb weakness can not stay on upright tilted grid
3.5	hindlimbs plegic
4.0	moribund
5.0	death

**4. Results**



#### 4.1 Localization of SIRT2 protein in the central nervous system

SIRT2 has the strongest brain expression among all sirtuins. Several studies have shown oligodendrocytes to be the cell type in the central nervous system, in which SIRT2 is preferentially expressed (Li *et al.*, 2007; Michan and Sinclair, 2007; Southwood *et al.*, 2007; Werner *et al.*, 2007). In addition to these findings, several groups have found SIRT2 to be expressed in olfactory neurons, in neuronal NeuN-positive cell bodies of the cortex, in Purkinje cells, molecular layer neurons and fiber tracts in the cerebellum and in cultured hippocampal neurons (Yu *et al.*, 2005; Suzuki and Koike, 2007; Taylor *et al.*, 2008; Pandithage *et al.*, 2008; Maxwell *et al.*, 2011). Experiments to address the effects of the SIRT2 activity in different neurodegenerative models and the neuroprotective effects of its inhibition have been conducted so far in neuronal cells (Outeiro *et al.*, 2007; Suzuki and Koike, 2007; Luthi-Carter *et al.*, 2010).

As a first step in the project, we aimed to show the exact localization of SIRT2 in the central nervous system of mice. For that, we performed immunostaining of SIRT2 on sagittal brain sections of 3 month-old wild type mice by using an antibody recognizing the N-terminal of the protein (Santa Cruz, SC H95, sc-20966). The SIRT2 staining showed the localization of the protein predominantly in white matter tracts of the brain (Figure. 9). The protein was almost undetectable in gray matter of the cortex and the cerebellum, when staining intensities compared to very strong one in the corpus callosum and the white matter tracts of the cerebellum (Figure. 9).

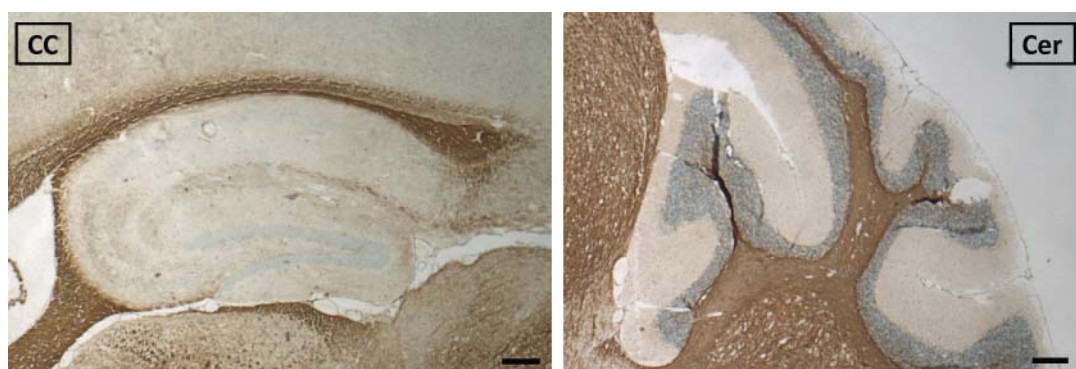


**Figure. 9 SIRT2 is enriched in white matter tracts of the brain.**

Immunostaining of SIRT2 on sagittal brain sections (5  $\mu\text{m}$  thick) of 3 month-old wild type mice showed the localization of the protein predominantly in white matter tracts. CC (corpus callosum), Cer (cerebellum). Scale bar, 200  $\mu\text{m}$ .

## 4.2 Analysis of the *Sirt2*<sup>null</sup> mice

Genetic deletion of the structural protein of the CNS myelin, proteolipid protein (PLP) resulted in an axonopathy in the CNS without any major myelin abnormalities (Griffiths *et al.*, 1998b; Edgar *et al.*, 2004). The major alteration in the protein composition of the Plp<sup>null</sup> myelin was the virtual absence of Sirtuin 2 (SIRT2) prior to the onset of axonal degeneration (Werner *et al.*, 2007). Due to these findings, we suggested that the axonal pathology observed in Plp<sup>null</sup> mice may be at least partially due to the lack of SIRT2.

To address this question, we aimed to analyze the mice lacking *Sirt2* expression. The complete *Sirt2*<sup>null</sup> mice were generated and provided by Dr. Maria Carla Motta (Massachusetts Institute of Technology, USA). In the following chapters, the experiments which were performed for the characterization of the mutant mice and for their analysis mainly in terms of myelination and axonal pathology will be explained in detail.

### 4.2.1 *Sirt2*<sup>null</sup> mice

The open reading frame of the wild type *Sirt2* gene was interrupted by the insertion of a puromycin cassette with the size of 2 kb in reverse orientation into exon 11 (Figure. 10A). PCR analysis to genotype the *Sirt2*<sup>null</sup> mice was designed to differentiate the mutant mice from the wild type by the amplification of 200 bp band which indicated the targeted allele (Figure. 10C). The targeted allele was successfully detected only in *Sirt2* homozygous and heterozygous mutant mice by using the primer (a) and the primer (b), which was designed to target the puromycin cassette (Figure. 10A). By sequence analysis, we investigated the exact position at which the puromycin cassette was inserted into exon 11 (Figure. 10B). The cassette was inserted right after the first 3 nucleotides (GAT) of the exon 11 and this insertion resulted in the introduction of an early stop codon into the open reading frame (Figure. 10B). Quantitative RT-PCR analysis indicated more than 50% reduction in *Sirt2* mRNA in the total brain of the mutant mice (Figure. 10D). This remaining mutant mRNA product was further analyzed by PCR (data not shown). Mutant mRNA was transcribed with the inserted puromycin cassette, and thereby presumably with a decreased stability. The introduction of the early stop codon into the open reading frame due to the insertion of the puromycin cassette is suggestive for an mRNA product translated into a non-functional SIRT2 protein. The targeting of the wild type *Sirt2* allele by this strategy did not alter the expression of the neighbouring genes, namely *Nfkbib* (nuclear factor of kappa light

polypeptide gene enhancer in B-cells inhibitor beta) and *Rin1* (Ras and Rab interactor like) (Figure. 10D).

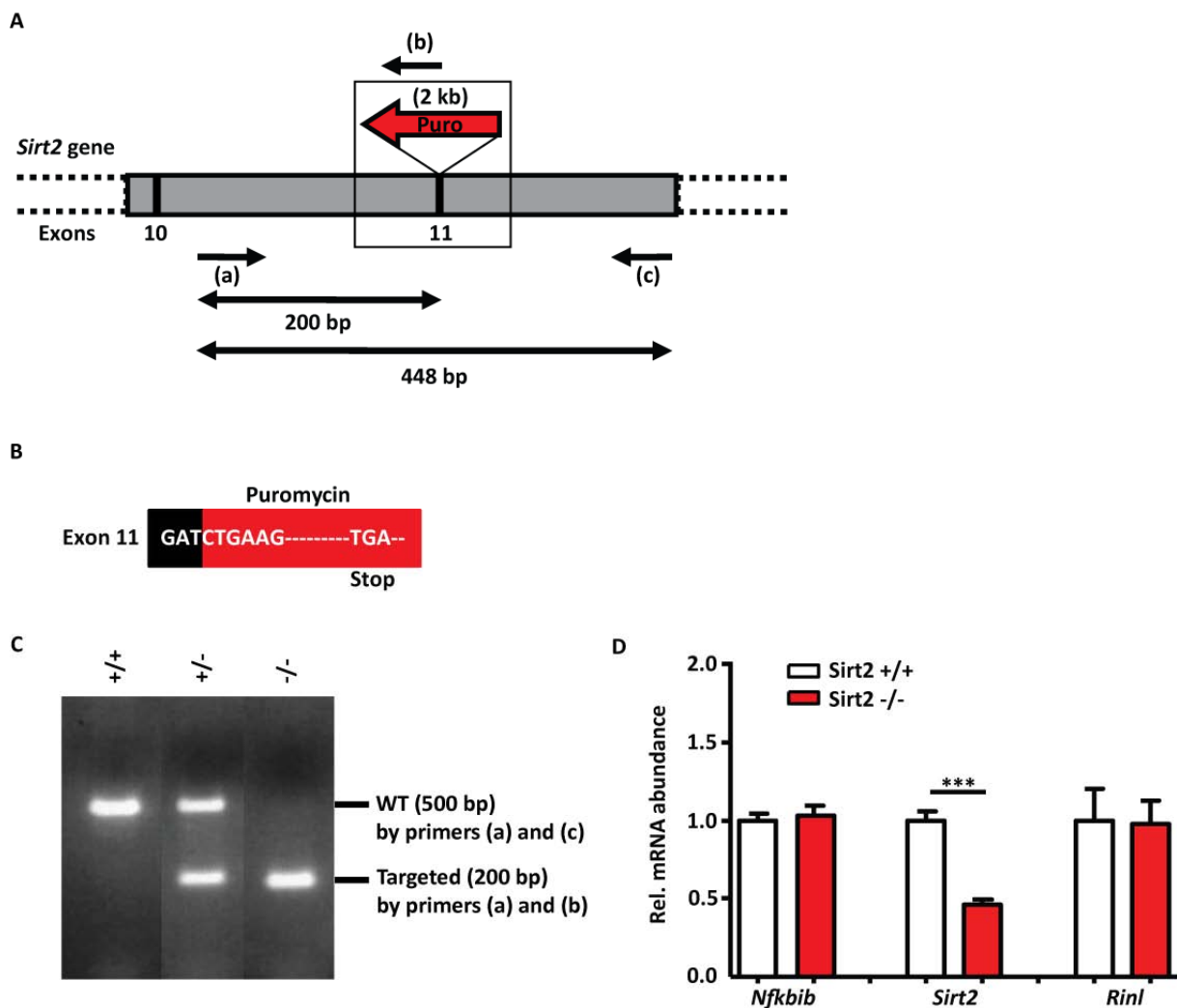


**Figure. 10** Genotyping the *Sirt2*<sup>null</sup> mice.

**(A)** Structure of the wild type *Sirt2* allele (with exons in black and introns in gray). Arrows (a, b and c) indicate positions of the primers. A puromycin cassette (puro) was inserted in reverse orientation into exon 11 to prevent the expression of a functional protein by interrupting the enzymatic center. **(B)** The detailed view of the boxed area in **(A)**. Sequence analysis revealed that the cassette was inserted right after the first 3 nucleotides (GAT) of the exon 11 and this insertion resulted in the introduction of an early stop codon into the open reading frame. **(C)** PCR-genotyping of *Sirt2* mutant mice. The primers (a) and (b) designed to detect the puromycin cassette resulted in the amplification of a 200 bp band only in *Sirt2* homozygous and heterozygous mutant, but not in wild type mice. **(D)** Quantitative RT-PCR detecting mRNA (*Sirt2* and 2 other genes flanking *Sirt2*) in total brain of adult wild type and *Sirt2*<sup>null</sup> mice. Quantitative analysis revealed more than 50% reduction in *Sirt2* mRNA in total brain. On the other hand, no change in mRNA abundance of the flanking genes *Nfkbib* (nuclear factor of kappa light polypeptide gene enhancer in B-cells inhibitor beta) and *Rin1* (Ras and Rab interactor like) was observed. Results were normalized to *Atp5b* and compared by the unpaired t-test (n=6). Values of p<0.05 were considered significant (\*\*\*p<0.0001). Error bars represent SEM. Rel.: relative.

By western blot analysis, we confirmed the absence of the SIRT2 protein in the mutant mice (Figure. 11). We used 2 different antibodies for this experiment. The antibody 1 was from Santa Cruz (sc-20966, H95) and recognizes an epitope located at the N-terminal of the SIRT2 protein. The antibody 2 was raised against C-terminal of mouse SIRT2 protein (Southwood et al., 2006). No protein was detected in the mutant brain (Figure. 11A), sciatic nerve (Figure. 11B) and myelin (Figure. 11C). Importantly, neither any truncated protein was observed in the mutant samples (data not shown). A clear reduction in the protein level was observed in the myelin samples from *Sirt2* heterozygous mutant mice (Figure. 11C).

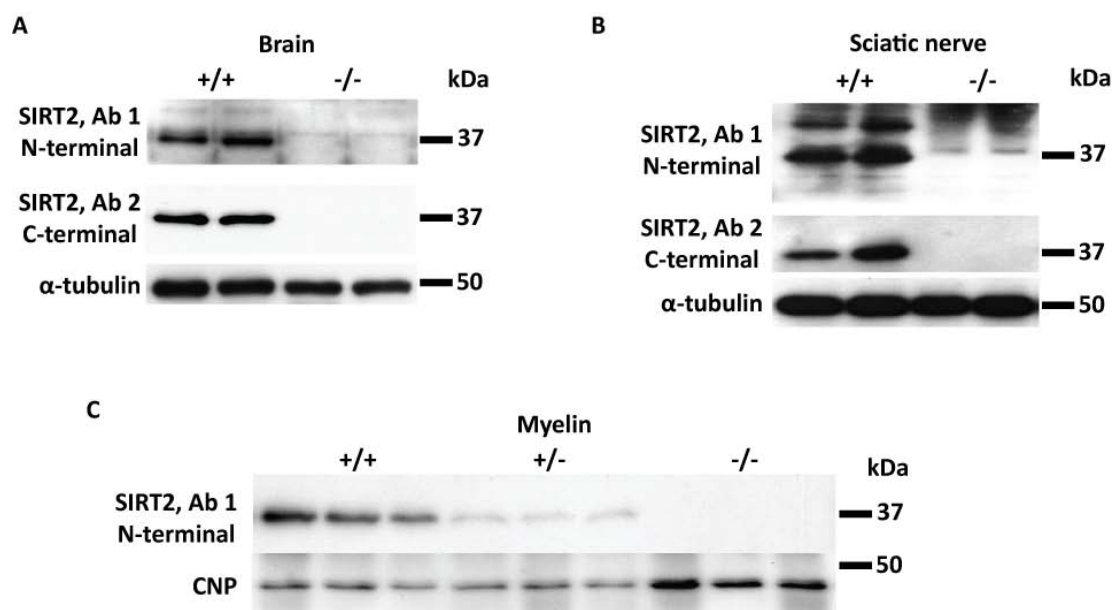


**Figure. 11 Absence of SIRT2 protein.**

Western blot analysis of protein lysates revealing a loss of SIRT2 in the brain (**A**), sciatic nerve (**B**) and myelin (**C**) of mutants compared to controls at the age of 2-3 months. The antibody 1 (Santa Cruz, sc-20966, H95) and antibody 2 (Southwood et al., 2006) against SIRT2 recognize the N-terminal and C-terminal of the protein, respectively. Note the reduction in the protein level in *Sirt2* +/- myelin compared to wild type (**C**). CNP and  $\alpha$ -tubulin were used as loading controls (n=2 (**A and B**) and n=3 (**C**) per genotype).

#### 4.2.2 Myelination in the absence of SIRT2

SIRT2 was shown to be enriched in myelin in an equivalent extent to that of PLP/DM20 and CNP (Werner *et al.*, 2007). We asked the question whether this myelin protein is indispensable for myelin formation and maintenance. To address this question, we used electron microscopy to analyze the optic nerves (Figure. 12) and sciatic nerves (Figure. 13) of adult (9 week-old) control and *Sirt2<sup>null</sup>* mice. Freeze substitution of high-pressure frozen samples and imaging were carried out in collaboration with Dr. Wiebke Möbius. We did not observe any principal alteration in myelin sheath thickness or ultrastructure in the absence of SIRT2 in the central and peripheral nervous systems. The axons of all calibers were wrapped with a myelin sheath of an apparently appropriate thickness and ultrastructure.

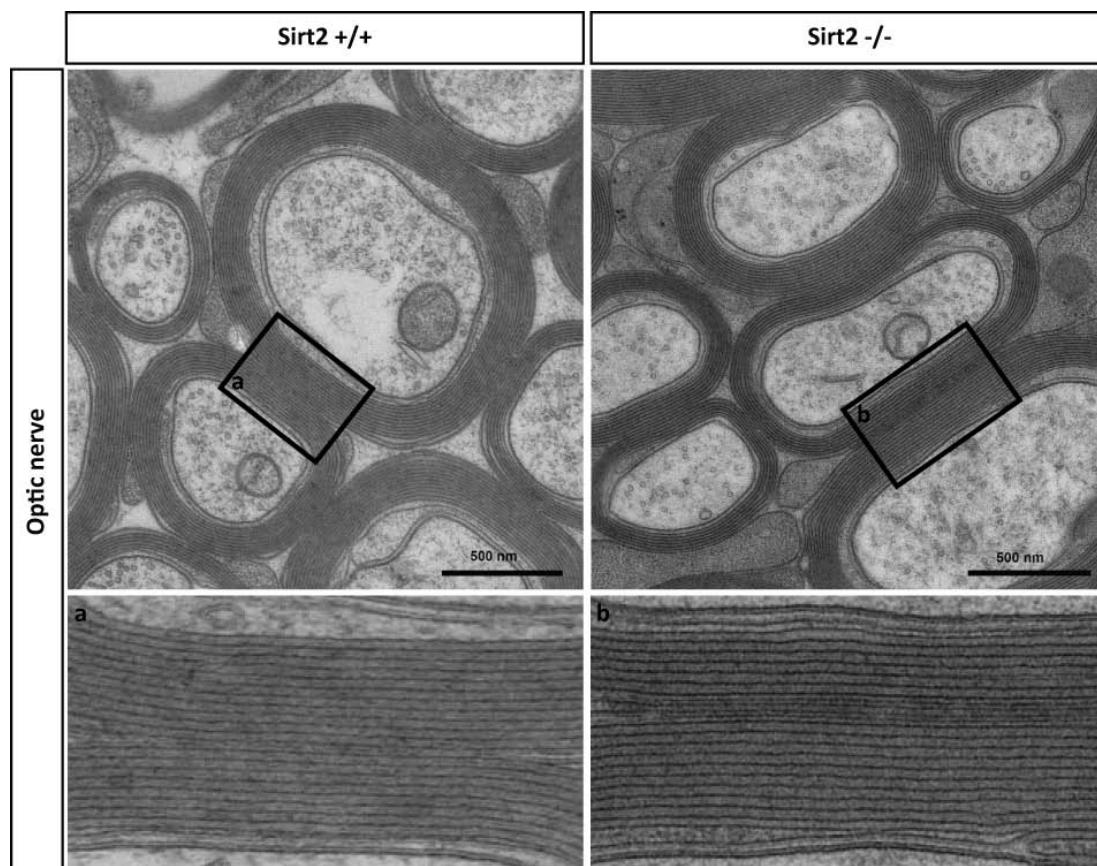


**Figure. 12** Normal myelination in CNS of *Sirt2<sup>null</sup>* mice.

Electron micrographs of 50 nm-thick cross sections from the optic nerves of 9 week-old control and *Sirt2<sup>null</sup>* mice. No principal alteration in myelin sheath thickness or ultrastructure was observed in the absence of SIRT2 in the central nervous system (CNS). The axons of all calibers were wrapped with a myelin sheath of an apparently appropriate thickness and ultrastructure. **a and b**, higher magnifications of the boxed areas. Scale bar, 500 nm.

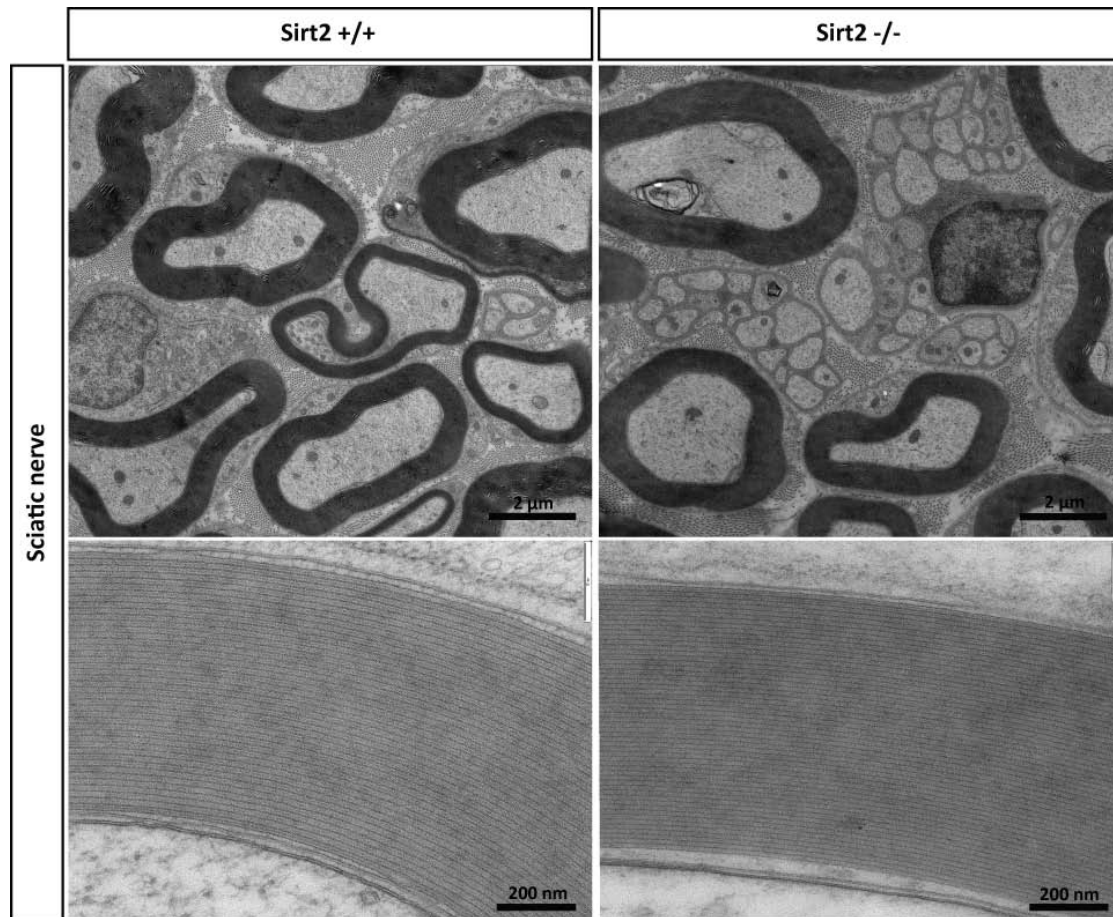


**Figure. 13 Normal myelination in PNS of  $Sirt2^{null}$  mice.**

Electron micrographs of 50 nm-thick cross sections from the sciatic nerves of 9 week-old control and  $Sirt2^{null}$  mice. No principal alteration in myelin sheath thickness or ultrastructure was observed in the absence of SIRT2 in the peripheral nervous system (PNS). The axons of all calibers were wrapped with a myelin sheath of an apparently appropriate thickness and ultrastructure. Bottom panel: images of myelin sheath at higher magnification are given. Scale bar, 2  $\mu\text{m}$  and 200 nm.

Additionally, we aimed to quantify the myelin sheath thickness and to analyze the axon diameter distribution. To achieve this, we analyzed electron micrographs of 50 nm-thick cross sections from the optic nerves and sciatic nerves of 2-3 month-old control and  $Sirt2^{null}$  mice (Figure. 14A and 15A). More than 150 axons per mouse were analyzed to measure the diameters of the axon and the complete fiber including the myelin sheath. The ratio of these 2 values was calculated to find out the g-ratio and to quantify the myelin sheath thickness. In neither of the tissues, a difference was observed in the mean of the g-ratio values among the 2 genotypes (Figure. 14B and 15B). Mutant mice had no change in the distribution of g-ratios of individual fibers over the axon diameter in either of the tissues, compared to the control mice (Figure. 14C and 15B). The material for this analysis was prepared prior to the PhD project start and parts of the data was

included into my Master Thesis manuscript from 2007. Quantification of the axon size distribution and the average axon diameter in both CNS and PNS revealed no obvious difference between mutant and control mice (Figure. 14D and E, 15 D and E).

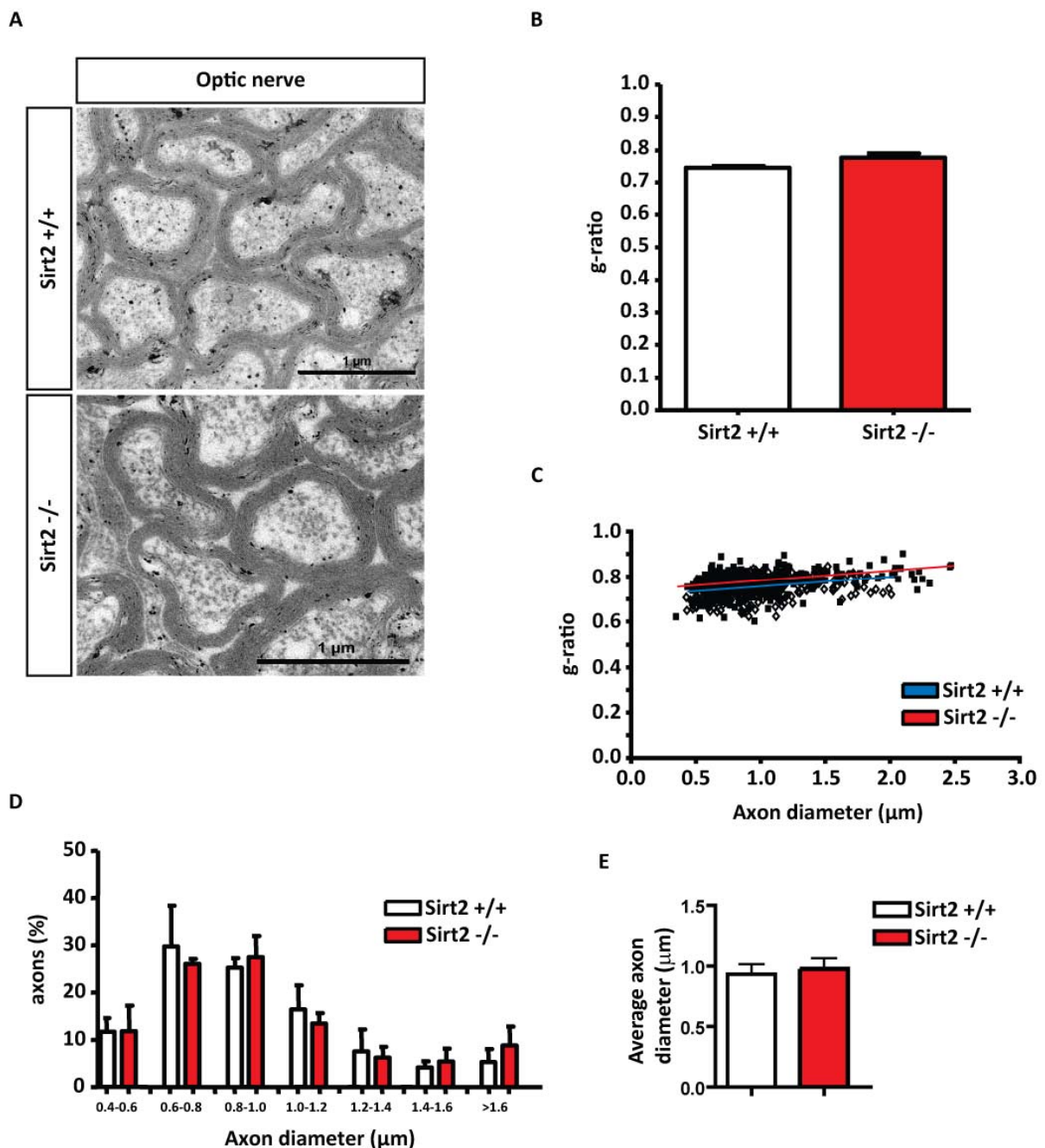


**Figure. 14** Quantification of myelin thickness and axon diameter in CNS of *Sirt2<sup>null</sup>* mice.

(A) Electron micrographs of 50 nm-thick cross sections from the optic nerves of 2-3 month-old control and *Sirt2<sup>null</sup>* mice were analyzed to calculate the myelin thickness and axon diameters. Scale bar, 1 µm. (B and C) Normal myelin sheath thickness (g-ratios) in the optic nerve of mutant and wild type mice. Mean g-ratio values of 3 animals per genotype were calculated and plotted as bar graph (B). g-ratios of individual fibers were plotted versus axon diameter as a Scatter plot in (C) (white and black boxes show the values for wild type and mutant, respectively). Quantification of the axon size distribution (D) and the average axon diameter (E) in the optic nerve revealed no obvious difference between mutant and control mice. Error bars represent SEM.

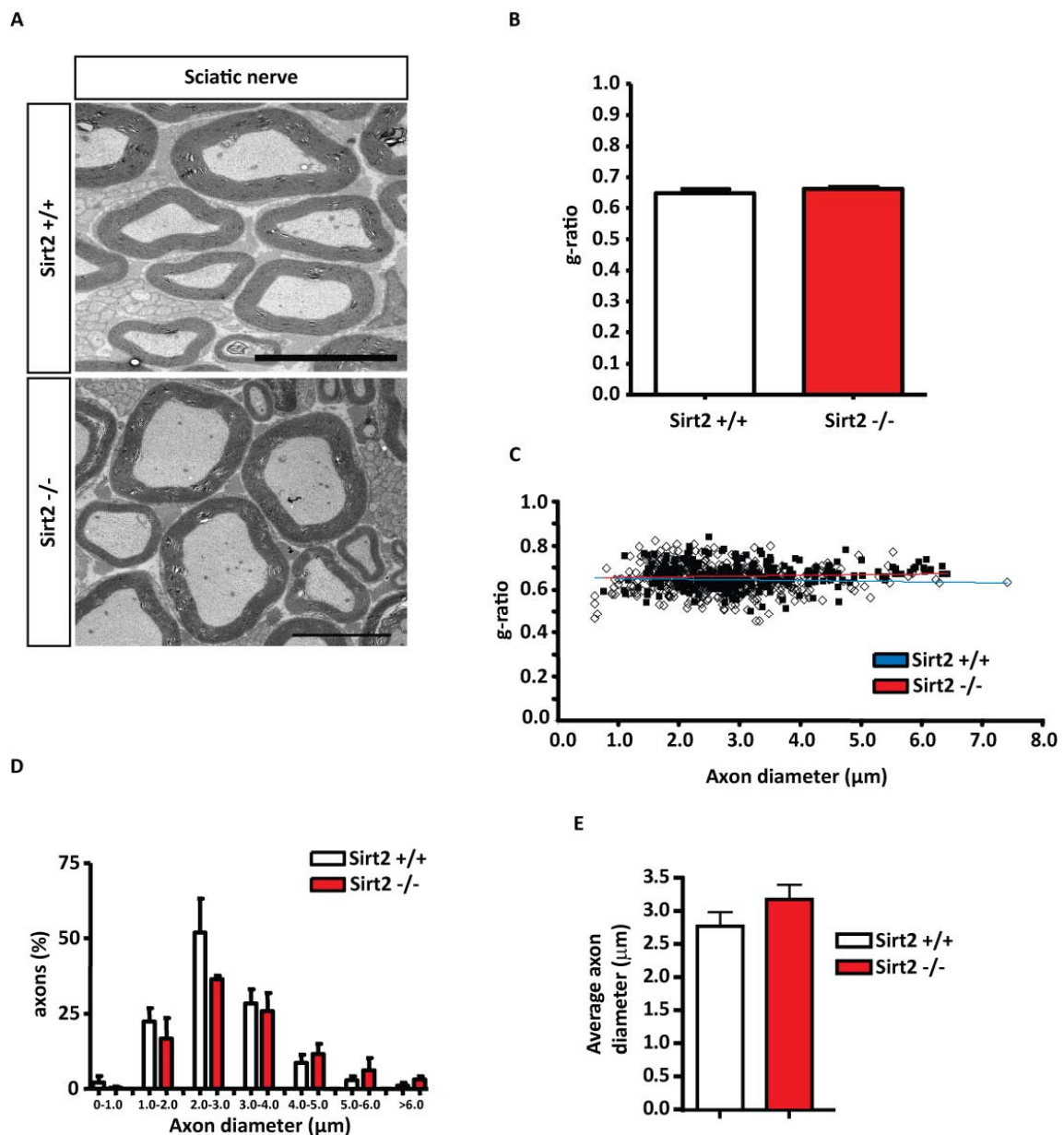


**Figure. 15** Quantification of myelin thickness and axon diameter in PNS of *Sirt2<sup>null</sup>* mice.

Electron micrographs of 50 nm-thick cross sections from the sciatic nerves of 2-3 month-old control and *Sirt2<sup>null</sup>* mice were analyzed to calculate the myelin thickness and axon diameters. Scale bar, 5  $\mu\text{m}$ . **(B and C)** Normal myelin sheath thickness (g-ratios) in the sciatic nerve of mutant and wild type mice. Mean g-ratio values of 3 animals per genotype were calculated and plotted as bar graph **(B)**. g-ratios of individual fibers were plotted versus axon diameter as a Scatter plot in **(C)**. (white and black boxes show the values for wild type and mutant, respectively). Quantification of the axon size distribution **(D)** and the average axon diameter **(E)** in the sciatic nerve revealed no obvious difference between mutant and control mice. Error bars represent SEM.



The next step was to attempt to investigate the protein composition of the mutant myelin. We enriched myelin from the total brain lysates of 3 month-old control and mutant mice. We subjected these samples to one-dimensional separation by SDS-PAGE and stained the proteins by Silver impregnation to gain information on the protein repertoire of mutant myelin (Figure. 16A). The qualitative comparison did not reveal any difference between the genotypes. To compare the abundances of specific myelin proteins, we performed western blot experiment on CNS myelin preparations using antibodies against PLP/DM20, Septin8, myelin oligodendrocyte glycoprotein (MOG), and myelin basic protein (MBP). Steady state levels of these myelin proteins were unaltered in *Sirt2<sup>null</sup>* myelin (Figure. 16B). The only difference detected was increased protein level of CNP in *Sirt2<sup>null</sup>* myelin and sciatic nerve (Figure. 16C). This increase in the CNP protein abundance was not due to an up-regulation of the expression of *Cnp* gene (Figure. 16D).

In order to assess any defect in the early stages of CNS myelination because of the absence of SIRT2, we chose to investigate developing mutant brains at postnatal day 10. We dissected different regions of P10 brains and prepared protein lysates for further analysis. We focused on the brain regions like cerebellum (Figure. 17A) and brain stem (Figure. 17B), which start to be myelinated at earlier days. We compared the abundances of a number of myelin proteins (CNP, MOG and MAG) in *Sirt2<sup>null</sup>* brain regions to littermate controls. Densitometric quantification revealed no difference in the abundance of myelin proteins analyzed between the genotypes in myelinating regions of P10 brain (Figure. 17). There was a tendency towards an increase in CNP protein level in the cerebellum; however, this difference is not statistically significant ( $p=0.3380$ ) (Figure. 17A, left).

To address the question whether the onset of peripheral myelination was affected by the absence of SIRT2, we analyzed the methylene blue-Azur II stained semithin cross sections of the sciatic nerves at postnatal day 5, by using light microscopy. We observed a comparable number of axons being myelinated in both genotypes; however, numbers were not quantified (Figure. 18).

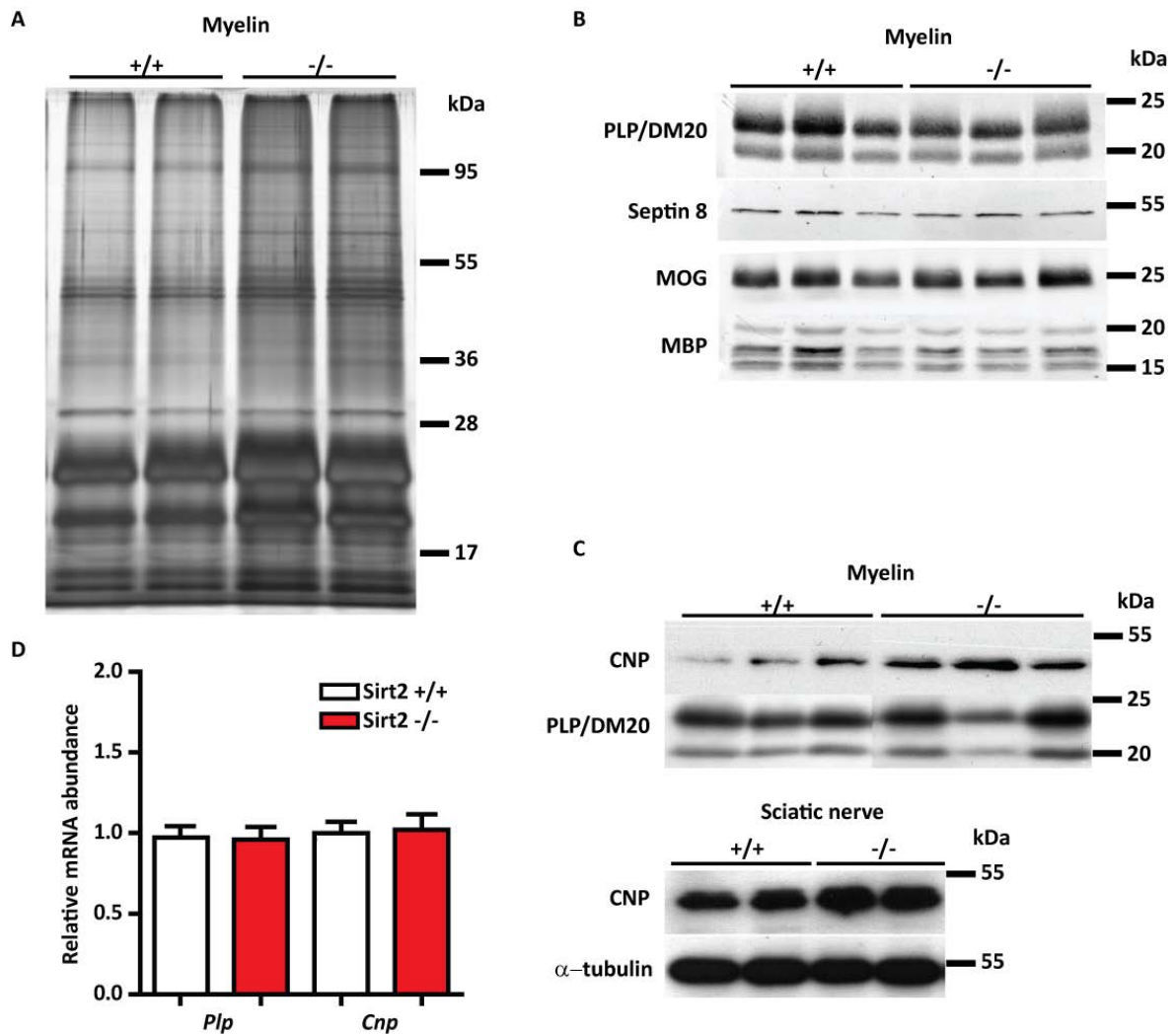


**Figure. 16** Levels of myelin proteins in *Sirt2*<sup>null</sup> mice.

**(A)** Protein lysates of myelin enriched samples from 3 month-old control and mutant mice were applied to one-dimensional separation by SDS-PAGE. Proteins were visualized by Silver staining. No difference was observed between the genotypes in terms of protein repertoire ( $n=2$  per genotype). **(B)** Semi-quantitative comparison of myelination by western blotting myelin proteins of CNS myelin preparations from mutant mice (age 3 months) and littermate controls. Steady state levels of PLP/DM20, Septin8, myelin oligodendrocyte glycoprotein (MOG), and myelin basic protein (MBP) are normal ( $n=3$  per genotype). **(C)** Semi-quantitative comparison by western blotting revealed increased protein level of CNP in *Sirt2*<sup>null</sup> myelin and sciatic nerve (bottom lane). Age: 2-3 months,  $n=2-3$  per genotype, loading controls: PLP/DM20 and  $\alpha$ -tubulin. **(D)** Quantitative RT-PCR analysis revealed no change in the expression of *Plp* and *Cnp* genes in total brain of adult mutant mice. Results were normalized to *Atp5b* ( $n=6$ ). Error bars represent SEM.

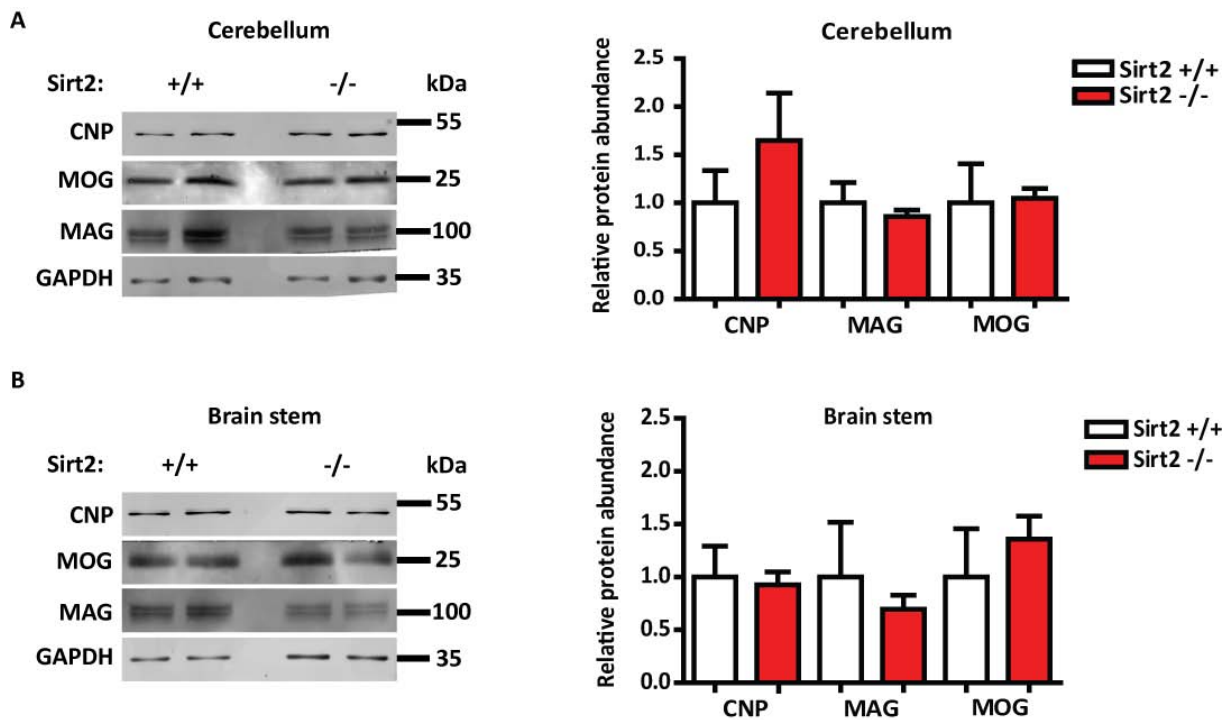


**Figure. 17** Quantification of myelin proteins in developing CNS of *Sirt2<sup>null</sup>* mice.

(**A and B**) Left: Western blot analysis of protein lysates showing the abundance of myelin proteins (CNP, MOG, and MAG) in the cerebellum and brain stem of mutant compared to control mice at the postnatal day 10 (n=2 per genotype shown). Right: Densitometric quantification revealed no difference in the abundance of myelin proteins analyzed between the genotypes in either of the brain regions at this age. Peak intensities ( $\pm$ SEM) were normalized to GAPDH (n=3 per genotype).

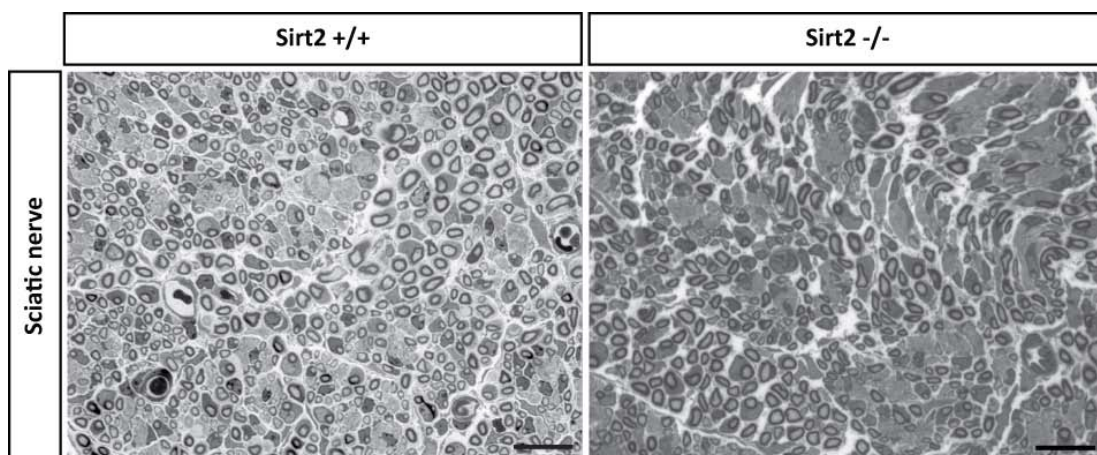


**Figure. 18** A closer look into peripheral myelination in *Sirt2<sup>null</sup>* mice at postnatal day 5.

Light microscopy of 500 nm-thick cross sections from the sciatic nerves at postnatal day 5 (P5) demonstrated widespread myelination in control and *Sirt2<sup>null</sup>* mice. Scale bar, 10  $\mu$ m.

In a model of Huntington's Disease, the expression of genes responsible for sterol biosynthesis was reported to be significantly down-regulated by the genetic or pharmacological inhibition of SIRT2 (Luthi-Carter *et al.*, 2010). The question arose whether the absence of SIRT2 in our mutant mice could result into a similar alteration in the synthesis of myelin lipids. To address this question, we extracted lipids from myelin enriched samples of control and *Sirt2<sup>null</sup>* brains. Myelin lipids were investigated by thin layer chromatography (TLC). We detected all myelin lipids in proportional amounts in both genotypes (n=2 per genotype) (Figure. 19). In addition to this, we also investigated the expression levels of the genes, which were shown to be down-regulated upon the inhibition of SIRT2 by Luthi-Carter *et al.*, in *Sirt2<sup>null</sup>* brains. We did not detect any significant changes in the mRNA abundance of these genes due to the absence of SIRT2 in our mutant mice.

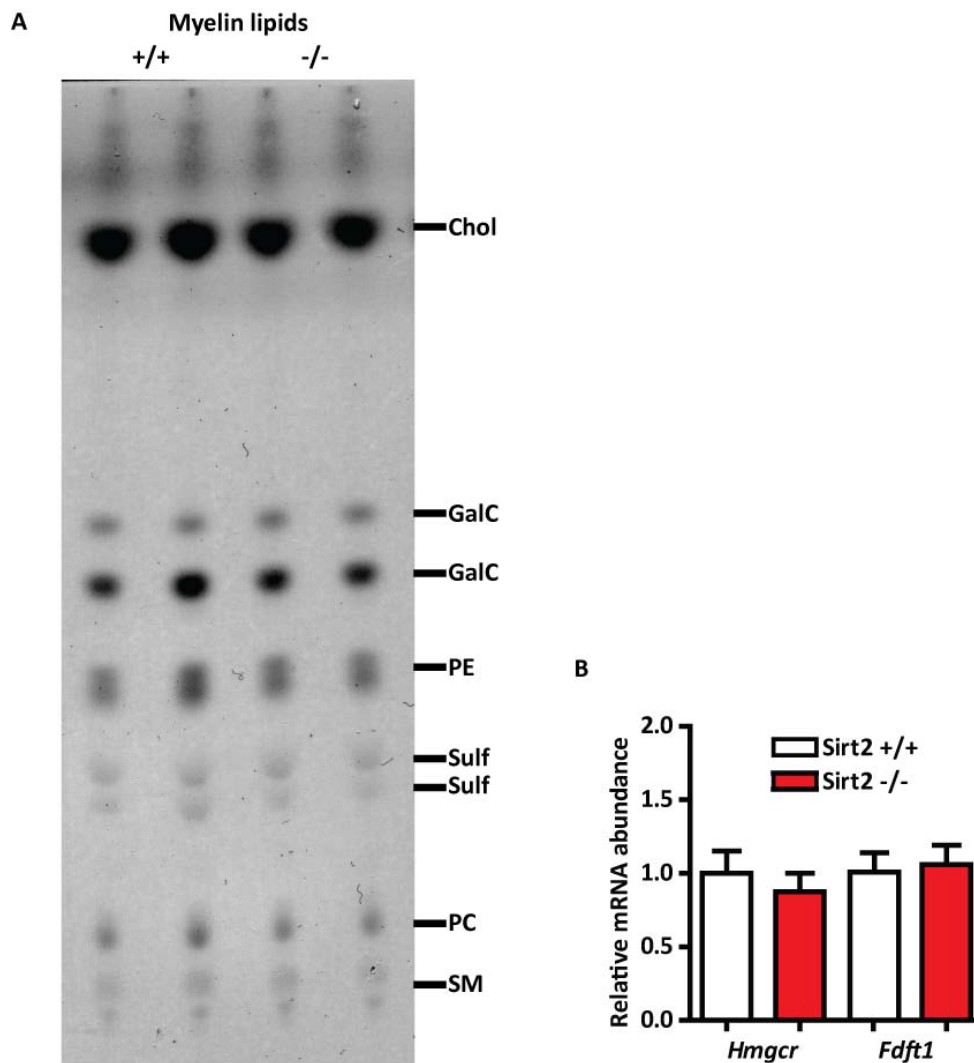


**Figure. 19 Analysis of the myelin lipids and expression of the genes regulating sterol biosynthesis in the absence of SIRT2.**

**(A)** Lipids were extracted from myelin enriched samples of 2 month-old control and *Sirt2<sup>null</sup>* brains and myelin lipids were investigated by thin layer chromatography (TLC). All myelin lipids in both genotypes were observed to be present in proportional amounts (n=2 per genotype). Chol: cholesterol, GalC: galactocerebroside, PE: phosphatidyl ethanolamine, Sulf: sulfatide, PC: phosphatidyl choline, SM: sphingomyelin. **(B)** Quantitative analysis revealed no change in the expression of the following genes in *Sirt2<sup>null</sup>* brains, which encode the major regulatory enzymes at sterol biosynthesis: *Hmgcr* (3-hydroxy-3-methylglutaryl-Coenzyme A reductase) and *Fdft1* (farnesyl-diphosphate farnesyltransferase 1 or squalene synthase). Results were normalized to *Top1* (n=6). Error bars represent SEM.

#### 4.2.3 Acetylation status of the proteins in the absence of SIRT2

SIRT2 is a myelin protein with a deacetylase function. The question arose what happens to the acetylation status of the myelin proteins in the absence of this deacetylase. To answer this question, we attempted to visualize the acetylated myelin proteins by western blot analysis and to identify any differential acetylation in the absence of SIRT2. For this experiment, we prepared CNS myelin fractions of all the 3 genotypes, including *Sirt2* heterozygous mice. TSA and nicotinamide were added into the homogenization and any other buffers used during the experiment to prevent unspecific deacetylation of proteins, at a final concentration of 500 nM and 10 mM, respectively. Membranes blotted with one-dimensionally separated myelin proteins were probed with antibodies against the acetylated lysine residues of the proteins.

Before conducting this experiment, the specificity of the antibodies was tested with a separate immunoblot experiment by using acetylated BSA as a competitive inhibitor. While incubating the antibody with acetylated BSA, all sites which are against acetylated lysine residues should be blocked by the competitive inhibitor. Therefore, pre-blocked antibody should not detect any protein at immunoblotting, if it is specific to what it was designed to detect. The specificity of both antibodies were confirmed by this approach (data not shown).

Two polyclonal antibodies from different companies exhibited slightly different binding affinities towards the same proteins. First antibody revealed certain proteins to be hyperacetylated in the *Sirt2* +/- and -/- myelin; however, this observation could not be confirmed by the second antibody (Figure. 20A).

SIRT2 has been reported to deacetylate  $\alpha$ -tubulin at the lysine-40 residue *in vitro* (North *et al.*, 2003). This makes it likely to observe hyperacetylated  $\alpha$ -tubulin in the absence of its deacetylase in our mutant mice. To clarify this, we checked the acetylation level of  $\alpha$ -tubulin in *Sirt2*<sup>null</sup> material by western blotting using an antibody which recognizes specifically the acetylated  $\alpha$ -tubulin. Neither in brain nor in myelin samples of *Sirt2*<sup>null</sup> mice, we observed hyperacetylated tubulin (Figure. 20B). Additionally, we investigated the acetylation level of  $\alpha$ -tubulin in the developing CNS of *Sirt2*<sup>null</sup> mice (Figure. 21A and B). At postnatal day 10, both control and mutant mice exhibited comparable levels of tubulin acetylation in cerebellum and brain stem (Figure. 21C).

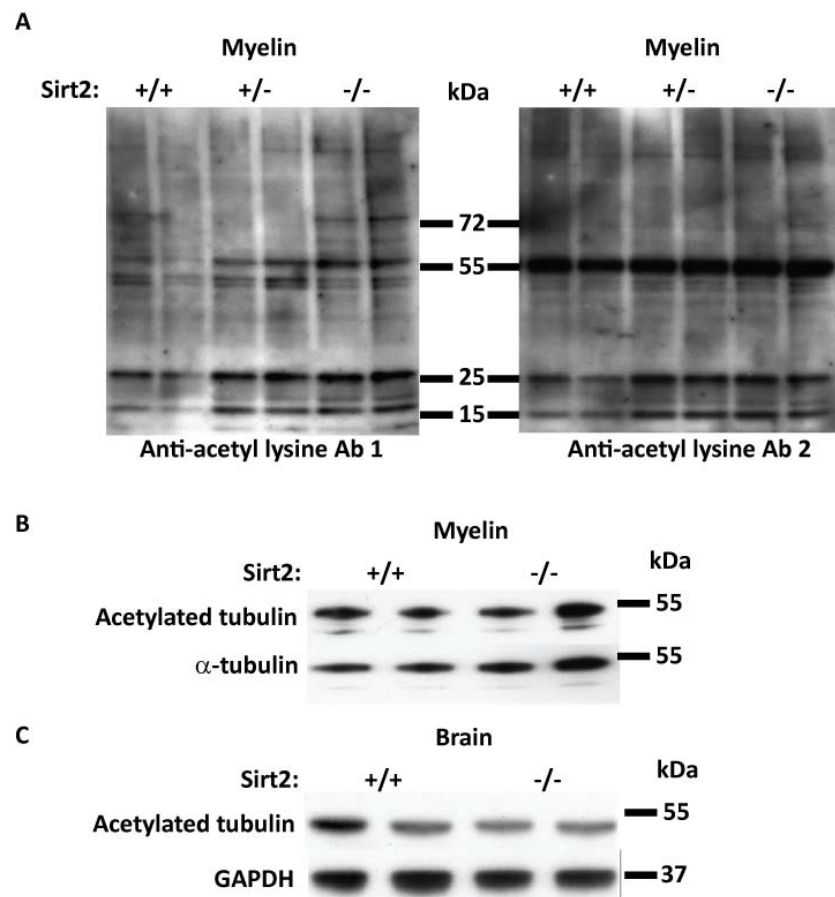


**Figure. 20** Acetylation levels of myelin proteins and  $\alpha$ -tubulin in the absence of SIRT2.

**(A)** Western blot analysis of acetylated proteins in myelin enriched samples of 2.5 month-old Sirt2 +/+, +/- and -/- mice by using two different antibodies against acetyl lysine residues of proteins (n=2 per genotype). The antibodies exhibited slightly different binding affinities towards the same proteins. First antibody revealed certain proteins to be hyperacetylated in the Sirt2 +/- and -/- myelin; however, this observation could not be confirmed by the second antibody. Ab 1: polyclonal rabbit antibody against acetyl lysine from Cell Signaling, Ab 2: polyclonal rabbit antibody against acetyl lysine from Immunechem. **(B and C)** Western blot analysis of acetylated tubulin showed lack of hyperacetylation of this protein in 2.5 month-old Sirt2<sup>null</sup> myelin and brain, respectively (n=2 per genotype, loading controls:  $\alpha$ -tubulin and GAPDH).

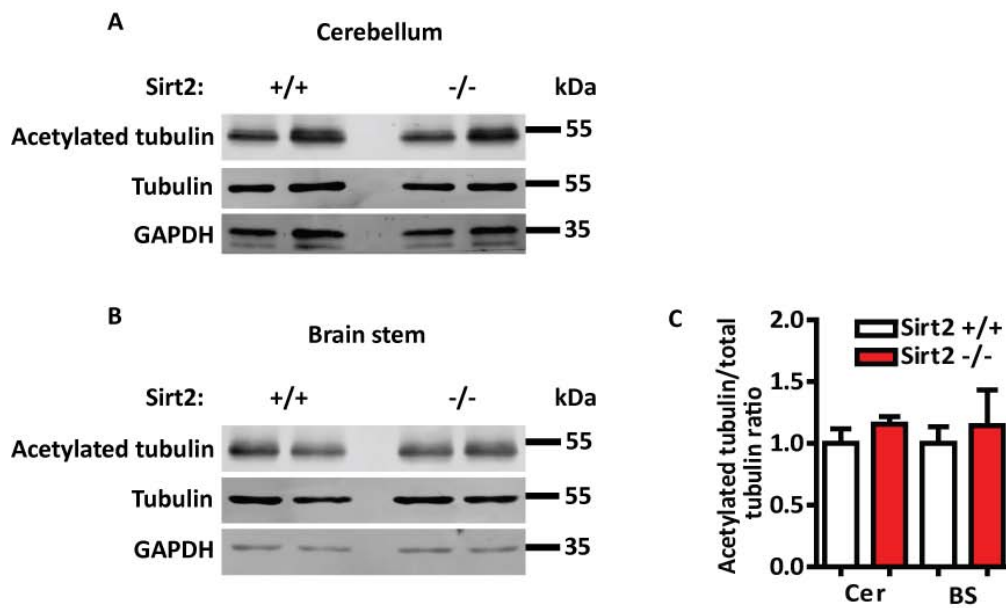


**Figure. 21** Acetylation levels of  $\alpha$ -tubulin in the developing CNS of *Sirt2<sup>null</sup>* mice.

**(A and B)** Western blot analysis of protein lysates showing the acetylated tubulin in the cerebellum and brain stem of mutant compared to control mice at postnatal day 10 (n=2 per genotype shown). **(C)** Densitometric quantification reveals no difference in the acetylation levels of  $\alpha$ -tubulin between the genotypes in either of the brain regions at this age. Peak intensities ( $\pm$ SEM) were normalized to GAPDH (n=3 per genotype). Cer (cerebellum), BS (brain stem)

#### 4.2.4 Expression levels of other sirtuins and cytoplasmic HDACs in the absence of SIRT2

Except from SIRT2, sirtuin family has six more members in mammals. All members possess the same  $\text{NAD}^+$ -dependent enzymatic activity. We asked the question whether there was any compensation taking place by an up-regulation of the expression of any of the other sirtuins, when SIRT2 was missing. Therefore, we performed quantitative RT-PCR experiment to investigate the expression of *Sirtuin* genes in the brain of adult mutant mice. The abundance of *Sirt5*, one of the mitochondrial sirtuins and *Sirt7*, which localizes in the nucleolus was detected increased in *Sirt2<sup>null</sup>* brain, whereas the others remain unaltered (Figure. 22).



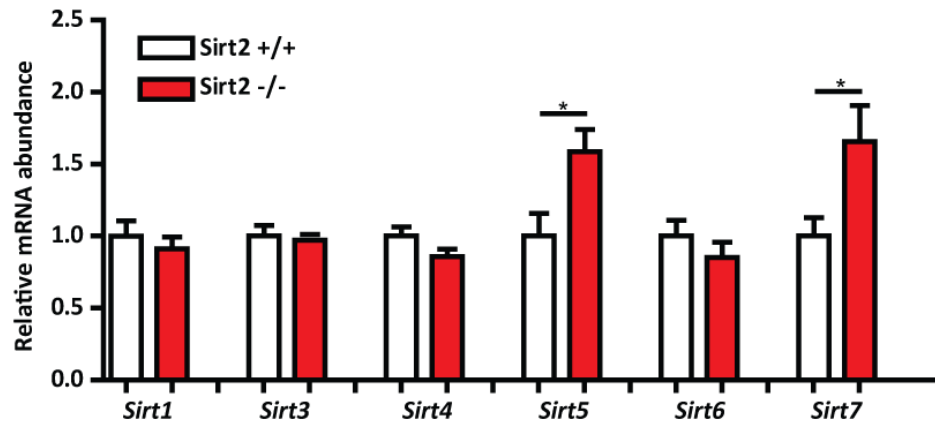


**Figure. 22 Relative mRNA abundance of other sirtuins in *Sirt2*<sup>null</sup> brain.**

Quantitative RT-PCR analysis was performed to investigate the expression of *Sirtuin* genes in total brain of adult mutant mice. The abundance of *Sirt5* and *Sirt7* was detected increased in *Sirt2*<sup>null</sup> brain, whereas the others remain unaltered. Results were normalized to *Top1* (n=5-6) and compared by the unpaired t-test. Values of p<0.05 were considered significant (\*p=0.0276 and 0.0418). Error bars represent SEM.

Among eleven members of the class I, II and IV non-sirtuin histone deacetylases, four of them, HDAC4, -5, -6 and 7, were reported to localize in the cytoplasm (Shen *et al.*, 2005). Additionally, HDAC6 co-immunoprecipitated *in vitro* with SIRT2 and was reported to have tubulin deacetylation activity (Hubbert *et al.*, 2002; Matsuyama *et al.*, 2002; Zhang *et al.*, 2003; North *et al.*, 2003). Therefore, we aimed to investigate any possible compensation taking place by an upregulation of the expression of any of the other cytoplasmic histone deacetylases, when SIRT2 was missing. To achieve this, we performed quantitative RT-PCR experiment to check the expression of *Hdac4*, -5, -6 and -7 genes in the brain of adult mutant mice. The abundance of *Hdac4* and *Hdac5* was detected increased in *Sirt2*<sup>null</sup> brain, whereas the abundance of *Hdac6* and *Hdac7* remained unaltered (Figure. 23A). All four cytoplasmic HDAC proteins were detected in the total brain lysate, without any abundance increase in *Sirt2*<sup>null</sup> material (Figure. 23B). Only HDAC4 was detected to be incorporated into the myelin fraction, with a slight abundance increase in *Sirt2*<sup>null</sup> myelin. However, the difference was not quantified (Figure. 23B). Such a possible increase for HDAC4 abundance in mutant mice was not observed when total brain lysates were compared (Figure. 23C).

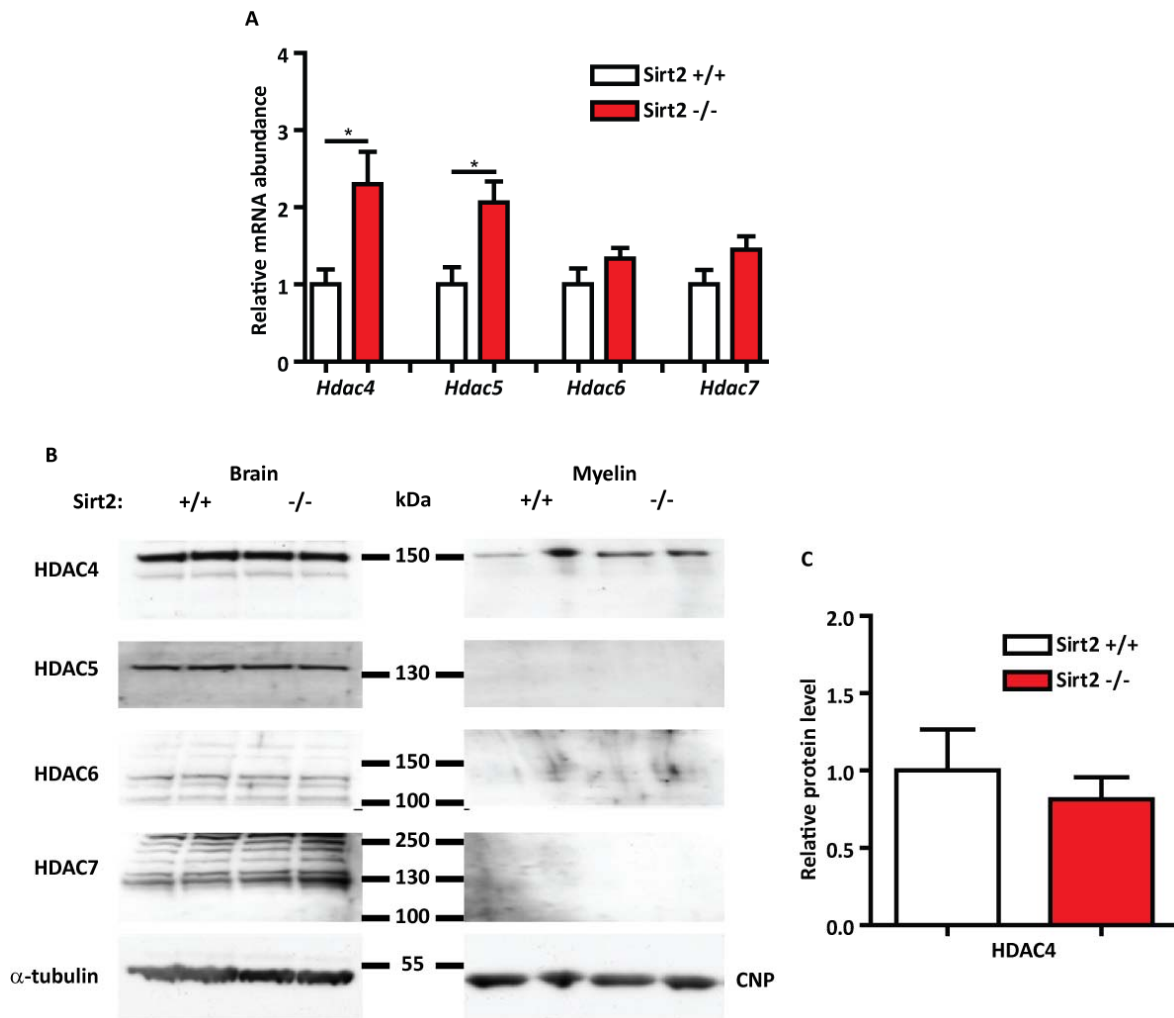


**Figure. 23** Relative mRNA abundance of cytoplasmic histone deacetylases (HDACs) in *Sirt2<sup>null</sup>* brain.

**(A)** Relative mRNA abundance of cytoplasmic histone deacetylases in *Sirt2<sup>null</sup>* brain. Quantitative RT-PCR analysis was performed to investigate the expression of cytoplasmic histone deacetylases in total adult brain of mutant mice. The abundance of *Hdac4* and *Hdac5* was detected increased in *Sirt2<sup>null</sup>* brain, whereas the abundance of *Hdac6* and *Hdac7* remained unaltered. Results were normalized to *Top1* (n=6) and compared by the unpaired t-test. Values of  $p < 0.05$  were considered significant (\* $p = 0.0172$  and  $0.0136$ ). Error bars represent SEM. **(B)** Western blot analysis of protein lysates were performed to investigate the abundance of cytoplasmic HDAC proteins in the brain and myelin enriched fraction of mutant compared to control mice at the age of 2.5 months (n=2 per genotype). All 4 HDACs were detected in the total brain lysate, without any abundance increase in *Sirt2<sup>null</sup>* material. Out of 4 HDACs, only HDAC4 was detected to be incorporated into the myelin fraction, with a slight abundance increase in *Sirt2<sup>null</sup>* myelin. Loading controls:  $\alpha$ -tubulin and CNP. **(C)** Densitometric quantification revealed no difference in the abundance of HDAC4 protein between the genotypes in the total brain lysate. Peak intensities ( $\pm$ SEM) were normalized to  $\alpha$ -tubulin (n=3 per genotype).

#### 4.2.5 Analysis of CNS axonopathy and inflammation in the absence of SIRT2

We hypothesized that the lack of Sirt2 expression might lead to a phenotype in mutant mice, which is similar to that in *Plp<sup>null</sup>* animals. To investigate this, we performed experiments to analyze axonopathy and inflammation in CNS and deficits in the motor performance.

We performed immunostaining of amyloid precursor protein (APP) and MAC3 on sagittal brain sections of 7 month-old wild type and mutant mice. APP was used to mark axonal spheroids and MAC3 was used to mark the activated microglia, indicating neuroinflammation. Experiments showed neither axonal degeneration nor microglial activation in *Sirt2<sup>null</sup>* brain (Figure. 24A). Absence of APP-positive swellings and activated microglia was observed in the entire mutant brain, but anterior commissure was chosen to be used in the images as a representative white matter tract region in the brain. Quantification of the protein level of the astrocytic marker GFAP showed no increase in mutant brains, indicating an absence of astrogliosis (Figure. 24B).

As a next step, we attempted to analyze *Sirt2<sup>null</sup>* mice in terms of motor behavior. The rotarod test was chosen to be conducted to assess the motor performance. The latency of the mice to fall from a rotating rod was measured. The experiment was done with 2 cohorts of animals at different ages. Both control and mutant mice at the age of 6-8 weeks showed a comparable performance on the rotarod (Figure. 25A). However, we observed a decline in the performance of older *Sirt2* heterozygous and homozygous mutant mice (age: 4-5 months) on the rotarod compared to wild type (Figure. 25B). Although the differences were statistically significant, it should be noted that all mice could stay on the rotating rod more than 3 min. To assess the hindlimb problems, the number of hindlimb slips of the mice during 2m-walk on a grid was counted. Mutant mice did not slip more frequently than the control mice.

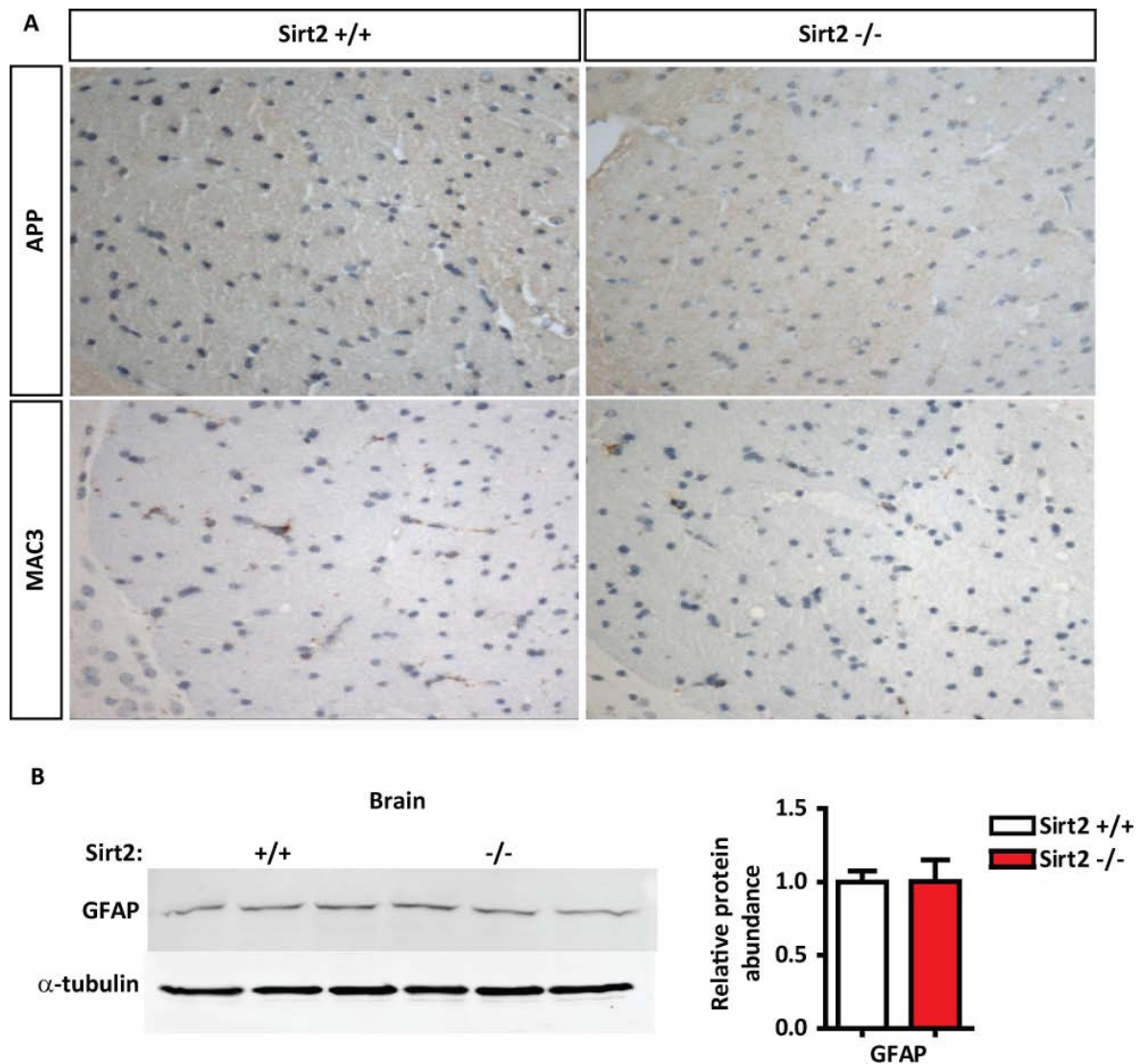


**Figure. 24** *Sirt2<sup>null</sup>* mice showed neither axonal degeneration nor microglial activation in the brain.

**(A)** Immunostaining of APP and MAC3 on sagittal brain sections (5 $\mu$ m thick) of 7 month-old wild type and *Sirt2<sup>null</sup>* mice indicated lack of axonal degeneration and neuroinflammation in the entire brain of the mutant mice. Anterior commissures are exemplified in the images. **(B)** Western blot analysis on brain lysates of 2 month-old *Sirt2<sup>null</sup>* and control animals was performed by using antibody against GFAP. An increase in the astrocytic marker GFAP is indicative for astrogliosis. Densitometric quantification revealed no difference in the abundance of GFAP protein between the genotypes in the total brain lysate. Peak intensities ( $\pm$ SEM) were normalized to  $\alpha$ -tubulin (n=3 per genotype).

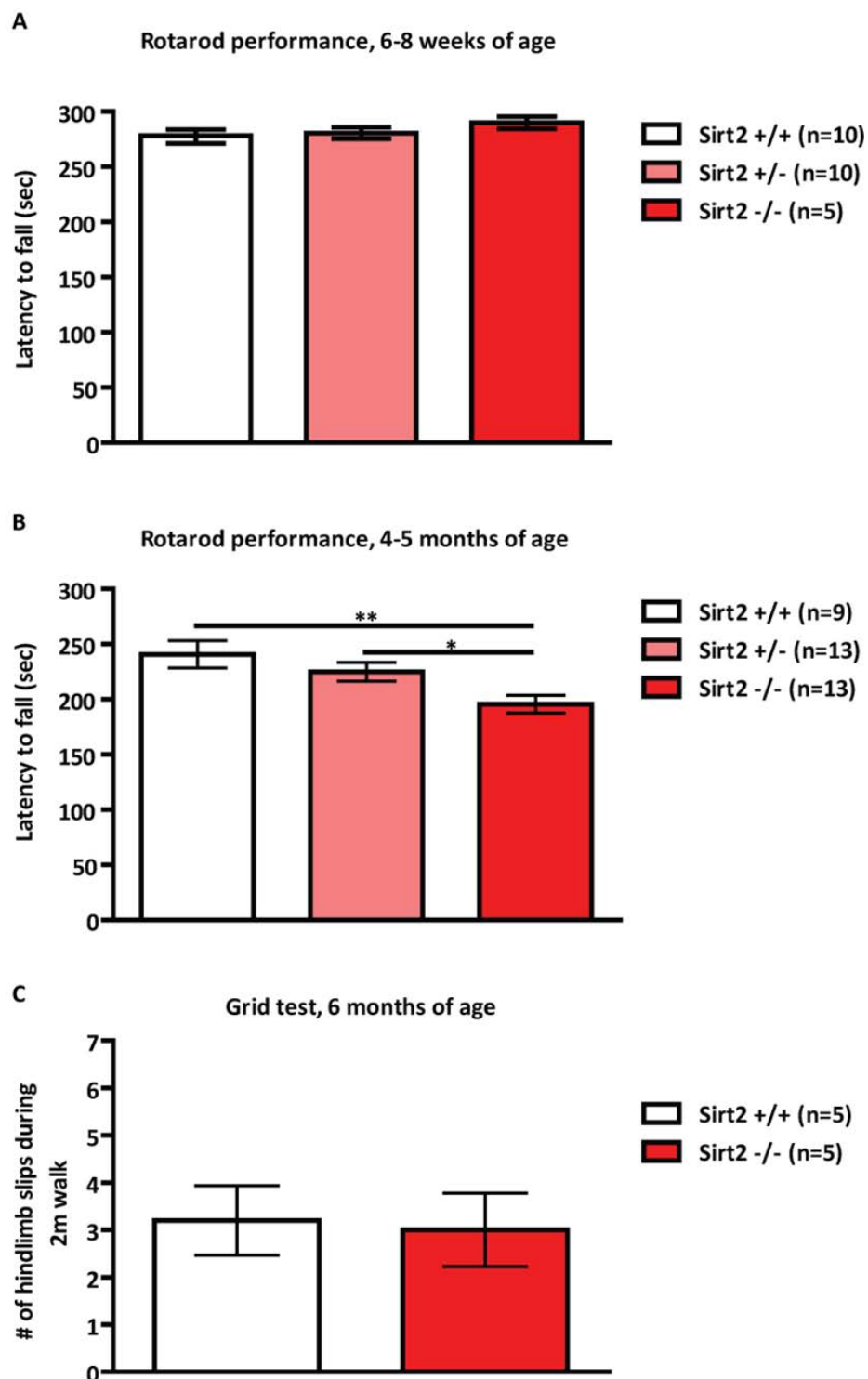


**Figure. 25 Motor performance and motoric behavior in *Sirt2*<sup>null</sup> mice.**

**(A and B)** The latency of the mice to fall from a rotating rod was measured to assess the motor performance. The mice were subjected to 6 **(A)** or 3 **(B)** trials per day. Scores obtained on the last day of a 3-day training period were plotted. Result of each trial was taken as a single data point (n=animal number\*trial number), and all scores were pooled to generate a mean and SEM. **(C)** The number of hindlimb slips of the mice during 2m-walk on a grid was counted to assess the hindlimb problems. Results were compared by the unpaired t-test. Values of  $p < 0.05$  were considered significant. Error bars represent SEM. The differences in rotarod performance among the genotypes were statistically significant only for 4-5 months of age **(B)** (\*\* $p=0.0022$  and \* $p=0.0142$ ).

### 4.3 Double mutant mice lacking the expression of Sirt2 and Cnp

Analysis of the mice lacking Sirt2 expression revealed no apparent CNS axonopathy. This suggested that SIRT2 may not be the only key player of the yet unexplained axonoprotective function of PLP.

We continued our project with a second hypothesis and asked the question whether SIRT2 serves as a regulator of glial response when axons are under stress or metabolically challenged. To address this question, we aimed to genetically genetically an axonal stress to the system. We generated Sirt2\*Cnp1 double null mutant mice. Mice which lack the expression of Cnp develop axonal swellings and neurodegeneration throughout the brain (Lappe-Siefke *et al.*, 2003). Our goal was to find out whether the extent of axonal degeneration caused by the lack of Cnp1 will be altered by the additional absence of SIRT2.

#### 4.3.1 SIRT2 protein level in the Cnp<sup>null</sup> myelin

Before generating Sirt2\*Cnp1 double null mutant mice, we asked the question whether SIRT2 protein will be also absent from Cnp<sup>null</sup> myelin, like it is from Plp<sup>null</sup>. To investigate this, we performed western blot experiments to detect SIRT2 protein in the myelin samples of wild type and Cnp<sup>null</sup> mice. Western blot analysis showed that Cnp<sup>null</sup> myelin does not lack SIRT2 (Figure. 26A) and quantitative analysis of the band intensities revealed no statistically significant difference in SIRT2 abundance among genotypes (Figure. 26B).

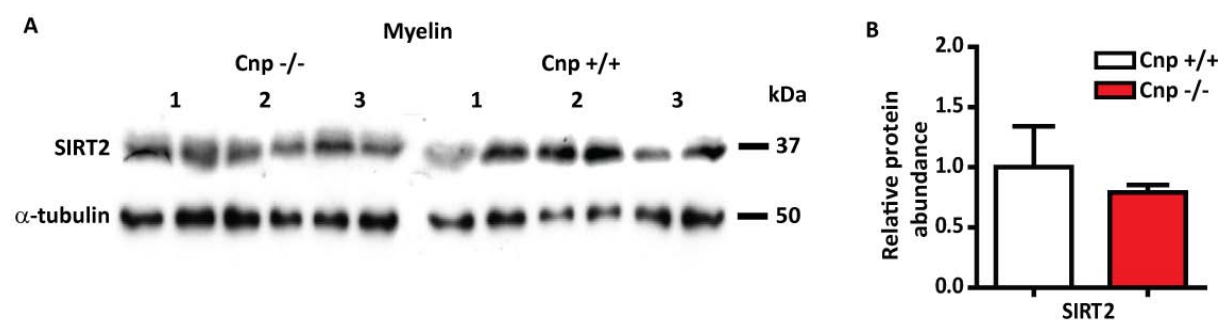


**Figure. 26 SIRT2 abundance in Cnp<sup>null</sup> myelin.**

(A) Western blot analysis of myelin samples were performed to investigate the abundance of SIRT2 in Cnp<sup>null</sup> mice compared to wild type at the age of 2.5 months (n=3 per genotype, 2 technical replicates for each sample). Cnp<sup>null</sup> myelin does not lack SIRT2. ( $\alpha$ -tubulin was used as loading control). (B) Densitometric quantification revealed no difference in the abundance of SIRT2 protein between the genotypes in the myelin. Peak intensities ( $\pm$ SEM) were normalized to  $\alpha$ -tubulin (n=3 per genotype).

#### 4.3.2 Premature lethality in $Sirt2^{null*}Cnp^{null}$ mice

Systematic monitoring of  $Sirt2^{null*}Cnp^{null}$  mice revealed that double mutant mice showed hindlimb problems starting at the age of 50 days. This phenotype progressed rapidly into a stage of severe hindlimb spasticity. This phenotype was accompanied by strong kyphosis (hunchback formation) and this was indicative for significant axonal degeneration. These double mutant mice survived maximum till the age of 120 days; however, the majority died at the age of 3 months (Figure. 27). Interestingly,  $Sirt2^{+/-}Cnp^{-/-}$  mice also suffer from a reduced lifespan compared to either single mutant. The heterozygosity of Sirt2 gene reduced the maximum lifespan of  $Cnp^{null}$  mice to the age of 8 months (Figure. 27).

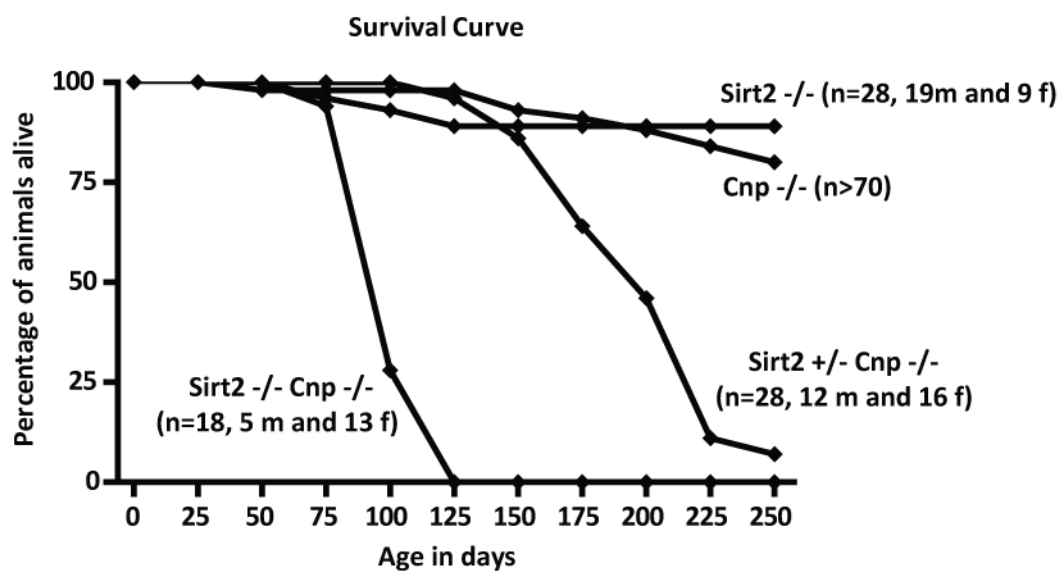


**Figure. 27** Premature lethality in  $Sirt2^{null*}Cnp^{null}$  mice.

$Sirt2^{null*}Cnp^{null}$  and  $Sirt2^{+/-}Cnp^{null}$  mice have a reduced lifespan compared to either single mutant. Double mutant mice survive maximum till the age of 4 months. The heterozygosity of Sirt2 gene reduced the lifespan of  $Cnp^{null}$  mice up to maximum the age of 8 months.

#### 4.3.3 Enhanced axonal degeneration in $Sirt2^{null*}Cnp^{null}$ mice

We performed immunostaining of APP on sagittal brain sections of 3-4 month-old double mutant mice and single mutant control mice. As expected,  $Sirt2^{null}$  brain was free of any APP-positive axonal swellings, whereas in  $Cnp^{null}$  brain, degenerating axons were detected especially in white matter tracts (Figure. 28). Remarkable observation was that the entire brain of  $Sirt2^{null*}Cnp^{null}$  mice was filled with APP-positive degenerating axons (Figure. 28), indicating a significantly enhanced axonal degeneration compared to  $Cnp^{null}$  mice. Anterior commissure and corpus callosum are shown in Figure. 28.

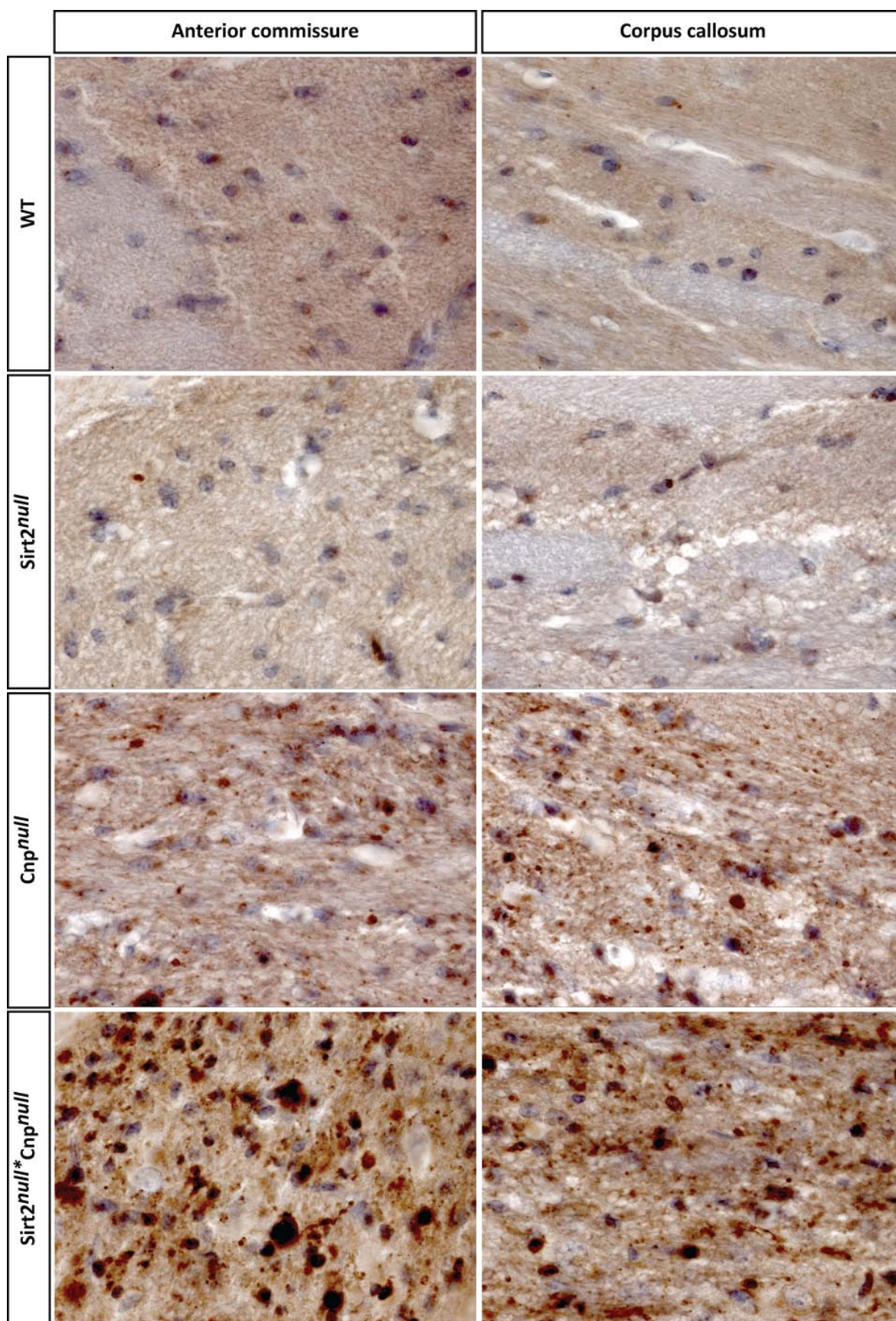


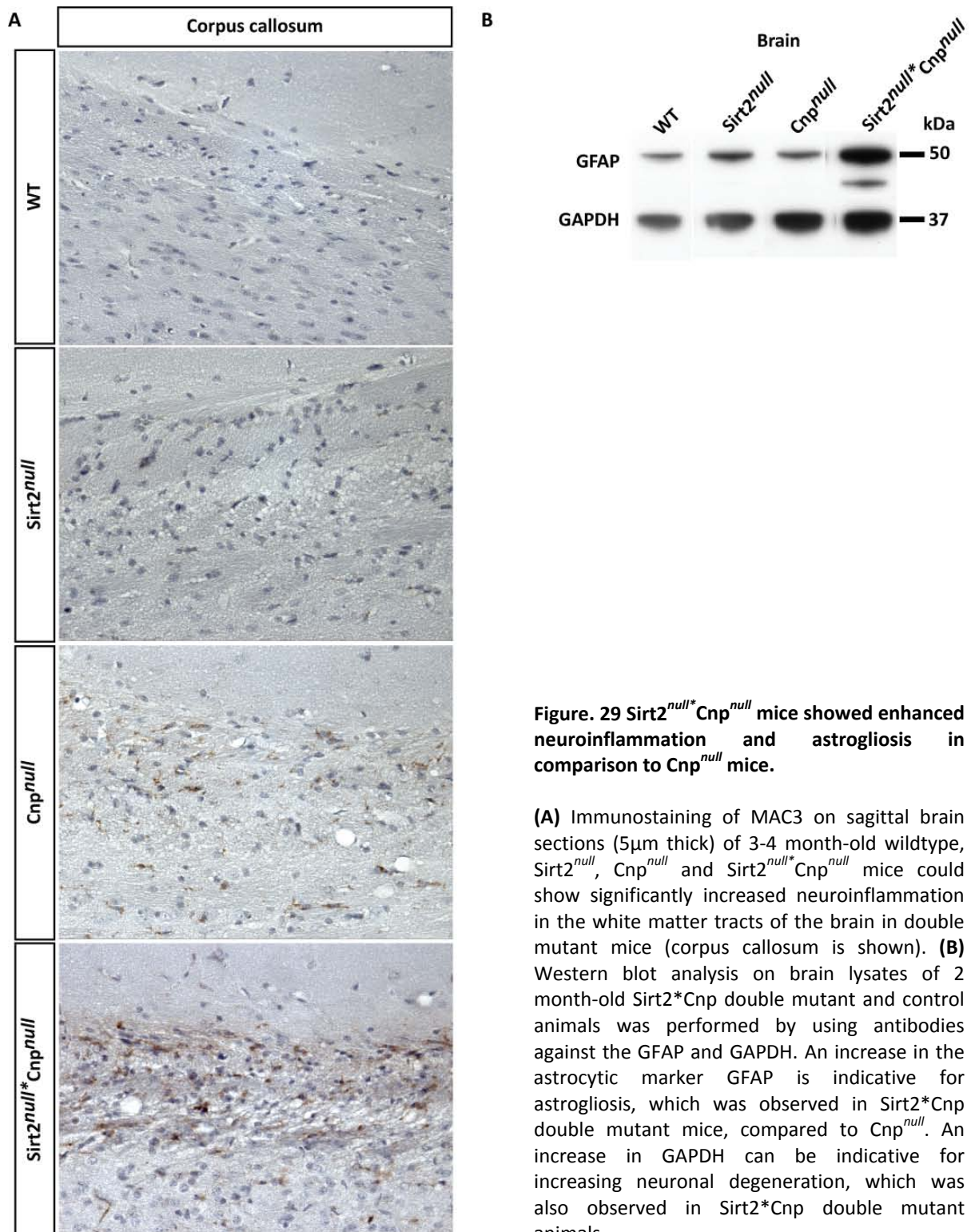


**Figure. 28**  $Sirt2^{null*}Cnp^{null}$  mice showed enhanced axonal degeneration in comparison to  $Cnp^{null}$  mice.

Immunostaining of APP on sagittal brain sections (5 $\mu$ m thick) of 3-4 month-old wildtype,  $Sirt2^{null}$ ,  $Cnp^{null}$  and  $Sirt2^{null*}Cnp^{null}$  mice could show significantly increased axonal degeneration in the white matter tracts of the brain in double mutant mice (anterior commissure and corpus callosum are shown).

#### **4.3.4 Enhanced inflammation and astrogliosis in $Sirt2^{null*}Cnp^{null}$ mice**

To investigate the microglia activation, immunostaining with MAC3 on sagittal brain sections of 3-4 month-old double mutant mice and single mutant control mice were performed. As expected,  $Sirt2^{null}$  brain was free of inflammation, whereas in  $Cnp^{null}$  brain, MAC3-positive activated microglia could be observed (Figure. 29A). In double mutant mice, the inflammation was significantly enhanced, especially in white matter tracts (Figure. 29A). Corpus callosum is shown in Figure. 29A. Additionally, quantitative analysis of the protein level of the astrocytic marker GFAP showed an increase in double mutant brain, indicating a dramatic astrogliosis (Figure. 29B).



#### 4.4 EAE induction in *Sirt2*<sup>null</sup> mice

To test whether the absence of SIRT2 results in an increased vulnerability to axonal degeneration from CNS inflammation, we chose to perform experimental autoimmune encephalomyelitis (EAE), a widely used animal model of multiple sclerosis. We immunized female wild type, *Sirt2* heterozygous and homozygous mutant mice at the age of 6-8 weeks by subcutaneous injection of MOG (35-55) peptide, emulsified in an adjuvant, in order to induce EAE. Once right after the immunization and once more 48 hours later, 500 ng of Pertussis toxin is administered intraperitoneally. The mice were clinically scored on a daily basis in terms of loss of tail tone, hindlimb problems and paralysis. Detailed phenotype explanation of each clinical score is listed in 3.2.9.5.

Average day of onset was for *Sirt2* +/+ animals 13.2, for *Sirt2* +/- animals 15.4, and for *Sirt2* -/- animals 17, without any statistically significant difference. There was no statistically significant difference in terms of the clinical course of EAE in the affected animals among three genotypes (Figure. 30). 3 out of 8 *Sirt2*<sup>null</sup> animals which were injected did not get clinically affected throughout the clinical monitoring.

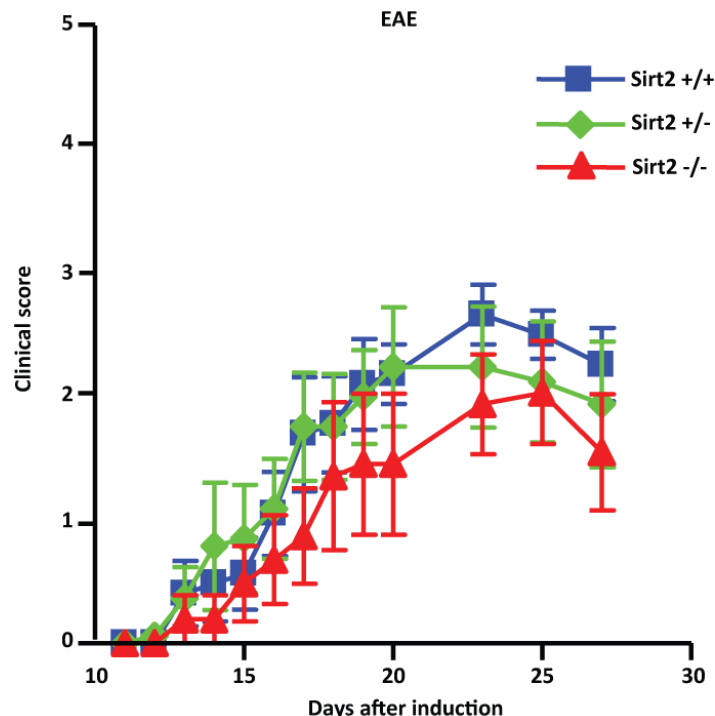


**Figure. 30** No change in the clinical course of EAE in *Sirt2*<sup>null</sup> mice.

*Sirt2* heterozygous and homozygous mutant mice did not show any significant change in the clinical course of EAE. 6-8 week-old female mice were injected with MOG (35-55) peptide to induce EAE and clinically scored daily. Data of 6 +/+, 8 +/- and 5 -/- mice were plotted. Error bars represent SEM.

#### 4.5 Acrylamide treatment in *Sirt2*<sup>null</sup> mice to induce axonal stress

We aimed to investigate whether the absence of SIRT2 results in a higher vulnerability to axonal degeneration from additional stresses such as neurotoxins. We chose to orally administer acrylamide to wild type, *Sirt2* heterozygous and homozygous mutant mice. Acrylamide is a well characterized toxin resulting in axonal degeneration without lymphocytic inflammatory response (Schaumburg *et al.*, 1974; Ko *et al.*, 2000).

Before performing the experiment on three genotypes, we monitored the effect of acrylamide at different concentrations on wild type mice to find out the proper dose to cause axonal impairments without achieving lethality. 6 week-old male mice (n=3 for each concentration) were treated with acrylamide by adding it to the drinking water. Mice were trained prior to the onset of the treatment on 3 consecutive days by performing on the rotarod as described in section 3.2.10.2. After initiation of acrylamide treatment, we monitored the rotarod performance and the change in weight of the mice for 3-4 weeks.

When exposed to acrylamide at 6 weeks of age, wild-type develop mild gait unsteadiness and when challenged with the rotarod test, they had mild difficulty in maintaining their balance on the rotating rods with a small decline in the retention time on the rotarod compared to untreated mice (Nguyen *et al.*, 2009). We achieved these effects without any major weight loss on wild type mice when using acrylamide at a concentration of 200 parts per million (ppm) (Figure. 31A and B).

When we exposed *Sirt2* heterozygous and homozygous mutant mice to acrylamide for 5 weeks, we did not observe any statistically significant difference in the performance at the rotarod between the genotypes (Figure. 32A and B). There was a decline in the performance due to the treatment; however, the extent of this decline did not differ in mutant mice. When the mice were monitored after 24 days of treatment while they were walking on a grid for 2 m long, we observed that the number of hindlimb slips of acrylamide-intoxicated *Sirt2*<sup>null</sup> mice was significantly higher than that of control mice (Figure. 32C). Additionally, the forelimbs of the mutant mice had a tendency to slip more frequently than the wild type mice; however, the difference was not significant between the genotypes, due to the high variance in the behavior of individual animals (Figure. 32C).

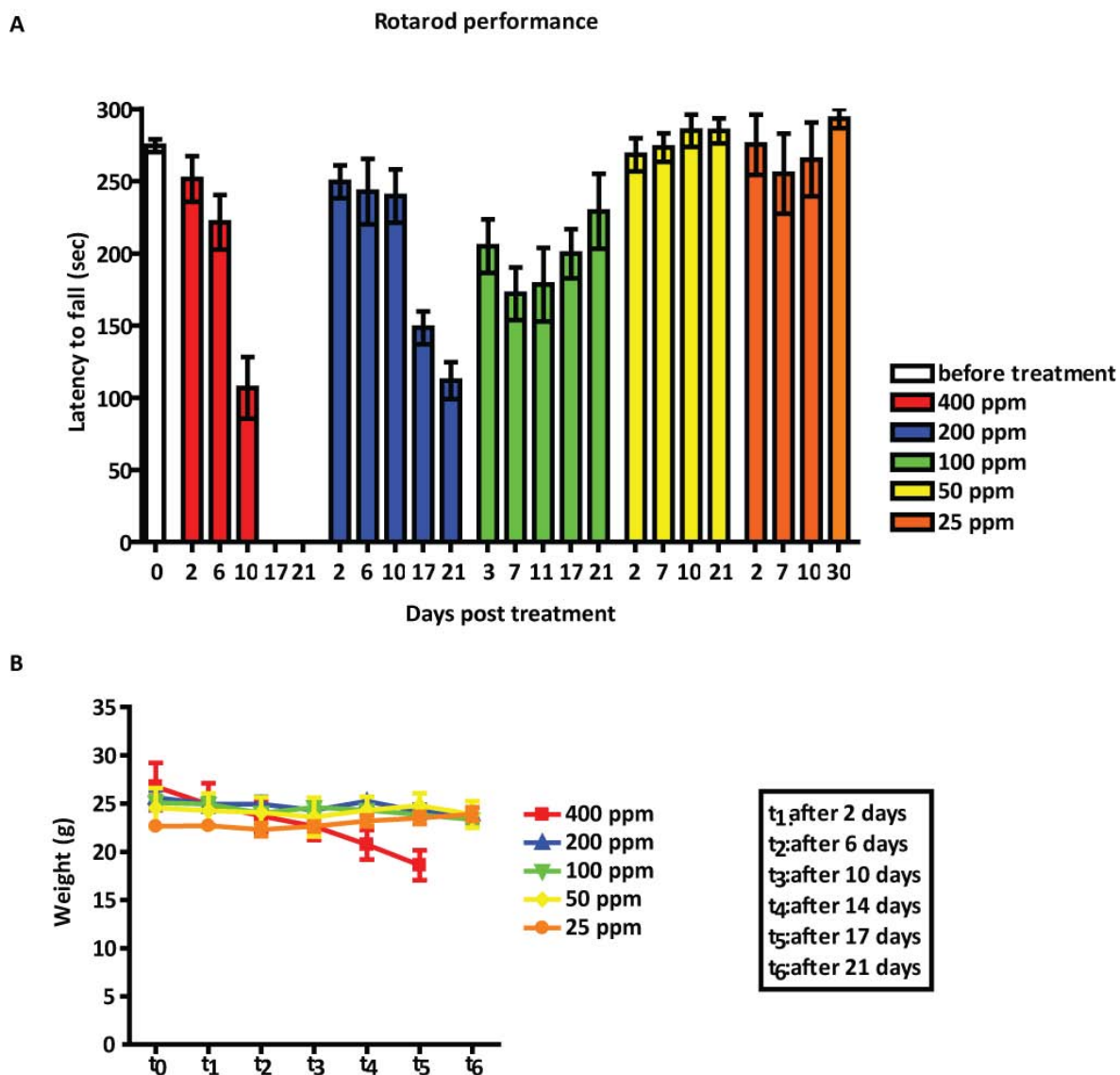
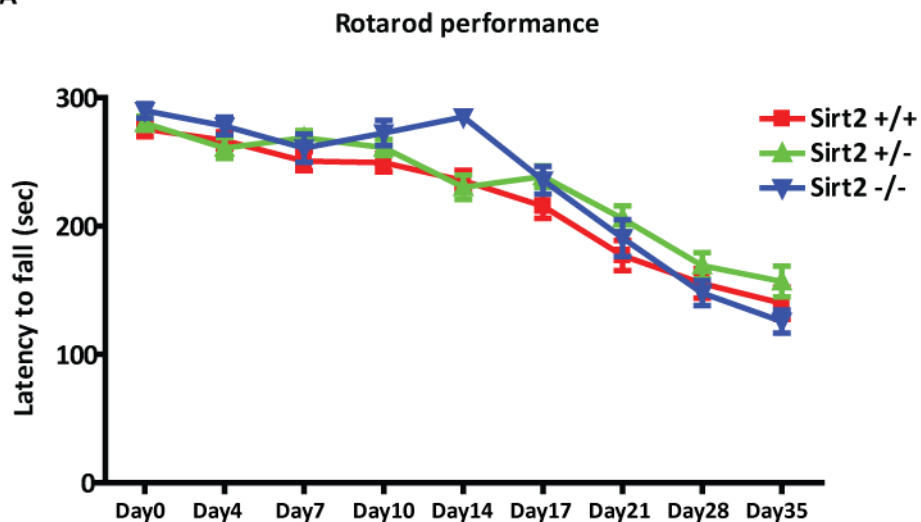


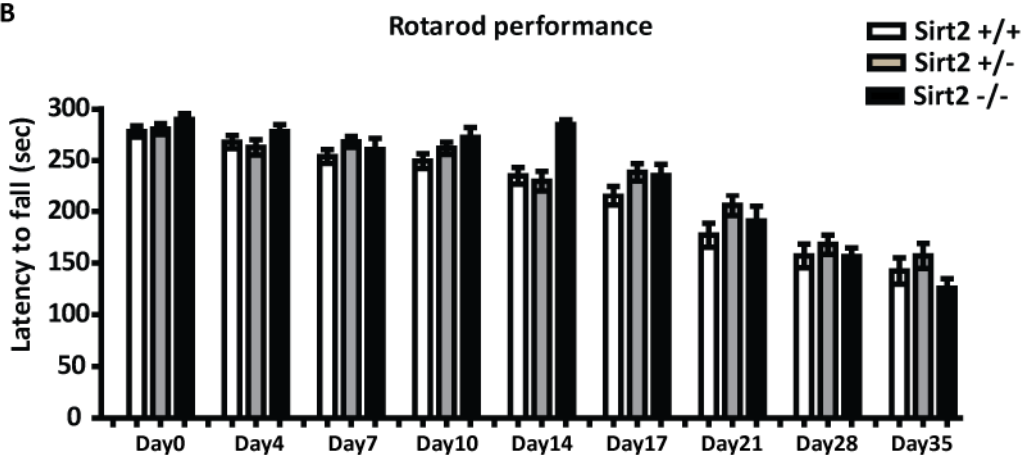
**Figure. 31** The effects of different doses of acrylamide on wild type mice.

(A) Acrylamide was applied to the drinking water of 6 week-old male mice (n=3 for each concentration). Mice were trained prior to the onset of the treatment on 3 consecutive days by performing on the rotarod (3 trials per mouse per day). After the initiation of the treatment, the rotarod performance was monitored for 3-4 weeks. Results of all trials on a single day were pooled to generate a mean and SEM. Ppm, parts per million. (B) The change in weight of the mice was monitored during the 3 week-treatment.

A



B



C

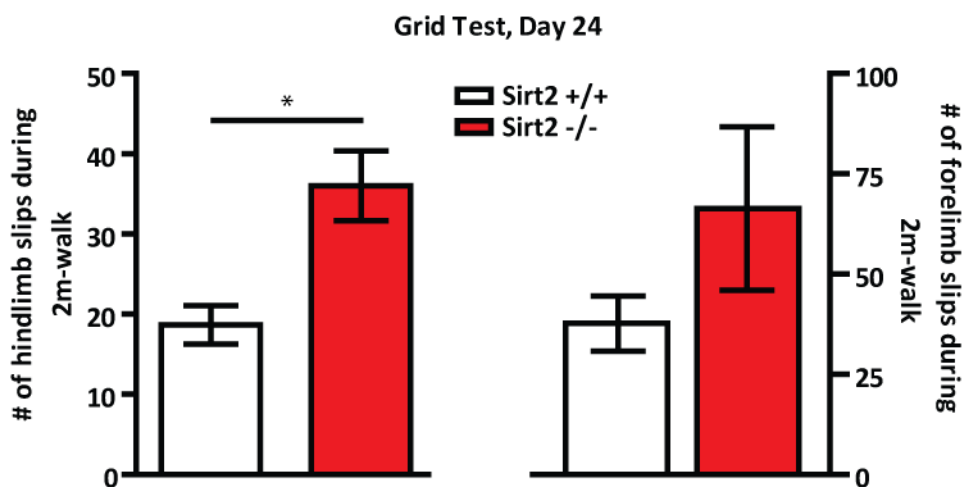


**Figure. 32 Monitoring the motoric behavior of acrylamide-intoxicated *Sirt2*<sup>null</sup> mice.**

**(A and B)** Acrylamide was applied to the drinking water of 6-9 week-old male wild type, *Sirt2* heterozygous and homozygous mutant mice (at a concentration of 200 ppm). Mice were trained prior to the onset of the treatment on 3 consecutive days by performing on the rotarod (6 trials per mouse per day). After the initiation of the treatment, the rotarod performance was monitored every 3-4 days for 5 weeks long. Results of all trials on a single day were pooled to generate a mean and SEM. Ppm, parts per million. (n=5-10 per genotype). **(C)** The number of slips of the fore-and hindlimbs of the intoxicated mice during 2 m-walk on a grid were counted. (n=3 per genotype). Results were compared by the unpaired t-test. Values of  $p < 0.05$  were considered significant (\* $p = 0.0253$ ). Error bars represent SEM.

#### 4.6 5XFAD mice with a decreased dose of *Sirt2* gene

To test whether the absence of SIRT2 results in an increased vulnerability to plaque development and axonal degeneration from the overexpression of mutated amyloid precursor protein (APP) and presenilins, we crossed *Sirt2*<sup>null</sup> mice with the APP/PS1 double transgenic mice that coexpress five familial Alzheimer's disease (FAD) mutations. Mutations in the genes for amyloid precursor protein (APP) and presenilins (PS1, PS2) cause FAD by increasing the production of beta-amyloid 42 (A $\beta$ 42) with the presence of amyloid plaque pathology. By generating APP/PS1 double transgenic mice coexpressing five FAD mutations (5XFAD mice), plaque development was accelerated and cerebral A $\beta$ 42 levels were increased (Oakley *et al.*, 2006). These mice were also reported to develop an age-dependent motor phenotype in addition to working memory deficits and an age-dependent axonopathy (Jawhar *et al.*, 2010). However, a decline in the lifespan below one year of age was not reported. Our preliminary observation was a reduction in the lifespan of 5XFAD transgenic mice up 10 months of age due to the heterozygosity of *Sirt2* gene (Figure. 33). When analyzing the cortex and subiculum of *Sirt2*<sup>+/-</sup> 5XFAD, we observed an increase in the plaque load compared to the 5XFAD mice (data not shown).

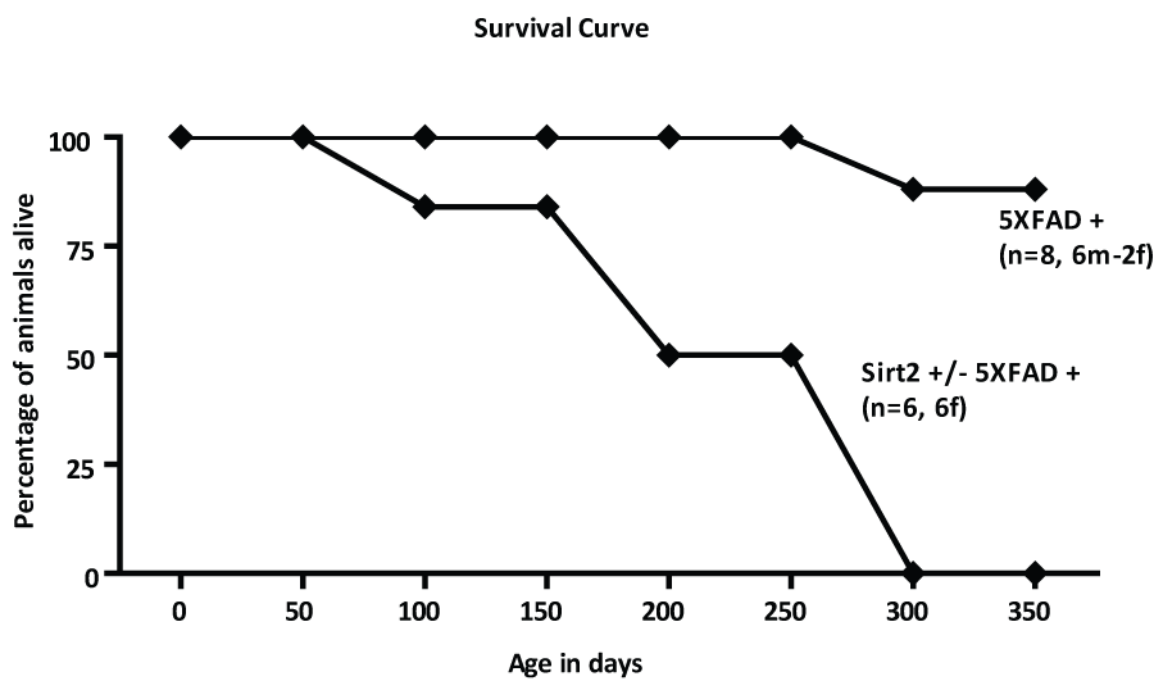


**Figure. 33 Lifespan of *Sirt2* heterozygous mutant mice carrying the 5XFAD transgene.**

The heterozygosity of *Sirt2* gene reduced the lifespan of 5XFAD transgenic mice up to maximum the age of 10 months.



**5. Discussion**

### 5.1 SIRT2 is an oligodendroglial protein

SIRT2 is strongly expressed in the peripheral and central nervous system. There are convincing evidence showing that oligodendrocytes are the cells predominantly expressing SIRT2 in the central nervous system (Li *et al.*, 2007; Michan and Sinclair, 2007; Southwood *et al.*, 2007; Werner *et al.*, 2007). SIRT2 was indicated to be incorporated into the myelin sheath in a PLP-dependent manner (Werner *et al.*, 2007), which has not been completely understood yet. However, there are groups investigating the effects of SIRT2 activity in different neurodegenerative models. In their studies, the neuroprotective effects of the inhibition of SIRT2 was shown mainly in neuronal cells (Outeiro *et al.*, 2007; Suzuki and Koike, 2007; Luthi-Carter *et al.*, 2010). It should be noted that inhibition of the activity of the protein was mainly achieved by pharmacological treatments and mainly in cultured cells. In addition to these findings, several groups have found SIRT2 to be expressed in olfactory neurons, in neuronal NeuN-positive cell bodies of the cortex, in Purkinje cells, molecular layer neurons and fiber tracts in the cerebellum and in cultured hippocampal neurons (Yu *et al.*, 2005; Suzuki and Koike, 2007; Taylor *et al.*, 2008; Pandithage *et al.*, 2008; Maxwell *et al.*, 2011).

It was important for us to show the exact localization of SIRT2 in brain. The mutant mice that we analyzed in our project is a complete knockout, which lacks the expression of the protein in the entire body and the brain. This was not conditional mutant, which lacks the expression of the protein in a certain type of cell. And we gathered data indicating a neuroprotective effect of an oligodendroglial protein. Therefore, it was important to emphasize its oligodendroglial localization. Our data shows intense immunostaining of SIRT2 in white matter tracts of the brain (Figure. 9). The protein was almost undetectable in gray matter of the cortex and the cerebellum, when staining intensities compared to the very strong one in the corpus callosum and the white matter tracts of the cerebellum (Figure. 9). We are denying the neuronal expression of SIRT2 by no means. When we stained mixed cultures of primary oligodendrocytes and neurons, we did detect SIRT2 in Tuj1-positive neurons; however, the degree of expression was significantly low when compared that in oligodendrocytes (data not shown).

### 5.2 Sirt2<sup>null</sup> mice: a tool to study the effects of the lack of a myelin-associated deacetylase

It is still a mystery why axons degenerate in the absence of myelin proteins. When oligodendrocytes are unable to express one gene or myelin lacks one of its components, this does not lead to a major myelin abnormality, but to a CNS axonopathy. One of the examples for this is

the phenotype developed by the genetic deletion of the structural protein of the CNS myelin, proteolipid protein (PLP) (Griffiths *et al.*, 1998b; Edgar *et al.*, 2004). This shows that it is important for the axons not only to be enwrapped by the proper amount of myelin membranes provided by the oligodendrocytes, but to be enwrapped by these with the proper protein composition. The detailed analysis of Plp<sup>null</sup> myelin to find out secondary molecular changes revealed the virtual absence of Sirtuin 2 (SIRT2) prior to the onset of axonal degeneration (Werner *et al.*, 2007). Due to these findings, we suggested that the axonal pathology observed in Plp<sup>null</sup> mice may be at least partially due to the lack of SIRT2. The best tool to be used to understand the function of SIRT2 in a potential axonoprotection is the mice lacking its expression.

The complete *Sirt2*<sup>null</sup> mice were generated and provided by Dr. Maria Carla Motta (Massachusetts Institute of Technology, USA). The strategy used to interrupt the open reading frame of the wild type *Sirt2* gene was the insertion of a puromycin cassette with the size of 2 kb in reverse orientation into exon 11 (Figure. 10A). The insertion of this cassette resulted in the introduction of an early stop codon into the open reading frame (Figure. 10B). There was a mutant mRNA transcribed with more than 50% reduction in abundance in the total brain of the mutant mice (Figure. 10D). We showed that this mutant mRNA was transcribed with the inserted puromycin cassette. We suggested that the early stop codon introduced into the open reading frame would lead to an mRNA product translated into a non-functional SIRT2 protein. And we showed that the targeting of the wild type *Sirt2* allele by this strategy did not alter the expression of the neighbouring genes (Figure. 10D). By western blot analysis, we confirmed that our suggestion held true that there was no functional protein translated by the mutant mRNA. The SIRT2 protein was absent from the mutant brain, myelin and sciatic nerve tissue (Figure. 11). Importantly, neither any truncated protein was observed in the mutant samples (data not shown) and there was a clear reduction in the protein level in the myelin samples from *Sirt2* heterozygous mutant mice (Figure. 11C). These findings convinced us to use this mouse model to study the function of SIRT2 in nervous system.

### 5.3 SIRT2 is dispensable for myelin formation and maintenance

OL differentiation can be modulated by histone deacetylases which finetune the epigenetic patterning to facilitate myelin gene expression (Coprav *et al.*, 2009). SIRT2 might govern OL differentiation not by its histone deacetylase function, but more likely by modifying the cytoskeleton. Thereby, it might result into changes in OL morphology during differentiation. However, available data in the literature have been contradictory so far. *In vitro* data pinpointed

SIRT2 as an inhibitor of OL differentiation. According to Li *et al.*, 2007, when SIRT2 was overexpressed, the complexity of the OL arborisation was decreased and when it was knocked down, the expression of myelin basic protein (MBP) was elevated as a sign of accelerated OL differentiation. Also the overexpression of functional SIRT2 inhibited the arborization-inducing effect of co-transfected juxtalin (an OL-specific, differentiation-related protein with an actin-binding domain) (Zhang *et al.*, 2005). However, Ji *et al.* (2011) demonstrated that the binding of the transcription factor Nkx2.2 to the Sirt2 promoter via HDAC1 negatively regulated the expression of SIRT2 in oligodendroglial precursor cell lines and subsequently led to a delay in the differentiation of these precursor cells (Ji *et al.*, 2011). And in Schwann cells, Sirt2 expression was correlated with that of structural myelin components during both developmental myelination and remyelination after nerve injury (Beirowski *et al.*, 2011).

What is not questionable is that SIRT2 is a myelin protein. It was shown to be enriched in myelin in an equivalent extent to that of PLP/DM20 and CNP (Werner *et al.*, 2007). We asked the question whether this myelin protein is indispensable for myelin formation and maintenance. Our data showed that there was no principal alteration in myelin sheath thickness or ultrastructure in the absence of SIRT2 in both central and peripheral nervous systems of adult mice (Figure. 12 and 13). The axons of all calibers were enwrapped with a myelin sheath of an apparently appropriate thickness and ultrastructure. We quantified the myelin sheath thickness and analyzed the axon diameter distribution in adult wild type and mutant mice (Figure. 14A and 15A). We measured the diameters of the axon and the complete fiber including the myelin sheath. The ratio of these 2 values was calculated to find out the g-ratio and to quantify the myelin sheath thickness. In neither of the tissues, a difference was observed in the mean of the g-ratio values among the 2 genotypes (Figure. 14B and 15B). Mutant mice had no change in the distribution of g-ratios of individual fibers over the axon diameter in neither of the tissues, compared to the control mice (Figure. 14C and 15B). Quantification of the axon size distribution and the average axon diameter in both CNS and PNS revealed no obvious difference between mutant and control mice (Figure. 14D and E, 15 D and E).

Our analysis on the myelin of the adult mutant mice indicated no principal changes in the protein composition (Figure. 16A and B), except from an increase in the abundance of CNP protein in mutant myelin and sciatic nerve lysate (Figure. 16C). This increase in the protein abundance was not due to an increase of mRNA abundance of the gene (Figure. 16D). This increase might point to a possible interaction between these two proteins; however, the opposite regulation was not observed, meaning that the protein abundance of SIRT2 in Cnp<sup>null</sup> myelin was not altered (Figure.

26). This might be a structural compensation of the absence of a non-compact myelin component by the increase in abundance of another. However, we did not gathered enough data to explain the reasons of this increase in CNP protein abundance in Sirt2<sup>null</sup> material. It should be also noted that our experiments on the protein composition of Sirt2<sup>null</sup> myelin remains semi-quantitative. For example, a more detailed differential myelin proteome analysis by using two-dimensional differential fluorescence intensity gel electrophoresis followed by mass spectrometry-based protein identification (similar to what was performed for Plp<sup>null</sup> myelin (Werner *et al.*, 2007)) has not been performed for Sirt2<sup>null</sup> material.

In order to assess any defect in the early stages of CNS myelination because of the absence of SIRT2, we investigated the abundances of myelin proteins in developing mutant brains at postnatal day 10. Densitometric quantification revealed no difference in the abundance of myelin proteins analyzed between the wild type and mutant mice in myelinating regions of P10 brain (Figure. 17). There was a tendency towards an increase in CNP protein level in the cerebellum; however, this difference is not statistically significant (p=0.3380) (Figure. 17A, left). This shows that yet unexplained increase in the protein abundance of CNP might start at earlier stages of myelination. In order for us to claim that there is absolutely no delay in the onset of CNS myelination in the absence of SIRT2, we have to finalize our analysis of myelinated versus non-myelinated axon count and the quantification of myelin sheath thickness in the optic nerves of wild type and mutant mice at the postnatal day 10.

Our qualitative analysis on the onset of peripheral myelination in the absence of SIRT2 revealed a comparable number of axons being myelinated in mutant sciatic nerves at postnatal day 5. However, numbers were not quantified (Figure. 18). It should be noted that when Beirowski *et al.* ablated Sirt2 expression specifically in Schwann cells, they observed hypomyelination in sciatic nerves at postnatal day 1, 3 and 5. Therefore, our analysis is not complete till we also analyze the earlier ages and quantify the myelin sheath thickness and the number of myelinated axons in the PNS of our Sirt2<sup>null</sup> mice.

Our data showed no indication that in the absence of SIRT2, there was alteration in the synthesis of myelin lipids. We detected all myelin lipids in proportional amounts in both genotypes (Figure. 19). In addition to this, we also did not find any changes in the expression levels of the genes, which were shown to be down-regulated upon the inhibition of SIRT2 by Luthi-Carter *et al.*, in Sirt2<sup>null</sup> brains. Considering the fact that they observed the down-regulation of these genes

responsible for sterol biosynthesis in cultured neurons by the pharmacological inhibition of SIRT2 activity, we could speculate that such regulations might not take place *in vivo*.

#### 5.4 Potential substrates of SIRT2 in the central nervous system

SIRT2 is a histone deacetylase with a cytoplasmic localization. It can shuttle between the nucleus and the cytoplasm during mitosis (North and Verdin, 2007a) and plays an important role in the regulation of the cell cycle (Inoue *et al.*, 2007a). However, it is more reasonable to focus on its possible nonhistone targets in cytoplasm. Considering that SIRT2 is incorporated into myelin, the site of action of the protein is most likely myelin itself. Therefore, we focused our analysis on myelin to find out differentially acetylated myelin proteins in the absence of SIRT2. However, our semi-quantitative one dimensional analysis on acetylated myelin proteins by using two different antibodies did not give us yet the clear answer. Two polyclonal antibodies from different companies exhibited slightly different binding affinities towards the same proteins. First antibody revealed certain proteins to be hyperacetylated in the Sirt2 +/- and -/- myelin; however, this observation could not be confirmed by the second antibody (Figure. 20A). This was by no means a discouraging result. It showed that there are potential targets of SIRT2 action in myelin which were differentially acetylated in the absence or decrease of SIRT2 abundance. However, in order to identify these substrates, a more detailed proteomic approach has to be considered.

Already eight years ago, SIRT2 was published to deacetylate  $\alpha$ -tubulin at the lysine-40 residue *in vitro* (North *et al.*, 2003). We also investigated the acetylation level of  $\alpha$ -tubulin in Sirt2<sup>null</sup> material by western blotting. Neither in brain nor in myelin samples of Sirt2<sup>null</sup> mice, we observed hyperacetylated tubulin (Figure. 20B). Additionally, we investigated the acetylation level of  $\alpha$ -tubulin in the developing CNS of Sirt2<sup>null</sup> mice (Figure. 21A and B). At postnatal day 10, both control and mutant mice exhibited comparable levels of tubulin acetylation in cerebellum and brain stem (Figure. 21C). Our results suggested two things:  $\alpha$ -tubulin might not be the *in vivo* target of SIRT2 or there are other deacetylases compensating the absence of SIRT2.

SIRT2 was found among the many myelin proteins present in the exosomes, which are membrane microvesicles, released by oligodendrocytes (Krämer-Albers *et al.*, 2007). It is still not entirely known what the function of these exosomes secreted by oligodendrocytes is. These membrane microvesicles are secreted from cells by regulated fusion of multi-vesicular bodies with the plasma membrane. Such multivesicular bodies can be also observed in the adaxonal region of myelin sheath in the neighbourhood of the axonal membrane (unpublished data). If a transport of

myelin proteins, and in this case SIRT2, takes place from the myelin structure to the axon via these multivesicular bodies, the axon becomes also a potential site of action for SIRT2. This is a very interesting hypothesis, but also very difficult to address.

Emerging data should be considered which indicate protein acetylation to be a key regulatory mechanism for cellular metabolism. The acetylated proteins identified by global screens of lysine acetylation consists mainly of metabolic enzymes (Zhang *et al.*, 2009) and covers a considerable proportion of mitochondrial proteins (Kim *et al.*, 2006; Schwer *et al.*, 2006). Acetylation not only regulates the activity of the proteins, but also their stabilities. Recently, Jiang *et al.* (2011) showed in their recent study that SIRT2 deacetylated and thus stabilized the gluconeogenic rate-limiting enzyme phosphoenolpyruvate carboxykinase (PEPCK1) at least *in vitro*. If such regulation of other metabolic enzymes by SIRT2 is taking place *in vivo*, this can very well make SIRT2 a key enzyme to finetune the metabolism of the organism when needed.

### **5.5 Compensation of the absence of SIRT2 by other sirtuins and cytoplasmic histone deacetylases**

All members of sirtuin family in mammals have the NAD<sup>+</sup>-dependent enzymatic activity. SIRT2 is the one with the strongest expression in brain and the only one reported to localize in cytoplasm and be associated with  $\alpha$ -tubulin. We asked the question whether there was any compensation of the absence of SIRT2 in mutant mice taking place by an upregulation of the expression of any of the other sirtuins. Our data showed that the abundance of *Sirt5*, one of the mitochondrial sirtuins and *Sirt7*, which localizes in the nucleolus was detected increased in *Sirt2<sup>null</sup>* brain, whereas the others remain unaltered (Figure. 22). SIRT5 was linked to aging and energy metabolism (Michishita *et al.*, 2005). SIRT7 exhibited a constitutive nuclear localization in association with heterochromatic regions and nucleoli with a lack of *in vitro* deacetylation activity of histones or p53 peptides (Liszt *et al.*, 2005; Michishita *et al.*, 2005). We do not have the answer why the expression of these genes were up-regulated in *Sirt2<sup>null</sup>* brain. It appears reasonable to look their exact localization in oligodendrocytes and to investigate a possible change in their subcellular localization when SIRT2 is missing.

Four of the non-sirtuin histone deacetylases, HDAC4, -5, -6 and 7, were reported to localize in the cytoplasm (Shen *et al.*, 2005). Additionally, HDAC6 was implicated as an interaction partner of SIRT2, because they co-immunoprecipitated *in vitro* and HDAC6 was reported to have tubulin deacetylation activity (Hubbert *et al.*, 2002; Matsuyama *et al.*, 2002; Zhang *et al.*, 2003; North *et*

*al.*, 2003). To our surprise, our data did not show any up-regulation in the expression of *Hdac6* in the *Sirt2<sup>null</sup>* brain (Figure. 23A). Nor it was incorporated into myelin, which was unlikely to be happening. This could mean that the interaction between these two proteins which has been shown so far to take place *in vitro* might not hold true for *in vivo*. We detected increased abundance of *Hdac4* and *Hdac5* mRNA in *Sirt2<sup>null</sup>* brain (Figure. 23A). The interesting candidate here seems to be HDAC4, because it was also detected in the myelin fraction. Additionally, Shen *et al.*, (2005) presented immunolabeling of HDAC4 in myelinated fiber tracts of rat corpus callosum. There is possibility to have an increased HDAC4 protein in *Sirt2<sup>null</sup>* myelin compared to wild type. Additional experiments should be conducted to find out whether this increase has any functional relevance.

### 5.6 Absence of CNS axonopathy and inflammation in *Sirt2<sup>null</sup>* mice

Our hypothesis was that SIRT2 might be the key player of the yet unexplained axonoprotective function of PLP. That is why we expected that the lack of *Sirt2* expression might lead to a phenotype in mutant mice, which is similar to the in *Plp<sup>null</sup>* animals. To our surprise, our experiments showed neither axonal degeneration nor microglial activation in the brain of 7 month-old *Sirt2<sup>null</sup>* mice (Figure. 24A). There was no APP-positive swellings and MAC3-positive activated microglia in the entire brain of the mutant mice. Our data did not indicate any astrogliosis in *Sirt2<sup>null</sup>* brain (Figure. 24B).

As a next step, we analyzed *Sirt2<sup>null</sup>* mice in terms of motor behavior. Both control and mutant mice at the age of 6-8 weeks showed a comparable performance on the rotarod (Figure. 25A). There was a decline in the performance of older *Sirt2* heterozygous and homozygous mutant mice (age: 4-5 months) on the rotarod compared to wild type (Figure. 25B). Although the differences were statistically significant, it should be noted that all mice could stay on the rotating rod more than 3 min. Some researchers chose the maximum limit for running of the mice on the rotating rod as 3 min. In this experiment, it was set to 5 min. This difference might not have been caught at another experiment with different settings. We do not have enough data to claim that this difference in rotarod performance does not increase with age. However, this decline in the rotarod performance was not translated into any motoric phenotype, which could be observed at the cage behavior, or any hindlimb problems in mice. When we performed grid-test on wild type and *Sirt2<sup>null</sup>* mice, which is a more neutral test to monitor the hindlimb problems, we observed that mutant mice did not slip more frequently than the control mice.



It should be underlined that mouse strains matters in terms of the severity of the phenotypes that one is hunting for. The phenotype in the mouse with the *rumpshaker* mutation of *Plp* gene, which causes dysmyelination both in mice and humans, was shown to be significantly dependent on the genetic background in which the mutation is expressed. Whereas longevity was normal on the C3H background, breeding the mice into a c57BL/6 strain led to seizures and death at around one month of age (Al-Saktawi *et al.*, 2003). Interestingly, it was also found that unfolded protein response, which modifies the severity of the resulting phenotype, appeared to be activated in response to *Plp* mutations in specific mouse strains but not in others (McLaughlin *et al.*, 2007). The complete *Sirt2*<sup>null</sup> mice were generated on Fvb inbred strain. The first generation on this strain that we observed was free of degenerating axons and motor problems at the age of 10 months (data not shown). Throughout our project, we backcrossed these mutant mice into c57BL/6 strain for 10 generations. We pursued our analysis on the mutant mice after one generation of backcrossing; however, most of data shown in this manuscript were obtained from the animals which were backcrossed at least 3 generations into c57BL/6 strain. Change in the strain did not cause *Sirt2*<sup>null</sup> mice to develop a CNS axonopathy phenotype.

Our findings indicated that SIRT2 might not be the only key player of the yet unexplained axonoprotective function of PLP.

### 5.7 Modification of axonal degeneration by SIRT2

Analysis of the mice lacking *Sirt2* expression revealed that mice can survive without suffering from any apparent CNS axonopathy or reduced lifespan, when SIRT2 is missing. We continued our project with a second hypothesis and asked the question whether SIRT2 serves as a regulator of glial response when axons are under stress or metabolically challenged. Our goal has become to expose the mutant mice to the situations when the axons were already under certain insult. To achieve this, we used different approaches. First approach was to introduce genetically an axonal stress to the system. For this, we generated *Sirt2*\**Cnp1* double null mutant mice. Mice which lack the expression of *Cnp* develop axonal swellings and neurodegeneration throughout the brain (Lappe-Siefke *et al.*, 2003). This means the axons were already stressed in the absence of this protein from myelin. Our goal was to find out whether the extent of the axonal degeneration caused by the lack of *Cnp1* will be altered by the additional absence of *Sirt2*.

It is important to note that *Cnp*<sup>null</sup> myelin does not lack SIRT2 (Figure. 26A). The reason why axons degenerate in the absence of CNP might not be explained via SIRT2 action; however, we aimed to

test whether the absence of SIRT2 makes the axons more vulnerable to degenerate once they face a stress.

Our data showed that  $Sirt2^{null*}Cnp^{null}$  mice developed hindlimb problems starting at the age of 50 days. And this phenotype progressed rapidly into a stage of severe hindlimb spasticity. This phenotype was accompanied by strong kyphosis (hunchback formation) and this was indicative for significant axonal degeneration. These double mutant mice survived maximum till the age of 120 days; however, the majority died at the age of 3 months (Figure. 27). This is very significant difference when compared to the single mutants.  $Sirt2^{null}$  mice do not have any reduction in the lifespan, whereas  $Cnp^{null}$  mice can survive beyond one year of age. Interestingly,  $Sirt2^{+/-*}Cnp^{-/-}$  mice also suffered from a reduced lifespan compared to either single mutants. The heterozygosity of  $Sirt2$  gene (which causes 50% reduction in the gene dose and also in the abundance of the protein incorporated into myelin (Figure. 11C)) reduced the maximum lifespan of  $Cnp^{null}$  mice to the age of 8 months. This is a very important observation revealing that SIRT2 acts as a modifier of the disease progression.

We showed that the entire brain of  $Sirt2^{null*}Cnp^{null}$  mice was filled with APP-positive degenerating axons (Figure. 28), indicating a significantly enhanced axonal degeneration compared to  $Cnp^{null}$  mice. Massive axonal degeneration in the brain stem regions might be the explanation for premature lethality.

Furthermore, we observed that in double mutant mice, the inflammation was significantly enhanced, especially in white matter tracts (Figure. 29A). Quantification of the protein level of the astrocytic marker GFAP indicated a dramatic astrogliosis in double mutant mice (Figure. 29B).

Considering that  $Sirt2^{null}$  mice that we analyzed is a complete null mutant which lack the expression of the gene in the entire body, question can arise whether the enhanced axonal degeneration in  $Sirt2^{null*}Cnp^{null}$  mice can be attributed to the lack of SIRT2 from neuronal cells, no matter how weak the expression is in those cells compared to oligodendrocytes. In the course of our project, we also generated  $Sirt2^{null*}Plp^{null}$  mice, which showed neither reduced life span nor increased axonal degeneration compared to  $Plp^{null}$  mice (data not shown). This was not a surprise for us, because  $Plp^{null}$  mice is already lacking SIRT2 from myelin, and serves like a conditional knockout for this gene. And the lack of enhanced axonopathy observed  $Sirt2^{null*}Plp^{null}$  mice indicated that SIRT2 which is in oligodendrocytes and in myelin modifies the vulnerability of the axons to degeneration.

To test whether the absence of SIRT2 results in an increased vulnerability to axonal degeneration from CNS inflammation, we performed experimental autoimmune encephalomyelitis (EAE), which is a widely used animal model of multiple sclerosis. There was no statistically significant difference in terms of the clinical course of EAE in the affected animals among three genotypes (Figure. 30). 3 out of 8 *Sirt2<sup>null</sup>* animals which were injected did not get clinically affected throughout the clinical monitoring. We do not have a complete explanation for this phenotype. This might be attributed to the function of SIRT2 outside the central nervous system. SIRT2 as a component associated with the cytoskeleton might be important for dendritic cells migration to the lymph nodes.

We investigated the effects of the absence of SIRT2 on increasing the vulnerability to axonal degeneration from additional stresses such as neurotoxins. We intoxicated wild type, *Sirt2* heterozygous and homozygous mutant mice by oral treatment of acrylamide. Acrylamide is a well characterized toxin resulting in axonal degeneration without lymphocytic inflammatory response (Schaumburg *et al.*, 1974; Ko *et al.*, 2000). We did not obtain any indication of enhanced axonal degeneration in acrylamide-intoxicated *Sirt2* heterozygous and homozygous mutant mice compared to wild type mice, which resulted in changes in the performance of the mice at the rotarod (Figure. 32A and B). We believed rotarod was the best method to resolve the difference in the hindlimb problems that mice might be suffering due to the treatment. That is why we monitored the intoxicated mice while walking on a grid, and neutrally observed them to count the fore-and hindlimb slips. We observed that the number of hindlimb slips of acrylamide-intoxicated *Sirt2<sup>null</sup>* mice was significantly higher than that of control mice (Figure. 32C). Additionally, the forelimbs of the mutant mice had a tendency to slip more frequently than the wild type mice; however, the difference was not significant between the genotypes, due to the high variance in the behavior of individual animals. Axonal degeneration due to acrylamide intoxication affects first hindlimb of the treated mice and the forelimbs develop problems at later stages or prolonged durations of the treatment (Schaumburg *et al.*, 1974; Ko *et al.*, 2000). The quantification of axonal numbers in spinal cord and sciatic nerve of the intoxicated mice should be completed in future to show a possible increase in the axonal loss in *Sirt2* heterozygous and homozygous mutant mice compared to wild type mice in both regions upon treatment.

Our last experiment was designed to test whether the absence of SIRT2 results in an increased vulnerability to plaque development and axonal degeneration from the overexpression of mutated amyloid precursor protein (APP) and presenilins. We used this approach to introduce to the system another stress which is free of modifications in myelin gene expression. We crossed *Sirt2<sup>null</sup>* mice with the APP/PS1 double transgenic mice that coexpress five familial Alzheimer's

disease (FAD) mutations. APP/PS1 double transgenic mice coexpressing five FAD mutations (5XFAD mice) were generated to accelerate the plaque development and to increase cerebral Abeta42 levels were increased. These mice were also reported to develop an age-dependent axonopathy, quantified in spinal cord and brain stem (Jawhar *et al.*, 2010). A decline in the lifespan below one year of age was not reported. Strengthening our previous findings and fulfilling our expectations, we first had a preliminary observation showing a reduction in the lifespan of 5XFAD transgenic mice up to 10 months of age due to the heterozygosity of *Sirt2* gene (Figure. 33). Remembering how heterozygosity of *Sirt2* gene regulated the lifespan of *Cnp<sup>null</sup>* mice, this new observation was a supportive evidence of SIRT2 to be a modifier of the disease progression. These *Sirt2* +/- 5XFAD mice showed formation of a kyphosis and hindlimb problems at around 8 months of age. Single 5XFAD transgenic mice never develop such a phenotype at that age. When analyzing the cortex and subiculum of *Sirt2* +/- 5XFAD, we observed an increase in the plaque load compared to the 5XFAD mice (data not shown). Additionally, we observed an increase in the staining of phosphorylated APP, which specifically marks the axonal accumulation of APP, for example in brain stem of *Sirt2* +/- 5XFAD mice, compared to the single 5XFAD transgenic mice: however, the difference has not been quantified yet. Future analysis will include the analysis of different brain regions, and cortico spinal tract and *Sirt2* -/- 5XFAD mice will be also included into the analysis.

All our findings support the hypothesis that SIRT2 is a myelin-associated sensor for the state of the axons. The NAD<sup>+</sup>-dependency of its enzymatic activity suggests that its function can be coupled to the metabolism. And it is not surprising to expect the axons to be metabolically challenged when they are exposed to degenerating agents or mutations. And SIRT2 by its deacetylase activity can finetune the components of metabolism by modulating their activity or simply affecting their stability. What we observed in our study is how SIRT2 modifies the vulnerability of the axons to degeneration due to different causes. New findings on its substrates in brain will help us to understand the underlying molecular mechanisms of the axonoprotective function of SIRT2.

**6. References**

- Afshar, G., & Murnane, J. P. (1999). Characterization of a human gene with sequence homology to *Saccharomyces cerevisiae* SIR2. *Gene*, 234(1), 161-168.
- Al-Saktawi, K., McLaughlin, M., Klugmann, M., Schneider, A., Barrie, J. A., McCulloch, M. C., Montague, P., Kirkham, D., Nave, K. A., & Griffiths, I. R. (2003). Genetic background determines phenotypic severity of the Plp rumpshaker mutation. *J Neurosci Res*, 72(1), 12-24.
- Anekonda, T. S. (2006). Resveratrol--a boon for treating Alzheimer's disease? *Brain Res Rev*, 52(2), 316-326.
- Araki, T., Sasaki, Y., & Milbrandt, J. (2004). Increased nuclear NAD biosynthesis and SIRT1 activation prevent axonal degeneration. *Science*, 305(5686), 1010-1013.
- Bae, N. S., Swanson, M. J., Vassilev, A., & Howard, B. H. (2004). Human histone deacetylase SIRT2 interacts with the homeobox transcription factor HOXA10. *J Biochem*, 135(6), 695-700.
- Baur, J. A., Pearson, K. J., Price, N. L., Jamieson, H. A., Lerin, C., Kalra, A., Prabhu, V. V., Allard, J. S., Lopez-Lluch, G., Lewis, K., Pistell, P. J., Poosala, S., Becker, K. G., Boss, O., Gwinn, D., Wang, M., Ramaswamy, S., Fishbein, K. W., Spencer, R. G., Lakatta, E. G., Le Couteur, D., Shaw, R. J., Navas, P., Puigserver, P., Ingram, D. K., de Cabo, R., & Sinclair, D. A. (2006). Resveratrol improves health and survival of mice on a high-calorie diet. *Nature*, 444(7117), 337-342.
- Beirowski, B., Gustin, J., Armour, S. M., Yamamoto, H., Viader, A., North, B. J., Michan, S., Baloh, R. H., Golden, J. P., Schmidt, R. E., Sinclair, D. A., Auwerx, J., & Milbrandt, J. (2011). Sir-two-homolog 2 (Sirt2) modulates peripheral myelination through polarity protein Par-3/atypical protein kinase C (aPKC) signaling. *Proc Natl Acad Sci U S A*, 108(43), E952-961.
- Bielschowsky, M. (1908). "Eine Modifikation meines Silver-imprägnationsverfahrens zur Darstellung der Neurofibrillen." *J für Psychologie Neurologie* 12: 135-137.
- Bishop, N. A., & Guarente, L. (2007). Genetic links between diet and lifespan: shared mechanisms from yeast to humans. *Nat Rev Genet*, 8(11), 835-844.
- Black, J. C., Mosley, A., Kitada, T., Washburn, M., & Carey, M. (2008). The SIRT2 deacetylase regulates autoacetylation of p300. *Mol Cell*, 32(3), 449-455.
- Blander, G., & Guarente, L. (2004). The Sir2 family of protein deacetylases. *Annu Rev Biochem*, 73, 417-435.

- Blum, H., Beier, H., and Gross, H. J. (1987). "Improved silver staining of plant proteins, RNA and DNA in polyacrylamide gels." *Electrophoresis* 8: 93-99.
- Bordone, L., Cohen, D., Robinson, A., Motta, M. C., van Veen, E., Czopik, A., Steele, A. D., Crowe, H., Marmor, S., Luo, J., Gu, W., & Guarente, L. (2007). SIRT1 transgenic mice show phenotypes resembling calorie restriction. *Aging Cell*, 6(6), 759-767.
- Bouras, T., Fu, M., Sauve, A. A., Wang, F., Quong, A. A., Perkins, N. D., Hay, R. T., Gu, W., & Pestell, R. G. (2005). SIRT1 deacetylation and repression of p300 involves lysine residues 1020/1024 within the cell cycle regulatory domain 1. *J Biol Chem*, 280(11), 10264-10276.
- Brunet, A., Sweeney, L. B., Sturgill, J. F., Chua, K. F., Greer, P. L., Lin, Y., Tran, H., Ross, S. E., Mostoslavsky, R., Cohen, H. Y., Hu, L. S., Cheng, H. L., Jedrychowski, M. P., Gygi, S. P., Sinclair, D. A., Alt, F. W., & Greenberg, M. E. (2004). Stress-dependent regulation of FOXO transcription factors by the SIRT1 deacetylase. *Science*, 303(5666), 2011-2015.
- Chen, J., Zhou, Y., Mueller-Steiner, S., Chen, L. F., Kwon, H., Yi, S., Mucke, L., & Gan, L. (2005). SIRT1 protects against microglia-dependent amyloid-beta toxicity through inhibiting NF-kappaB signaling. *J Biol Chem*, 280(48), 40364-40374.
- Chen, S., Owens, G. C., Makarenkova, H., & Edelman, D. B. (2010). HDAC6 regulates mitochondrial transport in hippocampal neurons. *PLoS One*, 5(5), e10848.
- Cheung, P., Allis, C. D., & Sassone-Corsi, P. (2000). Signaling to chromatin through histone modifications. *Cell*, 103(2), 263-271.
- Choudhary, C., Kumar, C., Gnad, F., Nielsen, M. L., Rehman, M., Walther, T. C., Olsen, J. V., & Mann, M. (2009). Lysine acetylation targets protein complexes and co-regulates major cellular functions. *Science*, 325(5942), 834-840.
- Coprav, S., Huynh, J. L., Sher, F., Casaccia-Bonnel, P., & Boddeke, E. (2009). Epigenetic mechanisms facilitating oligodendrocyte development, maturation, and aging. *Glia*, 57(15), 1579-1587.
- Creppe, C., Malinouskaya, L., Volvert, M. L., Gillard, M., Close, P., Malaise, O., Laguesse, S., Cornez, I., Rahmouni, S., Ormenese, S., Belachew, S., Malgrange, B., Chapelle, J. P., Siebenlist, U., Moonen, G., Chariot, A., & Nguyen, L. (2009). Elongator controls the migration and differentiation of cortical neurons through acetylation of alpha-tubulin. *Cell*, 136(3), 551-564.

- De Vos, K. J., Grierson, A. J., Ackerley, S., & Miller, C. C. (2008). Role of axonal transport in neurodegenerative diseases. *Annu Rev Neurosci*, 31, 151-173.
- Dent, E. W., & Gertler, F. B. (2003). Cytoskeletal dynamics and transport in growth cone motility and axon guidance. *Neuron*, 40(2), 209-227.
- Denu, J. M. (2005). The Sir 2 family of protein deacetylases. *Curr Opin Chem Biol*, 9(5), 431-440.
- Dhaunchak, A. S., Huang, J. K., De Faria Junior, O., Roth, A. D., Pedraza, L., Antel, J. P., Bar-Or, A., & Colman, D. R. (2010). A proteome map of axoglial specializations isolated and purified from human central nervous system. *Glia*, 58(16), 1949-1960.
- Dillin, A., & Kelly, J. W. (2007). Medicine. The yin-yang of sirtuins. *Science*, 317(5837), 461-462.
- Dompierre, J. P., Godin, J. D., Charrin, B. C., Cordelieres, F. P., King, S. J., Humbert, S., & Saudou, F. (2007). Histone deacetylase 6 inhibition compensates for the transport deficit in Huntington's disease by increasing tubulin acetylation. *J Neurosci*, 27(13), 3571-3583.
- Donmez, G., & Guarente, L. (2010). Aging and disease: connections to sirtuins. *Aging Cell*, 9(2), 285-290.
- Donmez, G., Wang, D., Cohen, D. E., & Guarente, L. (2010). SIRT1 suppresses beta-amyloid production by activating the alpha-secretase gene ADAM10. *Cell*, 142(2), 320-332.
- Dryden, S. C., Nahhas, F. A., Nowak, J. E., Goustin, A. S., & Tainsky, M. A. (2003). Role for human SIRT2 NAD-dependent deacetylase activity in control of mitotic exit in the cell cycle. *Mol Cell Biol*, 23(9), 3173-3185.
- Edgar, J. M., McLaughlin, M., Werner, H. B., McCulloch, M. C., Barrie, J. A., Brown, A., Faichney, A. B., Snaidero, N., Nave, K. A., & Griffiths, I. R. (2009). Early ultrastructural defects of axons and axon-glia junctions in mice lacking expression of Cnp1. *Glia*, 57(16), 1815-1824.
- Edgar, J. M., McLaughlin, M., Yool, D., Zhang, S. C., Fowler, J. H., Montague, P., Barrie, J. A., McCulloch, M. C., Duncan, I. D., Garbern, J., Nave, K. A., & Griffiths, I. R. (2004). Oligodendroglial modulation of fast axonal transport in a mouse model of hereditary spastic paraplegia. *J Cell Biol*, 166(1), 121-131.
- Ford, E., Voit, R., Liszt, G., Magin, C., Grummt, I., & Guarente, L. (2006). Mammalian Sir2 homolog SIRT7 is an activator of RNA polymerase I transcription. *Genes Dev*, 20(9), 1075-1080.



- Frye, R. A. (1999). Characterization of five human cDNAs with homology to the yeast SIR2 gene: Sir2-like proteins (sirtuins) metabolize NAD and may have protein ADP-ribosyltransferase activity. *Biochem Biophys Res Commun*, 260(1), 273-279.
- Frye, R. A. (2000). Phylogenetic classification of prokaryotic and eukaryotic Sir2-like proteins. *Biochem Biophys Res Commun*, 273(2), 793-798.
- Fukushima, N., Furuta, D., Hidaka, Y., Moriyama, R., & Tsujiuchi, T. (2009). Post-translational modifications of tubulin in the nervous system. *J Neurochem*, 109(3), 683-693.
- Galiano, M. R., Andrieux, A., Deloulme, J. C., Bosc, C., Schweitzer, A., Job, D., & Hallak, M. E. (2006). Myelin basic protein functions as a microtubule stabilizing protein in differentiated oligodendrocytes. *J Neurosci Res*, 84(3), 534-541.
- Gallagher, S.R. (2006). "Electrophoretic Separation of Proteins." *Current Protocols in Molecular Biology*. John Wiley & Sons, Inc. 10.2.1.
- Gallyas, F. (1979). Silver staining of myelin by means of physical development. *Neurol Res*, 1(2), 203-209.
- Gasser, S. M., & Cockell, M. M. (2001). The molecular biology of the SIR proteins. *Gene*, 279(1), 1-16.
- Gerard, G. F., D'Alessio, J. M., Kotewicz, M. L., & Noon, M. C. (1986). Influence on stability in *Escherichia coli* of the carboxy-terminal structure of cloned Moloney murine leukemia virus reverse transcriptase. *DNA*, 5(4), 271-279.
- Gravel, M., Peterson, J., Yong, V. W., Kottis, V., Trapp, B., & Braun, P. E. (1996). Overexpression of 2',3'-cyclic nucleotide 3'-phosphodiesterase in transgenic mice alters oligodendrocyte development and produces aberrant myelination. *Mol Cell Neurosci*, 7(6), 453-466.
- Griffiths, I., Klugmann, M., Anderson, T., Yool, D., Thomson, C., Schwab, M. H., Schneider, A., Zimmermann, F., McCulloch, M., Nadon, N., & Nave, K. A. (1998). Axonal swellings and degeneration in mice lacking the major proteolipid of myelin. *Science*, 280(5369), 1610-1613.
- Haberland, M., Montgomery, R. L., & Olson, E. N. (2009). The many roles of histone deacetylases in development and physiology: implications for disease and therapy. *Nat Rev Genet*, 10(1), 32-42.

Haigis, M. C., Mostoslavsky, R., Haigis, K. M., Fahie, K., Christodoulou, D. C., Murphy, A. J., Valenzuela, D. M., Yancopoulos, G. D., Karow, M., Blander, G., Wolberger, C., Prolla, T. A., Weindruch, R., Alt, F. W., & Guarente, L. (2006). SIRT4 inhibits glutamate dehydrogenase and opposes the effects of calorie restriction in pancreatic beta cells. *Cell*, 126(5), 941-954.

Hallows, W. C., Lee, S., & Denu, J. M. (2006). Sirtuins deacetylate and activate mammalian acetyl-CoA synthetases. *Proc Natl Acad Sci U S A*, 103(27), 10230-10235.

Hames, B.D.a.R., D. (1990). "Gel Electrophoresis of Proteins: A Practical Approach." 2<sup>nd</sup> ed. Oxford University Press, New York.

Han, Y., Jin, Y. H., Kim, Y. J., Kang, B. Y., Choi, H. J., Kim, D. W., Yeo, C. Y., & Lee, K. Y. (2008). Acetylation of Sirt2 by p300 attenuates its deacetylase activity. *Biochem Biophys Res Commun*, 375(4), 576-580.

Harlow, E., and Lane, D. (1988). "Antibodies: a laboratory manual." Cold Spring Harbor, NY: Cold Spring Harbor Laboratory.

Harting, K., & Knoll, B. (2010). SIRT2-mediated protein deacetylation: An emerging key regulator in brain physiology and pathology. *Eur J Cell Biol*, 89(2-3), 262-269.

Hartline, D. K., & Colman, D. R. (2007). Rapid conduction and the evolution of giant axons and myelinated fibers. *Curr Biol*, 17(1), R29-35.

Hasegawa, K., & Yoshikawa, K. (2008). Necdin regulates p53 acetylation via Sirtuin1 to modulate DNA damage response in cortical neurons. *J Neurosci*, 28(35), 8772-8784.

He, Y., Dupree, J., Wang, J., Sandoval, J., Li, J., Liu, H., Shi, Y., Nave, K. A., & Casaccia-Bonnel, P. (2007). The transcription factor Yin Yang 1 is essential for oligodendrocyte progenitor differentiation. *Neuron*, 55(2), 217-230.

Hill, C. M., Libich, D. S., & Harauz, G. (2005). Assembly of tubulin by classic myelin basic protein isoforms and regulation by post-translational modification. *Biochemistry*, 44(50), 16672-16683.

Hiratsuka, M., Inoue, T., Toda, T., Kimura, N., Shirayoshi, Y., Kamitani, H., Watanabe, T., Ohama, E., Tahimic, C. G., Kurimasa, A., & Oshimura, M. (2003). Proteomics-based identification of differentially expressed genes in human gliomas: down-regulation of SIRT2 gene. *Biochem Biophys Res Commun*, 309(3), 558-566.

- Hubbert, C., Guardiola, A., Shao, R., Kawaguchi, Y., Ito, A., Nixon, A., Yoshida, M., Wang, X. F., & Yao, T. P. (2002). HDAC6 is a microtubule-associated deacetylase. *Nature*, 417(6887), 455-458.
- Imai, S., Armstrong, C. M., Kaeberlein, M., & Guarente, L. (2000). Transcriptional silencing and longevity protein Sir2 is an NAD-dependent histone deacetylase. *Nature*, 403(6771), 795-800.
- Inoue, K. (2005). PLP1-related inherited dysmyelinating disorders: Pelizaeus-Merzbacher disease and spastic paraplegia type 2. *Neurogenetics*, 6(1), 1-16.
- Inoue, T., Hiratsuka, M., Osaki, M., & Oshimura, M. (2007). The molecular biology of mammalian SIRT proteins: SIRT2 in cell cycle regulation. *Cell Cycle*, 6(9), 1011-1018.
- Inoue, T., Hiratsuka, M., Osaki, M., Yamada, H., Kishimoto, I., Yamaguchi, S., Nakano, S., Katoh, M., Ito, H., & Oshimura, M. (2007). SIRT2, a tubulin deacetylase, acts to block the entry to chromosome condensation in response to mitotic stress. *Oncogene*, 26(7), 945-957.
- Inoue, T., Nakayama, Y., Yamada, H., Li, Y. C., Yamaguchi, S., Osaki, M., Kurimasa, A., Hiratsuka, M., Katoh, M., & Oshimura, M. (2009). SIRT2 downregulation confers resistance to microtubule inhibitors by prolonging chronic mitotic arrest. *Cell Cycle*, 8(8), 1279-1291.
- Jahn, O., Tenzer, S., & Werner, H. B. (2009). Myelin proteomics: molecular anatomy of an insulating sheath. *Mol Neurobiol*, 40(1), 55-72.
- Janke, C., & Kneussel, M. (2010). Tubulin post-translational modifications: encoding functions on the neuronal microtubule cytoskeleton. *Trends Neurosci*, 33(8), 362-372.
- Jawhar, S., Trawicka, A., Jenneckens, C., Bayer, T. A., & Wirths, O. (2012). Motor deficits, neuron loss, and reduced anxiety coinciding with axonal degeneration and intraneuronal Abeta aggregation in the 5XFAD mouse model of Alzheimer's disease. *Neurobiol Aging*, 33(1), 196 e129-140.
- Ji, S., Doucette, J. R., & Nazarali, A. J. (2011). Sirt2 is a novel in vivo downstream target of Nkx2.2 and enhances oligodendroglial cell differentiation. *J Mol Cell Biol*.
- Jiang, W., Wang, S., Xiao, M., Lin, Y., Zhou, L., Lei, Q., Xiong, Y., Guan, K. L., & Zhao, S. (2011). Acetylation regulates gluconeogenesis by promoting PEPCK1 degradation via recruiting the UBR5 ubiquitin ligase. *Mol Cell*, 43(1), 33-44.

- Jin, Y. H., Kim, Y. J., Kim, D. W., Baek, K. H., Kang, B. Y., Yeo, C. Y., & Lee, K. Y. (2008). Sirt2 interacts with 14-3-3 beta/gamma and down-regulates the activity of p53. *Biochem Biophys Res Commun*, 368(3), 690-695.
- Jing, E., Gesta, S., & Kahn, C. R. (2007). SIRT2 regulates adipocyte differentiation through FoxO1 acetylation/deacetylation. *Cell Metab*, 6(2), 105-114.
- Johns, T. G., & Bernard, C. C. (1999). The structure and function of myelin oligodendrocyte glycoprotein. *J Neurochem*, 72(1), 1-9.
- Jung, M., Sommer, I., Schachner, M., & Nave, K. A. (1996). Monoclonal antibody O10 defines a conformationally sensitive cell-surface epitope of proteolipid protein (PLP): evidence that PLP misfolding underlies dysmyelination in mutant mice. *J Neurosci*, 16(24), 7920-7929.
- Kaeberlein, M., McVey, M., & Guarente, L. (1999). The SIR2/3/4 complex and SIR2 alone promote longevity in *Saccharomyces cerevisiae* by two different mechanisms. *Genes Dev*, 13(19), 2570-2580.
- Karuppagounder, S. S., Pinto, J. T., Xu, H., Chen, H. L., Beal, M. F., & Gibson, G. E. (2009). Dietary supplementation with resveratrol reduces plaque pathology in a transgenic model of Alzheimer's disease. *Neurochem Int*, 54(2), 111-118.
- Kim, D., Nguyen, M. D., Dobbin, M. M., Fischer, A., Sananbenesi, F., Rodgers, J. T., Delalle, I., Baur, J. A., Sui, G., Armour, S. M., Puigserver, P., Sinclair, D. A., & Tsai, L. H. (2007). SIRT1 deacetylase protects against neurodegeneration in models for Alzheimer's disease and amyotrophic lateral sclerosis. *EMBO J*, 26(13), 3169-3179.
- Kim, S. C., Sprung, R., Chen, Y., Xu, Y., Ball, H., Pei, J., Cheng, T., Kho, Y., Xiao, H., Xiao, L., Grishin, N. V., White, M., Yang, X. J., & Zhao, Y. (2006). Substrate and functional diversity of lysine acetylation revealed by a proteomics survey. *Mol Cell*, 23(4), 607-618.
- Klugmann, M., Schwab, M. H., Puhlhofer, A., Schneider, A., Zimmermann, F., Griffiths, I. R., & Nave, K. A. (1997). Assembly of CNS myelin in the absence of proteolipid protein. *Neuron*, 18(1), 59-70.
- Kramer-Albers, E. M., Bretz, N., Tenzer, S., Winterstein, C., Mobius, W., Berger, H., Nave, K. A., Schild, H., & Trotter, J. (2007). Oligodendrocytes secrete exosomes containing major myelin and stress-protective proteins: Trophic support for axons? *Proteomics Clin Appl*, 1(11), 1446-1461.
- Ko, M. H., Chen, W. P., & Hsieh, S. T. (2000). Cutaneous nerve degeneration induced by acrylamide in mice. *Neurosci Lett*, 293(3), 195-198.

- Kotewicz, M. L., D'Alessio, J. M., Driftmier, K. M., Blodgett, K. P., & Gerard, G. F. (1985). Cloning and overexpression of Moloney murine leukemia virus reverse transcriptase in *Escherichia coli*. *Gene*, 35(3), 249-258.
- Kouzarides, T. (2000). Acetylation: a regulatory modification to rival phosphorylation? *EMBO J*, 19(6), 1176-1179.
- Laemmli, U. K. (1970). Cleavage of structural proteins during the assembly of the head of bacteriophage T4. *Nature*, 227(5259), 680-685.
- Lagouge, M., Argmann, C., Gerhart-Hines, Z., Meziane, H., Lerin, C., Daussin, F., Messadeq, N., Milne, J., Lambert, P., Elliott, P., Geny, B., Laakso, M., Puigserver, P., & Auwerx, J. (2006). Resveratrol improves mitochondrial function and protects against metabolic disease by activating SIRT1 and PGC-1alpha. *Cell*, 127(6), 1109-1122.
- Landry, J., Slama, J. T., & Sternglanz, R. (2000). Role of NAD(+) in the deacetylase activity of the SIR2-like proteins. *Biochem Biophys Res Commun*, 278(3), 685-690.
- Lappe-Siefke, C., Goebbels, S., Gravel, M., Nicksch, E., Lee, J., Braun, P. E., Griffiths, I. R., & Nave, K. A. (2003). Disruption of Cnp1 uncouples oligodendroglial functions in axonal support and myelination. *Nat Genet*, 33(3), 366-374.
- Larocca, J. N., & Rodriguez-Gabin, A. G. (2002). Myelin biogenesis: vesicle transport in oligodendrocytes. *Neurochem Res*, 27(11), 1313-1329.
- Li, W., Zhang, B., Tang, J., Cao, Q., Wu, Y., Wu, C., Guo, J., Ling, E. A., & Liang, F. (2007). Sirtuin 2, a mammalian homolog of yeast silent information regulator-2 longevity regulator, is an oligodendroglial protein that decelerates cell differentiation through deacetylating alpha-tubulin. *J Neurosci*, 27(10), 2606-2616.
- Li, Y., Matsumori, H., Nakayama, Y., Osaki, M., Kojima, H., Kurimasa, A., Ito, H., Mori, S., Katoh, M., Oshimura, M., & Inoue, T. (2011). SIRT2 down-regulation in HeLa can induce p53 accumulation via p38 MAPK activation-dependent p300 decrease, eventually leading to apoptosis. *Genes Cells*, 16(1), 34-45.
- Linnington, C., Webb, M., & Woodhams, P. L. (1984). A novel myelin-associated glycoprotein defined by a mouse monoclonal antibody. *J Neuroimmunol*, 6(6), 387-396.

- Liszt, G., Ford, E., Kurtev, M., & Guarente, L. (2005). Mouse Sir2 homolog SIRT6 is a nuclear ADP-ribosyltransferase. *J Biol Chem*, 280(22), 21313-21320.
- Liu, G., Su, L., Hao, X., Zhong, N., Zhong, D., Singhal, S., & Liu, X. (2011). Salermide upregulates death receptor 5 expression through the ATF4-ATF3-CHOP axis and leads to apoptosis in human cancer cells. *J Cell Mol Med*.
- Lowry, O. H., Rosebrough, N. J., Farr, A. L., & Randall, R. J. (1951). Protein measurement with the Folin phenol reagent. *J Biol Chem*, 193(1), 265-275.
- Luo, J., Nikolaev, A. Y., Imai, S., Chen, D., Su, F., Shiloh, A., Guarente, L., & Gu, W. (2001). Negative control of p53 by Sir2alpha promotes cell survival under stress. *Cell*, 107(2), 137-148.
- Luthi-Carter, R., Taylor, D. M., Pallos, J., Lambert, E., Amore, A., Parker, A., Moffitt, H., Smith, D. L., Runne, H., Gokce, O., Kuhn, A., Xiang, Z., Maxwell, M. M., Reeves, S. A., Bates, G. P., Neri, C., Thompson, L. M., Marsh, J. L., & Kazantsev, A. G. (2010). SIRT2 inhibition achieves neuroprotection by decreasing sterol biosynthesis. *Proc Natl Acad Sci U S A*, 107(17), 7927-7932.
- Lynn, E. G., McLeod, C. J., Gordon, J. P., Bao, J., & Sack, M. N. (2008). SIRT2 is a negative regulator of anoxia-reoxygenation tolerance via regulation of 14-3-3 zeta and BAD in H9c2 cells. *FEBS Lett*, 582(19), 2857-2862.
- Marin-Husstege, M., Muggironi, M., Liu, A., & Casaccia-Bonnel, P. (2002). Histone deacetylase activity is necessary for oligodendrocyte lineage progression. *J Neurosci*, 22(23), 10333-10345.
- Matsuyama, A., Shimazu, T., Sumida, Y., Saito, A., Yoshimatsu, Y., Seigneurin-Berny, D., Osada, H., Komatsu, Y., Nishino, N., Khochbin, S., Horinouchi, S., & Yoshida, M. (2002). In vivo destabilization of dynamic microtubules by HDAC6-mediated deacetylation. *EMBO J*, 21(24), 6820-6831.
- Maxwell, M. M., Tomkinson, E. M., Nobles, J., Wizeman, J. W., Amore, A. M., Quinti, L., Chopra, V., Hersch, S. M., & Kazantsev, A. G. (2011). The Sirtuin 2 microtubule deacetylase is an abundant neuronal protein that accumulates in the aging CNS. *Hum Mol Genet*.
- McLaughlin, M., Karim, S. A., Montague, P., Barrie, J. A., Kirkham, D., Griffiths, I. R., & Edgar, J. M. (2007). Genetic background influences UPR but not PLP processing in the rumpshaker model of PMD/SPG2. *Neurochem Res*, 32(2), 167-176.
- Michan, S., & Sinclair, D. (2007). Sirtuins in mammals: insights into their biological function. *Biochem J*, 404(1), 1-13.

- Michishita, E., Park, J. Y., Burneskis, J. M., Barrett, J. C., & Horikawa, I. (2005). Evolutionarily conserved and nonconserved cellular localizations and functions of human SIRT proteins. *Mol Biol Cell*, 16(10), 4623-4635.
- Milne, J. C., & Denu, J. M. (2008). The Sirtuin family: therapeutic targets to treat diseases of aging. *Curr Opin Chem Biol*, 12(1), 11-17.
- Milne, J. C., Lambert, P. D., Schenk, S., Carney, D. P., Smith, J. J., Gagne, D. J., Jin, L., Boss, O., Perni, R. B., Vu, C. B., Bemis, J. E., Xie, R., Disch, J. S., Ng, P. Y., Nunes, J. J., Lynch, A. V., Yang, H., Galonek, H., Israelian, K., Choy, W., Iffland, A., Lavu, S., Medvedik, O., Sinclair, D. A., Olefsky, J. M., Jirousek, M. R., Elliott, P. J., & Westphal, C. H. (2007). Small molecule activators of SIRT1 as therapeutics for the treatment of type 2 diabetes. *Nature*, 450(7170), 712-716.
- Mostoslavsky, R., Chua, K. F., Lombard, D. B., Pang, W. W., Fischer, M. R., Gellon, L., Liu, P., Mostoslavsky, G., Franco, S., Murphy, M. M., Mills, K. D., Patel, P., Hsu, J. T., Hong, A. L., Ford, E., Cheng, H. L., Kennedy, C., Nunez, N., Bronson, R., Frendewey, D., Auerbach, W., Valenzuela, D., Karow, M., Hottiger, M. O., Hursting, S., Barrett, J. C., Guarente, L., Mulligan, R., Demple, B., Yancopoulos, G. D., & Alt, F. W. (2006). Genomic instability and aging-like phenotype in the absence of mammalian SIRT6. *Cell*, 124(2), 315-329.
- Motta, M. C., Divecha, N., Lemieux, M., Kamel, C., Chen, D., Gu, W., Bultsma, Y., McBurney, M., & Guarente, L. (2004). Mammalian SIRT1 represses forkhead transcription factors. *Cell*, 116(4), 551-563.
- Mullis, K., Faloona, F., Scharf, S., Saiki, R., Horn, G., & Erlich, H. (1986). Specific enzymatic amplification of DNA in vitro: the polymerase chain reaction. *Cold Spring Harb Symp Quant Biol*, 51 Pt 1, 263-273.
- Muth, V., Nadaud, S., Grummt, I., & Voit, R. (2001). Acetylation of TAF(I)68, a subunit of TIF-IB/SL1, activates RNA polymerase I transcription. *EMBO J*, 20(6), 1353-1362.
- Nave, K. A. (2010). Myelination and support of axonal integrity by glia. *Nature*, 468(7321), 244-252.
- Nave, K. A., Lai, C., Bloom, F. E., & Milner, R. J. (1987). Splice site selection in the proteolipid protein (PLP) gene transcript and primary structure of the DM-20 protein of central nervous system myelin. *Proc Natl Acad Sci U S A*, 84(16), 5665-5669.
- Nguyen, T., Mehta, N. R., Conant, K., Kim, K. J., Jones, M., Calabresi, P. A., Melli, G., Hoke, A., Schnaar, R. L., Ming, G. L., Song, H., Keswani, S. C., & Griffin, J. W. (2009). Axonal protective effects of the myelin-associated glycoprotein. *J Neurosci*, 29(3), 630-637.

- Nie, H., Chen, H., Han, J., Hong, Y., Ma, Y., Xia, W., & Ying, W. (2011). Silencing of SIRT2 induces cell death and a decrease in the intracellular ATP level of PC12 cells. *Int J Physiol Pathophysiol Pharmacol*, 3(1), 65-70.
- North, B. J., Marshall, B. L., Borra, M. T., Denu, J. M., & Verdin, E. (2003). The human Sir2 ortholog, SIRT2, is an NAD<sup>+</sup>-dependent tubulin deacetylase. *Mol Cell*, 11(2), 437-444.
- North, B. J., & Verdin, E. (2007). Interphase nucleo-cytoplasmic shuttling and localization of SIRT2 during mitosis. *PLoS One*, 2(8), e784.
- North, B. J., & Verdin, E. (2007). Mitotic regulation of SIRT2 by cyclin-dependent kinase 1-dependent phosphorylation. *J Biol Chem*, 282(27), 19546-19555.
- Norton, W. T. (1984). Recent advances in myelin biochemistry. *Ann N Y Acad Sci*, 436, 5-10.
- Norton, W. T., & Poduslo, S. E. (1973). Myelination in rat brain: method of myelin isolation. *J Neurochem*, 21(4), 749-757.
- Oakley, H., Cole, S. L., Logan, S., Maus, E., Shao, P., Craft, J., Guillozet-Bongaarts, A., Ohno, M., Disterhoft, J., Van Eldik, L., Berry, R., & Vassar, R. (2006). Intraneuronal beta-amyloid aggregates, neurodegeneration, and neuron loss in transgenic mice with five familial Alzheimer's disease mutations: potential factors in amyloid plaque formation. *J Neurosci*, 26(40), 10129-10140.
- Okawara, M., Katsuki, H., Kurimoto, E., Shibata, H., Kume, T., & Akaike, A. (2007). Resveratrol protects dopaminergic neurons in midbrain slice culture from multiple insults. *Biochem Pharmacol*, 73(4), 550-560.
- Onyango, P., Celic, I., McCaffery, J. M., Boeke, J. D., & Feinberg, A. P. (2002). SIRT3, a human SIR2 homologue, is an NAD-dependent deacetylase localized to mitochondria. *Proc Natl Acad Sci U S A*, 99(21), 13653-13658.
- Outeiro, T. F., Kontopoulos, E., Altmann, S. M., Kufareva, I., Strathearn, K. E., Amore, A. M., Volk, C. B., Maxwell, M. M., Rochet, J. C., McLean, P. J., Young, A. B., Abagyan, R., Feany, M. B., Hyman, B. T., & Kazantsev, A. G. (2007). Sirtuin 2 inhibitors rescue alpha-synuclein-mediated toxicity in models of Parkinson's disease. *Science*, 317(5837), 516-519.
- Outeiro, T. F., Marques, O., & Kazantsev, A. (2008). Therapeutic role of sirtuins in neurodegenerative disease. *Biochim Biophys Acta*, 1782(6), 363-369.



- Pandithage, R., Lilischkis, R., Harting, K., Wolf, A., Jedamzik, B., Luscher-Firzlaff, J., Vervoorts, J., Lasonder, E., Kremmer, E., Knoll, B., & Luscher, B. (2008). The regulation of SIRT2 function by cyclin-dependent kinases affects cell motility. *J Cell Biol*, 180(5), 915-929.
- Parker, J. A., Arango, M., Abderrahmane, S., Lambert, E., Tourette, C., Catoire, H., & Neri, C. (2005). Resveratrol rescues mutant polyglutamine cytotoxicity in nematode and mammalian neurons. *Nat Genet*, 37(4), 349-350.
- Pedraza, L., Huang, J. K., & Colman, D. R. (2001). Organizing principles of the axoglial apparatus. *Neuron*, 30(2), 335-344.
- Perdiz, D., Mackeh, R., Pous, C., & Baillet, A. (2011). The ins and outs of tubulin acetylation: more than just a post-translational modification? *Cell Signal*, 23(5), 763-771.
- Pfister, J. A., Ma, C., Morrison, B. E., & D'Mello, S. R. (2008). Opposing effects of sirtuins on neuronal survival: SIRT1-mediated neuroprotection is independent of its deacetylase activity. *PLoS One*, 3(12), e4090.
- Picard, F., Kurtev, M., Chung, N., Topark-Ngarm, A., Senawong, T., Machado De Oliveira, R., Leid, M., McBurney, M. W., & Guarente, L. (2004). Sirt1 promotes fat mobilization in white adipocytes by repressing PPAR-gamma. *Nature*, 429(6993), 771-776.
- Piperno, G., LeDizet, M., & Chang, X. J. (1987). Microtubules containing acetylated alpha-tubulin in mammalian cells in culture. *J Cell Biol*, 104(2), 289-302.
- Pirollet, F., Margolis, R. L., & Job, D. (1992). Ca(2+)-calmodulin regulated effectors of microtubule stability in neuronal tissues. *Biochim Biophys Acta*, 1160(1), 113-119.
- Polevoda, B., & Sherman, F. (2002). The diversity of acetylated proteins. *Genome Biol*, 3(5), reviews0006.
- Poliak, S., & Peles, E. (2003). The local differentiation of myelinated axons at nodes of Ranvier. *Nat Rev Neurosci*, 4(12), 968-980.
- Poltorak, M., Sadoul, R., Keilhauer, G., Landa, C., Fahrig, T., & Schachner, M. (1987). Myelin-associated glycoprotein, a member of the L2/HNK-1 family of neural cell adhesion molecules, is involved in neuron-oligodendrocyte and oligodendrocyte-oligodendrocyte interaction. *J Cell Biol*, 105(4), 1893-1899.

- Qin, W., Chachich, M., Lane, M., Roth, G., Bryant, M., de Cabo, R., Ottinger, M. A., Mattison, J., Ingram, D., Gandy, S., & Pasinetti, G. M. (2006). Calorie restriction attenuates Alzheimer's disease type brain amyloidosis in Squirrel monkeys (*Saimiri sciureus*). *J Alzheimers Dis*, 10(4), 417-422.
- Richter-Landsberg, C. (2000). The oligodendroglia cytoskeleton in health and disease. *J Neurosci Res*, 59(1), 11-18.
- Rodgers, J. T., Lerin, C., Haas, W., Gygi, S. P., Spiegelman, B. M., & Puigserver, P. (2005). Nutrient control of glucose homeostasis through a complex of PGC-1alpha and SIRT1. *Nature*, 434(7029), 113-118.
- Rogina, B., & Helfand, S. L. (2004). Sir2 mediates longevity in the fly through a pathway related to calorie restriction. *Proc Natl Acad Sci U S A*, 101(45), 15998-16003.
- Roth, A. D., Ivanova, A., & Colman, D. R. (2006). New observations on the compact myelin proteome. *Neuron Glia Biol*, 2(1), 15-21.
- Rothgiesser, K. M., Erener, S., Waibel, S., Luscher, B., & Hottiger, M. O. (2010). SIRT2 regulates NF-kappaB dependent gene expression through deacetylation of p65 Lys310. *J Cell Sci*, 123(Pt 24), 4251-4258.
- Saher, G., Brugger, B., Lappe-Siefke, C., Mobius, W., Tozawa, R., Wehr, M. C., Wieland, F., Ishibashi, S., & Nave, K. A. (2005). High cholesterol level is essential for myelin membrane growth. *Nat Neurosci*, 8(4), 468-475.
- Saher, G., Quintes, S., & Nave, K. A. (2011). Cholesterol: a novel regulatory role in myelin formation. *Neuroscientist*, 17(1), 79-93.
- Sauve, A. A., Celic, I., Avalos, J., Deng, H., Boeke, J. D., & Schramm, V. L. (2001). Chemistry of gene silencing: the mechanism of NAD<sup>+</sup>-dependent deacetylation reactions. *Biochemistry*, 40(51), 15456-15463.
- Schaumburg, H. H., Wisniewski, H. M., & Spencer, P. S. (1974). Ultrastructural studies of the dying-back process. I. Peripheral nerve terminal and axon degeneration in systemic acrylamide intoxication. *J Neuropathol Exp Neurol*, 33(2), 260-284.
- Scher, M. B., Vaquero, A., & Reinberg, D. (2007). SirT3 is a nuclear NAD<sup>+</sup>-dependent histone deacetylase that translocates to the mitochondria upon cellular stress. *Genes Dev*, 21(8), 920-928.

- Schwer, B., Bunkenborg, J., Verdin, R. O., Andersen, J. S., & Verdin, E. (2006). Reversible lysine acetylation controls the activity of the mitochondrial enzyme acetyl-CoA synthetase 2. *Proc Natl Acad Sci U S A*, 103(27), 10224-10229.
- Schwer, B., North, B. J., Frye, R. A., Ott, M., & Verdin, E. (2002). The human silent information regulator (Sir)2 homologue hSIRT3 is a mitochondrial nicotinamide adenine dinucleotide-dependent deacetylase. *J Cell Biol*, 158(4), 647-657.
- Shen, S., Li, J., & Casaccia-Bonnel, P. (2005). Histone modifications affect timing of oligodendrocyte progenitor differentiation in the developing rat brain. *J Cell Biol*, 169(4), 577-589.
- Shen, S., Sandoval, J., Swiss, V. A., Li, J., Dupree, J., Franklin, R. J., & Casaccia-Bonnel, P. (2008). Age-dependent epigenetic control of differentiation inhibitors is critical for remyelination efficiency. *Nat Neurosci*, 11(9), 1024-1034.
- Sherman, D. L., & Brophy, P. J. (2005). Mechanisms of axon ensheathment and myelin growth. *Nat Rev Neurosci*, 6(9), 683-690.
- Shi, T., Wang, F., Stieren, E., & Tong, Q. (2005). SIRT3, a mitochondrial sirtuin deacetylase, regulates mitochondrial function and thermogenesis in brown adipocytes. *J Biol Chem*, 280(14), 13560-13567.
- Simons, M., & Trajkovic, K. (2006). Neuron-glia communication in the control of oligodendrocyte function and myelin biogenesis. *J Cell Sci*, 119(Pt 21), 4381-4389.
- Sorensen, B. K., Hojrup, P., Ostergard, E., Jorgensen, C. S., Enghild, J., Ryder, L. R., & Houen, G. (2002). Silver staining of proteins on electroblotting membranes and intensification of silver staining of proteins separated by polyacrylamide gel electrophoresis. *Anal Biochem*, 304(1), 33-41.
- Southwood, C. M., Peppi, M., Dryden, S., Tainsky, M. A., & Gow, A. (2007). Microtubule deacetylases, SirT2 and HDAC6, in the nervous system. *Neurochem Res*, 32(2), 187-195.
- Sprinkle, T. J. (1989). 2',3'-cyclic nucleotide 3'-phosphodiesterase, an oligodendrocyte-Schwann cell and myelin-associated enzyme of the nervous system. *Crit Rev Neurobiol*, 4(3), 235-301.
- Suzuki, K., & Koike, T. (2007). Mammalian Sir2-related protein (SIRT) 2-mediated modulation of resistance to axonal degeneration in slow Wallerian degeneration mice: a crucial role of tubulin deacetylation. *Neuroscience*, 147(3), 599-612.

- Tang, B. L., & Chua, C. E. (2008). SIRT2, tubulin deacetylation, and oligodendroglia differentiation. *Cell Motil Cytoskeleton*, 65(3), 179-182.
- Tapia, M., Wandosell, F., & Garrido, J. J. (2010). Impaired function of HDAC6 slows down axonal growth and interferes with axon initial segment development. *PLoS One*, 5(9), e12908.
- Taylor, C. M., Marta, C. B., Claycomb, R. J., Han, D. K., Rasband, M. N., Coetzee, T., & Pfeiffer, S. E. (2004). Proteomic mapping provides powerful insights into functional myelin biology. *Proc Natl Acad Sci U S A*, 101(13), 4643-4648.
- Taylor, D. M., Maxwell, M. M., Luthi-Carter, R., & Kazantsev, A. G. (2008). Biological and potential therapeutic roles of sirtuin deacetylases. *Cell Mol Life Sci*, 65(24), 4000-4018.
- Towbin, H., Staehelin, T., & Gordon, J. (1979). Electrophoretic transfer of proteins from polyacrylamide gels to nitrocellulose sheets: procedure and some applications. *Proc Natl Acad Sci U S A*, 76(9), 4350-4354.
- Tsukada, Y. and Kurihara, T. (1992). "2',3'-cyclic nucleotide 3'-phosphodiesterase: Molecular characterization and possible function significance." *Myelin: Biology and Chemistry*, (ed. Martenson, R.E) 449-480 (CRC Press, Boca Raton).
- Unlu, M., Morgan, M. E., & Minden, J. S. (1997). Difference gel electrophoresis: a single gel method for detecting changes in protein extracts. *Electrophoresis*, 18(11), 2071-2077.
- Vanrobaeys, F., Van Coster, R., Dhondt, G., Devreese, B., & Van Beeumen, J. (2005). Profiling of myelin proteins by 2D-gel electrophoresis and multidimensional liquid chromatography coupled to MALDI TOF-TOF mass spectrometry. *J Proteome Res*, 4(6), 2283-2293.
- Vaquero, A., Scher, M., Lee, D., Erdjument-Bromage, H., Tempst, P., & Reinberg, D. (2004). Human SirT1 interacts with histone H1 and promotes formation of facultative heterochromatin. *Mol Cell*, 16(1), 93-105.
- Vaquero, A., Scher, M. B., Lee, D. H., Sutton, A., Cheng, H. L., Alt, F. W., Serrano, L., Sternglanz, R., & Reinberg, D. (2006). SirT2 is a histone deacetylase with preference for histone H4 Lys 16 during mitosis. *Genes Dev*, 20(10), 1256-1261.
- Vaziri, H., Dessain, S. K., Ng Eaton, E., Imai, S. I., Frye, R. A., Pandita, T. K., Guarente, L., & Weinberg, R. A. (2001). hSIR2(SIRT1) functions as an NAD-dependent p53 deacetylase. *Cell*, 107(2), 149-159.

Voelter-Mahlknecht, S., Ho, A. D., & Mahlkecht, U. (2005). FISH-mapping and genomic organization of the NAD-dependent histone deacetylase gene, Sirtuin 2 (Sirt2). *Int J Oncol*, 27(5), 1187-1196.

Vogel, U. S., & Thompson, R. J. (1988). Molecular structure, localization, and possible functions of the myelin-associated enzyme 2',3'-cyclic nucleotide 3'-phosphodiesterase. *J Neurochem*, 50(6), 1667-1677.

Wang, F., Chan, C. H., Chen, K., Guan, X., Lin, H. K., & Tong, Q. (2011). Deacetylation of FOXO3 by SIRT1 or SIRT2 leads to Skp2-mediated FOXO3 ubiquitination and degradation. *Oncogene*.

Wang, F., & Tong, Q. (2009). SIRT2 suppresses adipocyte differentiation by deacetylating FOXO1 and enhancing FOXO1's repressive interaction with PPARgamma. *Mol Biol Cell*, 20(3), 801-808.

Wang, L., Zhang, L., Chen, Z. B., Wu, J. Y., Zhang, X., & Xu, Y. (2009). Icaritin enhances neuronal survival after oxygen and glucose deprivation by increasing SIRT1. *Eur J Pharmacol*, 609(1-3), 40-44.

Werner, H., Jung, M., Klugmann, M., Sereda, M., Griffiths, I. R., & Nave, K. A. (1998). Mouse models of myelin diseases. *Brain Pathol*, 8(4), 771-793.

Werner, H. B., Kuhlmann, K., Shen, S., Uecker, M., Schardt, A., Dimova, K., Orfaniotou, F., Dhaunchak, A., Brinkmann, B. G., Mobius, W., Guarente, L., Casaccia-Bonnel, P., Jahn, O., & Nave, K. A. (2007). Proteolipid protein is required for transport of sirtuin 2 into CNS myelin. *J Neurosci*, 27(29), 7717-7730.

Williams, B. P., & Price, J. (1992). What have tissue culture studies told us about the development of oligodendrocytes? *Bioessays*, 14(10), 693-698.

Wu, J., & Grunstein, M. (2000). 25 years after the nucleosome model: chromatin modifications. *Trends Biochem Sci*, 25(12), 619-623.

Yang, Y. H., Chen, Y. H., Zhang, C. Y., Nimmakayalu, M. A., Ward, D. C., & Weissman, S. (2000). Cloning and characterization of two mouse genes with homology to the yeast Sir2 gene. *Genomics*, 69(3), 355-369.

Yeung, F., Hoberg, J. E., Ramsey, C. S., Keller, M. D., Jones, D. R., Frye, R. A., & Mayo, M. W. (2004). Modulation of NF-kappaB-dependent transcription and cell survival by the SIRT1 deacetylase. *EMBO J*, 23(12), 2369-2380.

Yin, X., Peterson, J., Gravel, M., Braun, P. E., & Trapp, B. D. (1997). CNP overexpression induces aberrant oligodendrocyte membranes and inhibits MBP accumulation and myelin compaction. *J Neurosci Res*, 50(2), 238-247.

- Yu, T. T., McIntyre, J. C., Bose, S. C., Hardin, D., Owen, M. C., & McClintock, T. S. (2005). Differentially expressed transcripts from phenotypically identified olfactory sensory neurons. *J Comp Neurol*, 483(3), 251-262.
- Yu, W. P., Collarini, E. J., Pringle, N. P., & Richardson, W. D. (1994). Embryonic expression of myelin genes: evidence for a focal source of oligodendrocyte precursors in the ventricular zone of the neural tube. *Neuron*, 12(6), 1353-1362.
- Zhang, B., Cao, Q., Guo, A., Chu, H., Chan, Y. G., Buschdorf, J. P., Low, B. C., Ling, E. A., & Liang, F. (2005). Juxtanodin: an oligodendroglial protein that promotes cellular arborization and 2',3'-cyclic nucleotide-3'-phosphodiesterase trafficking. *Proc Natl Acad Sci U S A*, 102(32), 11527-11532.
- Zhang, J., Sprung, R., Pei, J., Tan, X., Kim, S., Zhu, H., Liu, C. F., Grishin, N. V., & Zhao, Y. (2009). Lysine acetylation is a highly abundant and evolutionarily conserved modification in *Escherichia coli*. *Mol Cell Proteomics*, 8(2), 215-225.
- Zhang, Y., Li, N., Caron, C., Matthias, G., Hess, D., Khochbin, S., & Matthias, P. (2003). HDAC-6 interacts with and deacetylates tubulin and microtubules in vivo. *EMBO J*, 22(5), 1168-1179.
- Zhang, Y., Zhang, M., Dong, H., Yong, S., Li, X., Olashaw, N., Kruk, P. A., Cheng, J. Q., Bai, W., Chen, J., Nicosia, S. V., & Zhang, X. (2009). Deacetylation of cortactin by SIRT1 promotes cell migration. *Oncogene*, 28(3), 445-460.
- Zhao, Y., Wang, L., Yang, J., Zhang, P., Ma, K., Zhou, J., Liao, W., & Zhu, W. G. (2010). Anti-neoplastic activity of the cytosolic FoxO1 results from autophagic cell death. *Autophagy*, 6(7), 988-990.

**7. Appendices**

**Appendix 1**

**Abbreviations**

2D-DIGE	Two-dimensional differential fluorescence intensity gel electrophoresis
A	Absorbance
ADP	Adenosine diphosphate
ALS	Amyotrophic lateral sclerosis
APP	Amyloid precursor protein
APS	Ammonium persulfate
ATP	Adenosine triphosphate
Atp5b	ATP synthase subunit beta
bit	Binary digit
bp	Base pairs
BSA	Bovine serum albumin
°C	Degrees of celsius (centigrades)
CBP	CREB-binding protein
CDC14B	Cell division cycle 14 homolog B
CDK	Cyclin dependent kinase
cDNA	Complementary DNA
CFA	Complete Freund adjuvant
Chol	Cholesterol
cm	Centimeter
CNP	2', 3'-cyclic nucleotide phosphodiesterase
CNS	Central nervous system
DAB	3,3'-diaminobenzidine
dATP	Deoxyadenosine triphosphate
dCTP	Deoxycytidine triphosphate
ddH <sub>2</sub> O	Double distilled water
DDSA	Dodecenyl succinic anhydride
dGTP	Deoxyguanosine triphosphate
DM20	Splice variant of PLP
DNA	Deoxyribonucleic acid
dNTP	Desoxyribonucleosidtriphosphate
dpi	Dots per inch
DTT	Dithiothreitol
dTTP	Deoxythymidine triphosphate



EAE	Experimental autoimmune encephalomyelitis
ECL	Enhanced chemiluminescence
EDTA	Ethylene diamine tetra acetic acid
EM	Electron microscopy
EtBr	Ethidium bromide
FAD	Familial Alzheimer's disease
FOXO3A	Forkhead transcription factor
g	Gravity
g	Gram
GAPDH	Glyceraldehyde 3-phosphate dehydrogenase
GalC	Galactocerebroside
GC	Guanine-cytosine content
GFAP	Glial fibrillary acidic protein
HAT	Histone acetyltransferases
HBSS	Hank's buffered salt solution
HDAC	Histone deacetylase
HE	Haematoxylin-Eosin
HEK	Human embryonic kidney
Hes5	Hairy and enhancer of split 5
HMGCR	3-hydroxy-3-methylglutaryl-Coenzyme A reductase
HOXA10	Homeobox transcription factor
hr	Hours
HRP	Horse-radish peroxidase
HS	Horse serum
IB	Immunoblotting
Id2	Inhibitor of DNA binding 2, dominant negative helix-Loop-helix protein
IHC	Immunohistochemistry
IPL	Intraperiod line
IRDye	Infrared dye
kb	Kilobases
kDa	Kilodalton
K&S	Karlsson and Schultz
L	Liter
LDS	Lithium dodecylsulfate
LFB	Luxol-Fast-Blue
m	Meter
M	Molar

mA	Milliampere
MAG	Myelin associated glycoprotein
MBP	Myelin basic protein
MDL	Major dense line
mg	Milligram
MGB	Modified Gitschier buffer
min	Minutes
ml	Milliliter
mM	Millimolar
mm	Millimeter
MNA	Methyl nadic anhydride
MOG	Myelin oligodendrocyte glycoprotein
MOPS	3-(N-morpholino)propanesulfonic acid
mRNA	Messenger ribonucleic acid
N	Normal
NAD	Nicotinamide adenine dinucleotide
NCBI	National Centre for Biotechnology Information
NF- $\kappa$ B	Nuclear factor 'kappa-light-chain-enhancer' of activated B-cells
Nfkbib	Nuclear factor of kappa light polypeptide gene enhancer in B-cells inhibitor
ng	Nanogram
nM	Nanomolar
nm	Nanometer
OAADPr	O-acetyl-ADP-ribose
OL	Oligodendrocyte
O/N	Overnight
P	Postnatal day
PAGE	Polyacrylamide gel electrophoresis
PB	Phosphate buffer
PBS	Phosphate buffered saline
PBST	PBS with Tween-20
PC	Phosphatidyl choline
PCR	Polymerase chain reaction
PE	Phosphatidyl ethanolamine
PEPCK1	Phosphoenolpyruvate carboxykinase
PFA	Paraformaldehyde
pg	Picogram

PGC-1 $\alpha$	Peroxisome proliferator-activated receptor gamma, coactivator 1 alpha
PL	Paranodal loops
PLP	Proteolipid protein
pM	Picomolar
PMD	Pelizaeus Merzbacher disease
pmol	Picomol
PMP22	Peripheral myelin protein 22
PMSF	Phenylmethanesulfonylfluoride
PNS	Peripheral nervous system
ppm	Parts per million
Puro	Puromycine
PVDF	Polyvinylidene difluoride
P0	Myelin protein zero
qRT-PCR	Quantitative real time PCR
RelA	V-rel reticuloendotheliosis viral oncogene homolog A
RinI	Ras and Rab interactor-like
RIPA	Radioimmunoprecipitation assay
RNA	Ribonucleic acid
rpm	Revolution per minute
RQ	Relative quantity
RT	Room temperature
S	Svedberg unit
SC	Schwann cell
SDS	Sodium dodecylsulfate
Sec	Seconds
SEM	Standard error of the mean
SIR	Silent information regulator proteins
Sir2	Silent information regulator 2 protein
siRNA	Small interference ribonucleic acid
SIRT2	Sirtuin 2
SM	Sphingomyelin
SPG-2	Spastic paraplegia type 2
SQS	Squalene synthase
Sulf	Sulfatide
TAE	Tris-acetate EDTA
Taq	<i>Thermus aquaticus</i>
TBS	Tris buffered saline

TBST	TBS with Tween-20
TEMED	Tetramethyldiamin
Top1	Topoisomerase I
tRNA	Transfer RNA
TSA	Trichostatin A
U	Unit
UV	Ultraviolet
V	Volt
W	Watts
WT	Wild type
β-ME	Beta mercaptoethanol
μg	Microgram
μl	Microliter
μm	Micrometer

**Appendix 2**

**Instruments**

Automated staining system	Discovery XT Staining Module (Ventana Medical Systems Inc)
Automated system for Epon embedding	EMTP Leica
Automated system for tissue dehydration and paraplast impregnation	MICROM HMP 110
Binocular	Zeiss Stemi DV4
Blotting units and apparatus	Invitrogen XcellSureLock Invitrogen Novex Semi-Dry Blotter
Developer machine	Kodak X-OMAT 1000
Gel documentation system	Intas
Homogenizer	KINEMATICA AG POLYTRON PT 3000 Precellys 24 PeqLab BioTech.
Incubators	Memmert (37°C) Heraeus (60°C) Innova 4000 (56°C)
Light Cycler	LightCycler 480, 7500 Fast Real Time PCR System, Roche
Light microscopes	Zeiss Axiophot upright microscope
Magnetic stirrers	Heidolph MR 2000 Heidolph MR 3001 IKAMAG RH IKAMAG RCT IKA RCT Basic
Microtomes	HM400 MICROM, Leica HI 1210 Ultracut S, Leica
Microwaves	Daewoo
Microtitre plate reader	Molecular Devices, ThermoMax
Paraplast embedding apparatus	MICROM AP280-1
PCR machines	Biometra T3 Thermocycler Biometra Tgradient
Peristaltic pump	Heraeus Pericor
pH meter	WTW Series inoLab pH 720
Pipetteboy	Integra Biosciences
Power supplies	BIO-RAD

	Pharmacia Fine Chemicals
	Pharmacia Biotech
Rotarod	Accelerator Rotarod 7650 for mice, Ugo Basile, Italy (Jones & Roberts)
Scales	Sartorius
Scanners	EPSON F-3200 EPSON Odyssey
SDS-PAGE gel casting and running units	BIO-RAD (Mini Protean 3) Invitrogen (Novex Mini Cell)
Shakers	Heidolph Reax 2 IKA LABORTECHNIK HS250basic IKA LABORTECHNIK KS125basic Assistent 348 Intelli-Mixer RM-2
Thermal plate sealer	4titude 4s2 Thermal Sealer
UV spectrophotometer	Eppendorf BioPhotometer 613
System for Ultrapure Lab water	Sartorius Arium 611
Table-top centrifuge	Heraeus BioFuge Pico (RT) Eppendorf Centrifuge 5403 (4°C) SIGMA 4K15C QIAGEN centrifuge
Table-top thermomixer	Eppendorf
Ultracentrifuge	Beckman XL70
Ultra-turrax	IKA Ultra-turrax Typ T8
UV table	HeroLab 40 Transilluminator
Vacuum concentrator	Eppendorf Concentrator 5301
Vibratome	Mikrotom Leica VT 1000S
Vortexer	Vortex Genie 2 (Bender and Hobein)

**Appendix 3**

**Chemicals**

Acetic acid	Merck
Acetic acid anhydride	Merck
Acrylamide (40% in water)	Sigma-Aldrich
Acrylamide/Bis-acrylamide (29:1) (30%)	SERVA
Agarose	AppliChem
Aluminium sulphate	Fluka
Ammonium nitrate	Merck
Ammonium persulfate (APS)	Merck
Ammonium sulfate ((NH <sub>4</sub> ) <sub>2</sub> SO <sub>4</sub> )	Merck
Bacto Agar	BD
Bicine	BIOMOL
Bis-Tris	Sigma-Aldrich
Bromophenol blue	International Biotechnologies
BSA	BIOMOL
Chloroform	Merck
Citric acid (C <sub>6</sub> H <sub>8</sub> O <sub>7</sub> ·xH <sub>2</sub> O)	Merck
Coomassie brilliant blue (R-250)	BIOMOL
Cresyl violet	Merck
Disodium hydrophosphate (Na <sub>2</sub> HPO <sub>4</sub> ·x2H <sub>2</sub> O)	Merck
EDTA	Merck
Eosin	Merck
Ethanol	Sigma-Aldrich
Formaldehyde (HCOH), 37%	Merck
Glycerol	Merck
Glycine	Merck
Glutaraldehyde (25%)	Electron Microscopy Sciences
Haematoxylin	Merck
Hydrochloric acid (HCl), fuming	Merck
Hydrochloric acid (HCl), 1N	Merck
Hydrogen peroxide	Merck
Isobutanol	Merck
Isopropanol	Merck
Kernechtrot	Merck
LDS	Fluka

Lithiumcarbonate	Riedel de Haen
Magnesium chloride (MgCl <sub>2</sub> )	Merck
Magnesium sulfate (MgSO <sub>4</sub> )	Merck
Methanol	Merck
Methylene blue	Merck
Milk powder	Frema REFORM
MOPS	BIOMOL
NH <sub>3</sub> (32%)	Merck
Nicotinamide	Sigma-Aldrich
Paraformaldehyde	SERVA
Phenol Red	Merck
PMSF	Boehringer Mannheim
Potassium bicarbonate (KHCO <sub>3</sub> )	Merck
Potassium dihydrogen phosphate (KH <sub>2</sub> PO <sub>4</sub> )	Merck
Potassium sulfate (K <sub>2</sub> SO <sub>4</sub> )	Merck
Pyridin	Merck
SDS	Sigma-Aldrich
Serva Blue G250	SERVA
Silver nitrate (AgNO <sub>3</sub> )	Merck
Sodium acetate	Merck
Sodium carbonate (Na <sub>2</sub> CO <sub>3</sub> )	Merck
Sodium chloride (NaCl)	Merck
Sodium deoxycholate	Sigma-Aldrich
Sodium dihydrogenphosphate (NaH <sub>2</sub> PO <sub>4</sub> )	Merck
Sodium hydroxide (NaOH, 1N)	Merck
Sodium thiosulphate (Na <sub>2</sub> S <sub>2</sub> O <sub>3</sub> )	Merck
Sucrose	Merck
TEMED	SERVA
Tert-amylalkohol	Merck
2,2,2 Tribromethanol (99%)	Sigma-Aldrich
Tris	Sigma-Aldrich
Tris-HCl	Sigma-Aldrich
tri-Sodium citrate dihydrate (C <sub>6</sub> H <sub>5</sub> O <sub>7</sub> Na <sub>3</sub> x2H <sub>2</sub> O)	Merck
Triton X-100	SERVA
TSA (5mM)	Sigma-Aldrich
Tween-20	Sigma-Aldrich
Xylene	Merck
β-ME	Fluka



**Appendix 4**

**Curriculum vitae**

**Burcu Kasapoglu**

**Mobile Phone:** +49 176 227 297 98 and +90 533 512 79 36

**Home Phone:** +49 551 200 29 05 and +90 212 575 50 26

**E-mail:** [kasapoglu@em.mpg.de](mailto:kasapoglu@em.mpg.de) and [burcu.kasapoglu@gmail.com](mailto:burcu.kasapoglu@gmail.com)

**Private address-1**

Rote Strasse 36, 37073, Göttingen, Germany

**Private address-2**

Sair Orhan Veli Sokak, 15/12, 34180, Bahcelievler, Istanbul, Turkey

**Work address**

Max-Planck-Institute of Experimental Medicine (MPI-EM), Department of Neurogenetics  
Hermann-Rein Str 3, 37075, Göttingen, Germany

**Personal Information**

**Date of birth:** 08.02.1983

**Place of birth:** Bakirkoy/Istanbul/TURKEY

**Nationality:** Turkish

**Gender:** Female

**Education**

<b>2007-present</b>	PhD student Göttingen Graduate School for Neurosciences and Molecular Biosciences (GGNB), Molecular Physiology of the Brain Program (CMPB) Max-Planck-Institute of Experimental Medicine Department of Neurogenetics, Göttingen, Germany
<b>2005-2007</b>	Master of Science (MSc) degree International Max Planck Research School MSc/PhD Program in Neurosciences Max-Planck-Institute of Experimental Medicine Department of Neurogenetics, Göttingen, Germany
<b>2000-2005</b>	Bachelor of Science (BSc) degree Department of Molecular Biology and Genetics The Middle East Technical University, Ankara, Turkey
<b>2003-2005</b>	Minor program Department of Psychology The Middle East Technical University, Ankara, Turkey
<b>1993- 2000</b>	Cagaloglu Anatolia Highschool (CAL), Istanbul, Turkey <u>Medium of Instruction:</u> German

### Fellowships and awards

- 2006-2007** Max Planck stipend for research scholars, MPI-EM, Göttingen
- 2005-2006** Stipend for master studies in Neurosciences, International Max Planck Research School, Göttingen

### Scientific Activities

#### PROJECTS

- PhD thesis project:  
“Role of myelin-associated NAD<sup>+</sup>-dependent deacetylase Sirtuin 2 in modifying axonal degeneration”  
Supervisor: Prof. Klaus-Armin Nave, PhD, Max-Planck-Institute of Experimental Medicine, Department of Neurogenetics, Göttingen, Germany  
(2007-present)
- MSc thesis project:  
“Molecular characterization of a novel myelin protein, NAD<sup>+</sup>-dependent deacetylase SIRT2” Supervisor: Prof. Klaus-Armin Nave, PhD, Max-Planck-Institute of Experimental Medicine, Department of Neurogenetics, Göttingen, Germany  
(2005-2007)
- Lab rotation project:  
“Investigation of proteolipid protein’s (PLP) interaction with endoplasmic reticulum lectins and differential gene expression in response to unfolded PLP in oligodendroglial cells”  
Supervisor: Prof. Klaus-Armin Nave, PhD, Max-Planck-Institute of Experimental Medicine, Department of Neurogenetics, Göttingen, Germany  
(2006)
- Lab rotation project:  
“Construction of the transgenic vectors for pan-neuronal expression of ribbon-specific ribeye protein at conventional synapses”  
Supervisor: Prof. Dr. Markus Missler, Center for Physiology, Georg-August-University, Göttingen, Germany  
(2006)
- Lab rotation project:  
“Purification of TAT-P25 fragments to investigate CDK5-mediated apoptosis”  
Supervisor: Prof. Dr. Mathias Bähr, Center for Neurological Medicine, Georg-August-University, Göttingen, Germany  
(2006)
- Lab rotation project:  
“Neural differential effect by knockdown and overexpression of TRIM 11, a PAX6 ubiquitin ligase”  
Supervisor: Prof. Dr. Anastasia Stoykova, Max-Planck-Institute of Biophysical Chemistry, Department of Molecular Cell Biology, Göttingen, Germany  
(2006)

- Bachelor project:  
“Responsive Tissue Engineering Carriers, poly(NIPAM) as a thermoresponsive cell carrier”  
Supervisor: Prof. Dr. Vasif N. Hasirci, Middle East Technical University, Ankara, Turkey  
(2003-2005)
- Summer practice project:  
“Molecular Analysis in Neurodegenerative Diseases, like SCA and ALS”  
Supervisor: Prof. Dr. A. Nazli Basak, Bogazici University, Istanbul, Turkey  
(July-August 2004)
- Summer practice project:  
“Cloning of the thermostable DNA polymerase gene from a thermophilic bacterium found in a hot spring water in Turkey”  
Supervisor: Rengul Cetin Atalay, MD, PhD, Bilkent University, Ankara, Turkey  
(June-October 2002)

### **SCIENTIFIC MEETINGS**

- Poster presentation at Society for Neuroscience’s annual meeting (Washington, DC, USA):  
“Sirtuin 2 contributes to a neuroprotective function of oligodendrocytes in white matter tracts”  
(12-16 November 2011)
- Poster presentation at 10<sup>th</sup> European meeting on Glial Cells in Health and Disease (Prague, Czech Republic):  
“The myelin protein Sirtuin 2 is necessary for the axonoprotective function of oligodendroglia ”  
(13-17 September 2011)
- Poster presentation at Neurizons 2011, From Molecules to Mind-Making Sense of the Brain (Göttingen, Germany):  
“The myelin protein Sirtuin 2 is necessary for axonoprotective function of oligodendrocytes”  
(25-28 May 2011)
- Attended to 24<sup>th</sup> Ernst Klenk Symposium in Molecular Medicine-Protein Aggregation and Brain Disease (Köln, Germany)  
(14-16 September 2008)
- Poster presentation at Biomed 2004, 11<sup>th</sup> International Biomedical Science and Technology Days (Hacettepe University, Ankara, Turkey):  
“Responsive Tissue Engineering Carriers”  
(06-10 September 2004)
- Attended to 3<sup>rd</sup> Ege International Biennial Graduate Neuroscience Summer School, *Developmental, Degenerative and Regenerative Neural Plasticity and Myths and Facts about Neural Stem Cells: from Dish to Bedside*, Ege University Faculty of Medicine and Center for Brain Research, Izmir, Turkey  
(05-09 July 2004)

## Skills

### TEACHING SKILLS

- Summer internship, student: Hikmet Taner Teker  
Project: "Sirtuin 2 in the central nervous system"  
(June-September 2010)
- Summer internship, student: Tuba Oguz  
Project: "Sequence analysis of SIRT2 exons in SPG patients"  
(June-September 2009)
- Lab rotation, student: Sina Mozaffari Jovin  
Project: "Energy-dependent protein deacetylation by Sirtuin 2 in the central nervous system myelin"  
(March-May 2008)

### ORAL PRESENTATION SKILLS

- Annual retreat of the PhD students of the CMPB graduate program  
"Sirtuin 2 and acetylated myelin proteins"  
(November 2009)
- Annual MPI-EM PhD student retreat (2006-2009)
- Biennial Joint Lab Symposium, Cell Biology of Myelinating Glia  
Max-Planck-Institute of Experimental Medicine, Department of Neurogenetics, Göttingen,  
Germany  
(2008 and 2010)

### LANGUAGE SKILLS

- Turkish: native language
- English: fluent in writing and speaking
- German: fluent in writing and speaking

### COMPUTER SKILLS

Adobe Illustrator CS3, Adobe Photoshop CS3, EndNote, GraphPad Prism 5, ImageJ, Microsoft Office